



Fakultät für Medizin

Institut für Strahlenbiologie

Role of tumour initiating cells in the radiation resistance of osteosarcoma

Olena Klymenko

Vollständiger Abdruck der von der Fakultät für Medizin der Technischen Universität München zur Erlangung des akademischen Grades eines

Doctor of Philosophy (Ph.D.)

genehmigten Dissertation.

Vorsitzender: Univ.-Prof. Dr. Roland M. Schmid

Betreuer: Univ.-Prof. Dr. Michael J. Atkinson

Prüfer der Dissertation:

1. Univ.-Prof. Dr. Gabriele Multhoff
2. Priv.-Doz. Dr. Anna Friedl

Die Dissertation wurde am 17.12.2013 bei der Fakultät für Medizin der Technischen Universität München eingereicht und durch die Fakultät für Medizin am 26.02.2014 angenommen.

To My Family

Acknowledgments

I would like to thank all of my colleagues and friends who gave me the possibility to complete this thesis for their support and encouragement.

First of all I would like to thank my advisor Prof. Dr. Michael J. Atkinson for believing in me and giving the opportunity to carry out my PhD thesis in his institute and supporting me at any possible level.

I would like to thank my supervisor Dr. Michael Rosemann for the great time we spent working together; for the very interesting project and the every day discussions and advices. It was my pleasure to work in your group.

With great pleasure I would like to thank Prof. Klaus R. Trott for bringing me to the field of radiation biology and for the great support during all the time, for all very interesting discussions and meetings and taking care.

I am grateful to the Fridericus Foundation for the financial support of the last half year of my project and giving me the opportunity to finish my work on time.

I am thankful to Dr. Joachim Ellwart for the collaboration and help in performing cell sortings for my project. Also I would like to thank Dr. Ingo Burtscher for the providing the red expressing plasmid and Dr. Nicolaos Deliolanis for the performing mice tumour fluorescent visualization *in vivo* and Dr. Guido Drexler for helping in optimizing the immunofluorescence analysis.

I would like to thank Prof. Dr. Gabriele Multhoff and PD Dr. Anna Friedl for being in my thesis committee and advising my work.

Also I would like to thank PhD program coordinators Dr. Katrin Offe and Desislava Zlatanova for the great support during my study as well as all program members for their kind co-operation.

I would like to give my thanks to Dr. Iria Gonzales Vasconcellos and Bahar Sanli-Bonazzi for the amazing time spent together and our friendship. Special thank to Bahar for the technical assistance for my experiments.

Also I would like to express my thanks to all my colleagues from the Institute of Radiation Biology (Head Prof. Dr. Michael J. Atkinson), from the Research Unit of Radiation Cytogenetics (Head Prof Dr. H. Zitzelsberger) HMGU and from the Institute of Pathology (Head Prof. Dr. med. Heinz Höfler) for their kind support and help.

Спасибо моим киевским друзьям и однокурсникам; и всем, с кем мне посчастливилось познакомиться в Мюнхене, за поддержку и незабываемые встречи.

I would like to thank my mother Larisa, my brother Sergiy and his family for their love and support during all these years.

Спасибо Мамочка за твою любовь и поддержку на всём протяжении моей работы.

At the end I would like to thank my father who is not longer living but always in my heart.

Index

Index

Summary	6
Zusammenfassung	7
Abbreviations	8
I. Introduction	10
1.1. The biology and incidence of osteosarcoma	10
1.2. The aetiology of osteosarcoma	10
1.3. Animal studies	11
1.4. Clinical manifestations and the treatment of osteosarcoma	12
1.5. Tumour initiating cells as a cause of treatment failure	14
1.6. The identification and selection of tumour initiating cells	16
1.6.1. Surface markers and side population	16
1.6.2. Genetic markers of stemness	19
1.7. The molecular characterisation of side population cells as potential tumour initiating cells	21
1.8. The radioresistance of tumour initiating cells	22
1.9. Clonogenic survival and DNA damage as the most important criterium of tumour radiosensitivity	25
1.10. Hypothesis	28
II. Materials	29
III. Methods	36
3.1. Establishment of Mouse Osteosarcoma (MOS) cell lines	36
3.2. Growth inhibition of MOS cell lines after ionising irradiation	37
3.3. MOS cell line cultivation and liquid nitrogen freezing	38
3.4. Irradiation of MOS cell lines	38
3.5. Analysis and sorting of MOS side population cells	39
3.5.1. Hoechst 33342 staining	39
3.5.2. Flow cytometry analysis and Fluorescence Activated Cell Sorting (FACS)	40
3.5.3. Isolation of side population cells by Fluorescence Activated Cell Sorting (FACS)	40
3.6. Semi-quantitative RT-PCR analysis of target genes expression	41
3.6.1. Total RNA extraction	41
3.6.2. Quantification of nucleic acids	42
3.6.3. cDNA synthesis (Reverse transcription) of total RNA	42
3.6.4. Semi-quantitative RT-PCR primers	43
3.6.5. Semi-quantitative RT-PCR reaction	44
3.6.6. Analysis of semi-quantitative RT-PCR amplifications	45
3.7. Proliferation activity (MTT assay)	48
3.8. Protein immunoblotting (Western Blot analysis)	48
3.8.1. Total protein extraction	48
3.8.2. Protein concentration measurement	49
3.8.3. Samples preparation for loading into SDS electrophoresis gels	49
3.8.4. SDS-PAGE (polyacrylamide) gel preparation	50
3.8.5. Electrophoretic separation of proteins	50
3.8.6. Transfer of separated proteins	51
3.8.7. Antibody detection of target protein	51
3.8.8. Detection of immunoblot signals	51
3.8.9. Stripping and re-probing	52
3.9. Clonogenic assay	52
3.9.1. Serial dilution growth assay of side population and SP-depleted main population cells (clonogenic potential)	52
3.9.2. Clonogenic cell survival after irradiation assay (limiting dilution technique)	52
3.10. Immunofluorescent detection of DNA double strand breaks (DSBs) after irradiation (γ H2AX and 53BP1 foci)	57
3.10.1. Immunofluorescent staining of γ H2AX and 53BP1 foci	57

3.10.2.	Analysis of γ H2AX and 53BP1 foci	59
3.11.	In vivo osteosarcoma mouse model	60
3.11.1.	Mammalian plasmid for expression of red fluorescence protein (RFP) tdTomato	60
3.11.2.	Plasmid amplification	61
3.11.3.	Digestion of plasmid DNA and fragment analysis	61
3.11.4.	Gel electrophoresis of plasmid DNA	62
3.11.5.	Transfection of MOS cells with pCAG-tdTomato	62
3.11.6.	Stable integration of pCAG-tdTomato into the MOS genome	63
3.11.7.	Single cell cloning of MOS cells stably expressing the red fluorescence protein	64
3.11.8.	Experimental animals	64
3.11.9.	In vivo injection of pCAG-tdTomato MOS cells into mice	64
3.11.10.	Epifluorescence imaging of tumour formation in vivo	65
3.11.11.	Histological examination	65
IV. Results		66
4.1.	Characterisation of MOS cell lines	66
4.1.1.	Fraction of side population cells in MOS cell lines	66
4.1.2.	Side population and SP-depleted main population cells from MOS-R-306 have different morphologies	68
4.1.3.	Repopulation of side population and SP-depleted main population cells during growth of seeded SP cells and SP-depleted MP cells	69
4.1.4.	Proliferation activity of cultured side population and SP-depleted main population cells (MTT assay)	72
4.1.5.	Clonogenicity of side population and SP-depleted main population cells	74
4.1.6.	MOS cell line side population and SP-depleted main population cells differ in mRNA expression of markers present in embryonic and adult normal stem cells	76
4.1.7.	Correlation between the mRNA expression of markers present in embryonic and adult normal stem cells and the fraction of side population cells in unsorted MOS cell lines	79
4.1.8.	Sox2 and Bmi1 protein expression in MOS cell lines	84
4.1.9.	Overexpression of p53 protein in MOS-R-1929	86
4.2.	Radiation sensitivity of MOS cell lines	87
4.2.1.	Clonogenic survival of MOS cell lines	87
4.2.2.	Comparison of the clonogenic survival after irradiation of side population cells and SP-depleted main population cells	90
4.2.3.	Radiation-induced DNA double strand breaks after ionising irradiation in MOS cells	93
4.2.4.	Change in the expression of stem cell markers after irradiation of MOS cell lines	99
4.2.5.	Sox2 and Bmi1 expression change after irradiation in MOS cell lines (western blot)	102
4.3	Generation of an in vivo mouse osteosarcoma model	103
V. Discussion		107
5.1	MOS cell lines showed a large degree of variability in their clonogenic survival, with only a slight correlation with residual DNA double strand breaks	107
5.2	MOS cells possess a distinct subset of cells with the properties of tumour initiating cells	109
5.3	Tumour initiating cells do not show inherent radioresistance	112
5.4.	Expression of tumour initiating cells markers in MOS cells does not correlate with their radiosensitivity	113
5.5.	MOS cell radiosensitivity correlates with the fraction of tumour initiating cells	115
5.6.	Outlook	115
5.7.	Conclusion	116
VI. References		117
Curriculum Vitae		125

Summary

Osteosarcoma (OS) is the most common bone tumour predominantly affecting children and adolescents. It is recognized as a very aggressive and highly metastatic disease. The 10-year survival rate of OS patients is around 60%. Although clinical data show that human OS may vary in their radiation response it considered to be relatively radioresistant.

Evidence from other tumour types suggest that the radiation response of a small subset of so-called Tumour Initiating Cells (TICs) possessing self-renewing capacity is responsible for tumour relapse and resistance to therapy. However, there is no convincing evidence on the inherent radiosensitivity of these cells. Thus, we aimed at evaluating the role of TICs for the inherent radiosensitivity of these cells in osteosarcoma.

We analysed a set of mouse osteosarcoma (MOS) cell lines previously established from radiation induced mouse bone tumours. We showed that MOS cell lines varied significantly in their radiosensitivities evaluated by clonogenic cell survival after ionizing radiation and DNA double strand breaks repair.

Using stem cell specific dye exclusion we identified and isolated TICs from the selected MOS cell lines. The fraction of TICs was measured by the Hoechst 33342 Side Population (SP) cytometric assay and varied from 0.14% to 15% between cell lines. We showed that these cells have a prominent clonogenic potential and over-express embryonic “core-transcription factors” such as Sox2 and Nanog compared to SP-depleted main population cells. Yet, we observed that putative stem cell markers are not universally specific for all analysed cell lines. In disagreement to our expectations we found that isolated TICs of MOS cell lines did not show inherent radioresistance compared to non-TICs using limiting dilution clonogenic cell survival. On the other hand, we found that the difference in radiosensitivity between the analysed MOS cell lines was well correlated to their fraction of TICs. For further investigation on the radiosensitivity of osteosarcoma *in vivo* we developed a mouse osteosarcoma fluorescent model that showed great potential for more complex investigations.

Our results suggest that osteosarcoma possess a distinct set of cells with properties of TICs. We conclude from our study that the TICs contribute to the tumour radiation response due to their interaction with their tumour surrounding environmental (niche).

Zusammenfassung

Osteosarkome sind die häufigsten Knochentumoren. Sie treten vor allem bei Kindern und Jugendlichen auf. Sie sind aggressiv und metastasieren früh. Die 10-Jahres Überlebensrate liegt heute bei 60%. Klinische Daten weisen darauf hin, dass ihr Ansprechen auf Strahlentherapie sehr variabel ist. Sie gelten allgemein als strahlenresistent.

Forschungsergebnisse an anderen Tumorentitäten weisen darauf hin, dass das Auftreten von Tumorrezidiven und Therapieresistenzen zurückzuführen sind auf die Reaktion einer kleinen Subpopulation von Krebszellen, die sogenannten „tumour initiating cells“ (TIC) auf die Bestrahlung. Es gibt keine überzeugenden Daten bezüglich der individuellen Strahlenempfindlichkeit der TIC in Osteosarkomen. Deshalb waren wir bestrebt, die Rolle der TIC für die Strahlenempfindlichkeit der Osteosarkome zu erforschen.

Dazu untersuchten wir eine Reihe von Osteosarkom Zelllinien, die früher schon aus in Mäusen strahleninduzierten Osteosarkomen isoliert worden waren. Deren Strahlenempfindlichkeit, gemessen an der Koloniebildungsfähigkeit und an Doppelstrangbrüchen nach Bestrahlung variierte signifikant zwischen den Osteosarkom Zelllinien.

TIC wurden in den ausgewählten Osteosarkom Zelllinien mit Hilfe des stammzellspezifischen Farbausschlussverfahrens identifiziert und isoliert. Der mit dem Hoechst 33342 Farbstoffausschlussverfahren gemessene Anteil an TIC an der Gesamtzellpopulation variierte zwischen den Zelllinien von 0,14% bis 15%. TIC besitzen ausgeprägtes klonogene Potenzial und exprimieren embryonale Transkriptionsfaktoren wie Sox2 und Nanog. Stärker als die übrigen Zellen. Jedoch sind die üblichen Stammzellmarker nicht generell in den TIC aller verwendeten Zelllinien positiv. Entgegen unserer Arbeitshypothese stellten wir fest, dass isolierte Osteosarkom TIC im Koloniebildungstest nicht strahlenresistenter sind als die übrigen Osteosarkomzellen. Dagegen fand sich eine signifikant positive Korrelation zwischen dem Anteil von TIC an der Gesamtzellpopulation und ihrer inhärenten Strahlenresistenz.

In Vorbereitung auf geplante Untersuchungen zur Strahlenresistenz der Osteosarkome *in vivo* wurde ein genetisch manipuliertes Modell entwickelt, welches für solche Experimente aussichtsreich erscheint.

Abbreviations

53BP1	Tumor suppressor p53-binding protein 1
A/b	Antibody
A260	Absorption at 260nm
A280	Absorption at 280nm
ABC transportes	ATP (Adenosine-triphosphate)-binding cassette transporters
bp	base pair
Bq	Becquerel (unit of radioactivity)
CD	Cluster of differentiation
cDNA	complementary deoxyribonucleic acid
Cs ¹³⁷	Caesium-137 radioisotop
Ct	Cycle threshold
Cy3	Cyanine 3 fluorescent dye
D	Dose
DMEM	Dulbecco's modified eagle's medium
DNA	Deoxyribonucleic acid
E.Coli	Escherichia coli
FACS	Fluorescent activated cell sorting
g	gram (unit of mass)
gDNA	genomic DNA
i.e.	that is
IgG	Immunoglobulin G (antibody isotype)
kDa	kilodalton
Klf4	Kruppel-like factor 4
l	liter (unit of volume)
LD	Lethal dose
LD ₅₀	Median lethal dose
MDR (Mdr)	Multiple drug resistance
MHz	Megahertz (unit of frequency)
ml	millilitre (unit of volume)
mm	millimetre (unit of length)
MOS cell line	Mouse osteosarcoma cell line
MTT	3-(4,5-Dimethylthiazol-2-yl)-2,5-Diphenyltetrazolium Bromide
mV	millivolt (unit of electric potential)

n	number
HRP	Horseradish peroxidase
Oct3/4	Octamer-binding transcription factor 3/4
OD	Optical density
p53	Tumour suppressor protein 53
pCAG	plasmid containing CAG promoter
PE	Plating efficiency
PI	Propidium iodide
RB1	Retinoblastoma gene human
RNA	Ribonucleic acid
RNase	Ribonuclease
RT	Reverse transcription
RT-PCR	Real time polymerase chain reaction
SDS-PAGE	Sodium dodecyl sulphate polyacrylamide gel electrophoresis
Semi-qRT-PCR	Semi-quantitative real time polymerase chain reaction
SF (S)	Survival fraction
SF2	Survival fraction at 2Gy
Sox2	SRY (sex determining region Y)-box 2 transcription factor
SP	Side population
SP-depleted MP	Side population-depleted main population
SYBR green	Synergy brand green dye
TBP	TATA-binding protein
TBq	Terabecquerel
tdTomato	tandem dimer Tomato
Th ²²⁷	Thorium-227 radioisotope
TICs	Tumour initiating cells
UV	Ultraviolet light
V	Volt (unit of electric potential)
VEGF	Vascular endothelial growth factor
WB	Western blot
γ H2AX	phosphorylation of histone H2AX at serine 139
μ g	microgram (unit of mass)
μ l	microliter (unit of volume)

I. Introduction

1.1. The biology and incidence of osteosarcoma

Sarcomas are relatively rare malignant tumours of connective tissue. They can be histopathologically divided into soft tissue sarcomas and bone sarcomas. Among the bone sarcomas the most frequent tumour type is osteoblastic osteosarcoma (osteosarcoma), an entity that predominantly affects children and adolescents (Raymond et al, 2002).

This tumour arises from the bone-forming osteoblastic cell lineage, most probably from primitive mesenchymal bone lineage-committed cells. The primary distinguishing characteristic of osteosarcoma is the production of an extracellular matrix, termed osteoid as well as the presence of malignant transformed osteoblasts. In the cellular matrix other mesenchymal cell types are present, which leads to a histological subdivision of osteosarcoma into osteoblastic, chondroblastic and fibroblastic osteosarcoma subtypes. For diagnostic purposes the presence of osteoid and any area of malignant bone-forming tissue in the lesion establishes the diagnosis of osteosarcoma (Cannon, 2007; Raymond et al, 2002).

The incidence of osteosarcoma is low about 4-5 cases per million population, with a slightly greater prevalence among males. Idiopathic osteosarcoma is largely a disease of the young (Raymond et al, 2002). The period of greatest risk is 10-14 years for girls and 15-18 years for boys. From 20 years of age the incidence falls almost to zero but rises again after 40 to give a second peak in later age (around 60) (Cannon, 2007; Ottaviani & Jaffe, 2009).

1.2. The aetiology of osteosarcoma

The aetiology of osteogenic osteosarcoma is still unknown. Multiple pathogenic factors are considered, including bone infection, existing Paget's disease, exposure to carcinogenic environmental agents as well as a number of genetic predisposition syndromes (Cannon, 2007). Among the inherited syndromes that are associated with an increased risk for the causation of osteosarcoma are Li-Fraumeni, Bloom and Rothmund-Thomson syndromes (Ward et al, 1984; Wong et al, 1997). The dominantly-inherited Li-Fraumeni syndrome is a familial cancer syndrome resulting from germ line mutations in the p53 tumour suppressor gene, leading to an increased incidence of sarcomas in children and adults (Malkin et al, 1990; Sakurai et al, 2013). In sporadic osteosarcoma, p53 mutations and RB1 gene loss of heterozygosity are frequent. It was

shown that 75% of osteosarcoma cases possess loss of heterozygosity of the p53 gene (Chang et al, 1993; Toguchida et al, 1989). Bone trauma can reveal or propagate the clinical appearance of the tumour rather than be a risk factor to its development (Raymond et al, 2002). A dramatically increased risk to develop osteosarcoma after exposure to radiation was reported in women who painted luminous dials on instruments and watches using radium-containing paint in the 1920-40s (Fry, 1998; Rowland et al, 1978). Radium, as well as Strontium and Plutonium, is a bone seeking radioisotope which may replace calcium in bones and therefore become incorporated into the bone matrix of humans or animals when introduced into the body. A dose and time dependent increase of bone sarcomas was shown in a retrospective study on children treated with injected Ra^{224} (Peteosthor) for bone tuberculosis in the 1950s (Chmelevsky et al, 1988; Spiess, 1995). More recently, an increased incidence of osteosarcoma in workers from the “Mayak” Production Association was shown to be associated with exposure from both internally deposited plutonium and external gamma radiation (Koshurnikova et al, 2000). External beam irradiation is considered to be a risk factor in the development of osteosarcoma. The presence of inactivated RB1 gene in retinoblastoma patients who survive radiation treatment was associated with a 500-fold increase in incidence of osteosarcoma in the radiation field, late in life (Ward et al, 1984; Wong et al, 1997).

1.3. Animal studies

In animal experiments the risk of developing osteosarcoma is dependent on the radiation dose delivered, the gender and the age of the animals at incorporation, as well as their genetic background (Luz et al, 1991). A large programme of research on the osteosarcoma risk of incorporation of short life α -emitters after intraperitoneal injection was performed in Munich in the 1970s (Gössner et al, 1976). This led to the study of the genetic factors that influence the development of osteosarcoma in mice after administering internal bone seeking α -emitters. The susceptible loci that were found to play a role in mouse radiation osteosarcoma predisposition were proposed to be important for bone tumour formation in man as well (Rosemann et al, 2002). During this study a set of cell lines from radiation induced osteosarcoma was developed for further studies. Some of these were used in the project described here.

1.4. Clinical manifestations and the treatment of osteosarcoma

Osteosarcoma is a locally invasive and highly metastatic disease (Raymond et al, 2002). At the time of the initial diagnosis approximately 15% of osteosarcoma cases already present with detectable lung metastasis, and up to 80% of patients are believed to have existing micro-metastasis in the lung (Longhi et al, 2006; Raymond et al, 2002). The diagnosis of a clinically manifest metastasis is a poor prognostic indicator (Harris et al, 1998). Osteosarcomas most commonly develop in the long bones of the peripheral skeleton, preferentially in the cell rich metaphyseal area, with 50% of all osteosarcoma cases occurring in the distal femur, followed in frequency by the proximal tibia and the proximal humerus. In about 10% of cases osteosarcoma affects other parts of the skeleton, notably the jaw, the skull, the spine and the pelvis. In these cases conventional surgical treatment is rather difficult (Cannon, 2007).

Before chemotherapy was introduced every osteosarcoma having disseminated disease was eventually lethal to the patient (Longhi et al, 2006). In the past, amputation of the affected limb was the only way to treat an appendicular osteosarcoma. One of the first chemotherapeutical agents shown to be active in osteosarcoma patients was high-dose methotrexate in 1970s. This drug is still included in almost all of the current osteosarcoma treatment protocols. However, the use of this cytotoxic drug as a monotherapy is not sufficient, and different combinations with other systemic cytotoxic agents have been explored (Cannon, 2007; Longhi et al, 2006).

As a consequence of these refinements, the treatment outcome of osteosarcoma has improved considerably. Over the last 30 years novel chemotherapy regimes have raised the 10-year survival rate from about 10% to the current ~ 60% (Longhi et al, 2006). This is still much lower than many other solid cancer types of childhood (German Childhood Cancer Registry 1980-2009), suggesting further improvement is possible.

Today, the standard treatment for osteosarcoma involves a multimodal approach involving a combination of neo-adjuvant chemotherapy followed by surgical treatment and cycles of adjuvant chemotherapy (Cannon, 2007). The chemotherapy prior to surgery has a critical role in inactivating potential micro-metastasis, but also serves to control the primary tumour growth. The treatment strategy selected depends on the presence or absence of metastasis at diagnosis, tumour grade and anatomical location if it is the primary or recurrent disease, and not unusually the refusal of amputation. The extent of the surgical treatment of osteosarcoma is defined by the extent of the tumour. If distal or proximal amputation can be

avoided it is preferable to perform modified amputation or limb salvage surgery (Cannon, 2007).

The standard protocols defining alternative regimes and durations of chemotherapy for osteosarcoma treatment are based on the outcome of randomised clinical trials. The choice of neo-adjuvant treatment for local and metastatic primary disease commonly includes doxorubicin, ifosfamide, cisplatin and high-dose methotrexate in different combinations (Geller & Gorlick, 2010). If the tumour response to neo-adjuvant treatment is good the post-surgery adjuvant treatment may include the same chemotherapeutic drugs (Geller & Gorlick, 2010). If the tumour response is poor, however, i.e. level of necrosis in post adjuvant surgery specimen is low, the tumour is classified as refractory or even a relapsed disease and the next chemotherapy cycles may be modified to include additional chemotherapy drugs such as cyclophosphamide, etoposide (Geller & Gorlick, 2010; Rodriguez-Galindo et al, 2002).

Radiotherapy is not used as a standard treatment of osteosarcoma. However, radiotherapy in combination with chemotherapy is the method of choice for those osteosarcoma patients where surgery is not feasible or when the patient refuses to undergo surgery. The combination of chemo-radiation treatment may also be used for tumour local growth control in the case of multifocal osteosarcoma (Longhi et al, 2006; Machak et al, 2003). Curative conventional external beam radiotherapy is typically administered using 6 – 18 MeV linear accelerated photons. The radiation dose delivered to the tumour target volume is around 70Gy. In the 1950s, before chemotherapy was introduced, Cade showed that high dose radiotherapy of the local tumour followed by amputation after a six month metastasis free interval, increased patients survival more than early amputation (Cade, 1955). Nowadays, it has been shown that the 5-year overall local control rate for non-metastatic osteosarcoma of the extremities, treated with neo-adjuvant chemotherapy cycles and followed by 60Gy local radiotherapy is rather good at about 50% - 60%. This mostly depends on the early chemotherapy response (Longhi et al, 2006; Machak et al, 2003). Non-metastatic high grade osteosarcoma treated with preoperative radiotherapy followed by adjuvant chemotherapy also was shown to increase the chance of successful limb salvage surgery with a good prognosis (Dincbas et al, 2005). Moreover, radiotherapy with a median dose of 66Gy locally delivered in combination with chemotherapy, was shown to improve survival of osteosarcoma patients when minimal residual disease after surgery had to be treated (DeLaney et al, 2005).

Newly developed particle beam radiotherapy (proton therapy, heavy ion therapy) shows early but promising results in the treatment of osteosarcoma patients. The advantage of

particle therapy is the low energy deposition within the entry volume of the particle beam, coupled with the steep dose deposition peak across the tumour volume. This is obtained by using variations in the beam energy to suit the Bragg peak to the physical form of the tumour (Combs et al, 2010; Matsunobu et al, 2012).

Studies on the indications and techniques for radiotherapy of osteosarcoma deserve more consideration. This may offer an opportunity to improve upon the standard treatment by avoiding gross limb dysfunction, decreasing psychological strain on the patient, and also increasing long term survival rate in radiotherapy resistant cases.

1.5. Tumour initiating cells as a cause of treatment failure

The question why cancer patients frequently relapse after aggressive tumour treatment is still under investigation. The reason for this may be the existence of a small subset of cells in the tumour mass, so called tumour initiating cells (TICs) (Visvader & Lindeman, 2008). The hypothesis of tumour initiating cells is based on the principle of normal stem cell clonal evolution and assumes a hierarchical proliferation of tumour cells. (Kummermehr J. & Trott K.R., 1996; Nguyen et al, 2012). Particular clinical feature of tumour biology, including unrestricted tumour growth, formation of distant metastasis and re-growth of tumour after radical treatment all support this hypothesis (Cannon, 2007).

This concept stipulates that only this small proportion of tumour initiating cells from the whole tumour volume have a self-renewal capacity and can maintain the tumour over long period of time. This model also stipulates that the majority of tumour cells do not have self-renewal properties and, thus, have limited proliferative potential (Nguyen et al, 2012). The origin of the tumour initiating cells in tumours remains unclear. Recent studies showed that tumour initiating cells may originate either from a series of transformation events affecting normal stem cells or that they may arise from de-differentiation of more differentiated progenitor cells after their oncogenic transformation (Figure 1) (Reya et al, 2001; Visvader & Lindeman, 2008). Reya reviewed evidence from leukaemia that suggests that both hematopoietic stem cells as well as lineage-committed progenitor hematopoietic cells could be the target for transformation into leukaemia (Reya et al, 2001). Breast cancer cells were suggested to reprogram (de-differentiate) into tumour initiating cells after irradiation (Lagadec 2012).

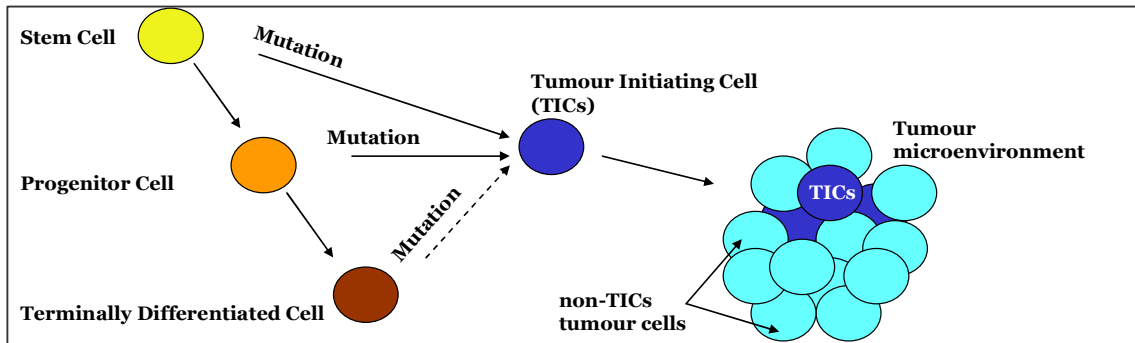


Figure 1: The evolution of tumour initiating cells. The simplified scheme shows that at any level of differentiation from a stem cell to a differentiated cell, irreversible mutation may occur. Such mutation would lead to a transformation of cell into the cell with tumour initiating properties and tumour development.

The tumour microenvironment was shown to play an important role in the maintenance of tumour initiating cells similar to the role played by the stem cell niche for normal stem cells (Borovski et al, 2011; Bütof et al; Peitzsch et al, 2013). The tumour initiating cells would not be equally distributed throughout the tumour and are suggested to reside in so called tumour “niches” which are represented either by perivascular, hypoxic or invasive sites (Borovski et al, 2011; Bütof et al; Peitzsch et al, 2013). Borovski described the interaction between the glioblastoma tumour initiating cells and the perivascular niches. Glioblastoma is a relatively well vascularised tumour and there is likely an interaction between glioblastoma tumour initiating cells and endothelial cells similar to neural stem cells and the vasculature niche (Borovski et al, 2011). Tumour initiating cells within this perivascular niche secrete the growth factor (VEGF) that promotes further formation of the vessels. The endothelial cells create new vasculature structures that would be able to maintain the stem like state of the tumour initiating cells through the activation of Notch pathway as was described by the production of nitric oxide (Borovski et al, 2011). In the hypoxic niche normal stem cells preferentially reside due to their slowly cycling and low oxygen consumption. The hypoxic environment and slow cell cycle progression may explain assumed tumour initiating cells radioresistance when compared to the cells in well oxygenated areas (Bütof et al; Peitzsch et al, 2013). The metastasis process is closely related to the invasive niche, also called pre-metastatic niche, where circulating tumour initiating cells may be hosted to grow into distinct metastasis (Peitzsch et al, 2013).

The reproductive potential of tumour initiating cells was investigated a long time ago in the classical approach to identify tumour initiating cells using quantitative limiting dilution transplantation *in vivo*. In 1958 Hewitt performed the first experiment to quantify the number

of human leukemia initiating cells in mice. He observed that after a titration of inoculated tumour cell numbers that the TD₅₀ value (the number of cells required to yield a tumour take rate of 50% of injected sites) was 3 cells i.e. not every cell injected could repopulate the tumour and thus cannot be considered as a tumour initiating cell (Hewitt, 1953; Hewitt, 1958). Since the serial dilution is a random process and the tumour take rate follows a Poisson distribution the new tumours originated from one or more cells with TICs properties.

In the 1950-60s it was also shown for solid tumours in mice that not all tumour cells could grow into a tumour after single cell transplantation into isogenic mice. The estimated TD₅₀ values varied between different solid tumours, ranging from 5 to 20.000 cells per inoculums (Hewitt et al, 1976; Kallman et al, 1967). This method has also been used in human cancers to identify tumorigenic properties of tumour initiating cells (Lapidot et al, 1994). One of the disadvantages of the quantitative transplantation technique is that it is both time and cost consuming.

1.6. The identification and selection of tumour initiating cells

1.6.1. Surface markers and side population

To predict the patient tumour therapy response it would be helpful to identify tumour initiating cells (TICs) that could allowed their quantification. The reason for the failure to identify genetic or molecular TICs markers with a predictive value might be that TICs usually not a large fraction of cells within any tumour, hence contributing to only a tiny portion of tumour DNA or RNA. Molecular features unique for TICs may be masked by the presence of a majority of non-TICs.

The quantitative transplantation assay provides the functional evidence for the existence of tumour initiating cells but it does not indentify these cells directly (Hewitt, 1953; Kallman et al, 1967). The introduction of flow cytometry capable of the separation of tumour initiating cells based on their expression of specific surface markers enabled the separation and investigation of individual tumour initiating cells (Basu-Roy et al, 2012a).

One of the first examples of specific surface markers that can be used to simplify the isolation and study of TICs came from studies on haematological malignancies and was reported in 1994 (Lapidot et al, 1994). The surface clusters of differentiation (CD) molecules found on normal hematopoietic cells were assumed to be present on leukaemia cells as well. In the experiment of Lapidot a very small CD34⁺/CD38⁻ cell population from a patient

suffering from leukaemia was isolated. The CD34⁺/CD38⁻ markers were selected as these represent immature hematopoietic cells, i.e. CD34⁺ is expressed by pluripotent bone marrow cells whereas CD38⁺ is a marker of lineage commitment (Olweus et al, 1994). After transplantation of these CD34⁺/CD38⁻ cells into SCID immunodeficient mice the proliferation of human acute myeloid leukaemia (AML) cells was observed in the recipient mice (Lapidot et al, 1994). On the contrary, CD34⁻/CD38⁻ cells failed to show the same rate of AML disease formation. This result clearly showed the tumorigenic potential of the CD34⁺/CD38⁻ cells and identified these cells as TICs (Lapidot et al, 1994). Despite the advantages of identifying TICs by CD surface markers expression it is may cause difficulties to do this in solid tumours where enzymatic cell disaggregation needed to produce a single cell population may lead to the destruction of surface proteins and loss of CD antigenes.

The other prominent approach to identify tumour initiating cells *in vitro* was also established from haematological research and was published in 1996 (Goodell et al, 1996). It was discovered during their experiments with bone marrow cells that a small subpopulation of cells treated with the vital dye Hoechst 33342 had a low dye content and could be distinguished from the remaining cells that had high dye content by flow cytometry when excited with UV-light and simultaneously detected at two emission wavelengths (red and blue). This low-staining cell fraction was called side population (SP) cells (Goodell et al, 1996; Petriz, 2007). Further, the authors showed that the presence of the side population cells was related to their high activity of the multidrug resistant protein (Mdr), an ABC motive protein involved in pumping out xenobiotic compounds, including many cytostatic drugs and the DNA specific dye Hoechst 33343. Thus, the assay for the cells was based on the property of normal stem cells to over-express Mdr ATP-binding cassette (ABC) transporters (such as Mdr /ABCG2) which lead to their active export of xenobiotic compounds from the cell, and to resistance to cytotoxic agents. The vital dye Hoechst 33342 binds to DNA in living cells and when bound to the DNA can be easily detected. In case the Hoechst 33342 is pumped out of the cell it does not bind to DNA and actually leads to a reduction of the blue wavelength emission as well as a reduction of red wavelength emission, resulting in a specific cytometric profile (Figure 2). The identified side population cells were shown to be significantly enriched for haematopoietic stem cells in competitive repopulation and long-term multilineage contribution experiments in lethally irradiated recipient mice (Goodell et al, 1996).

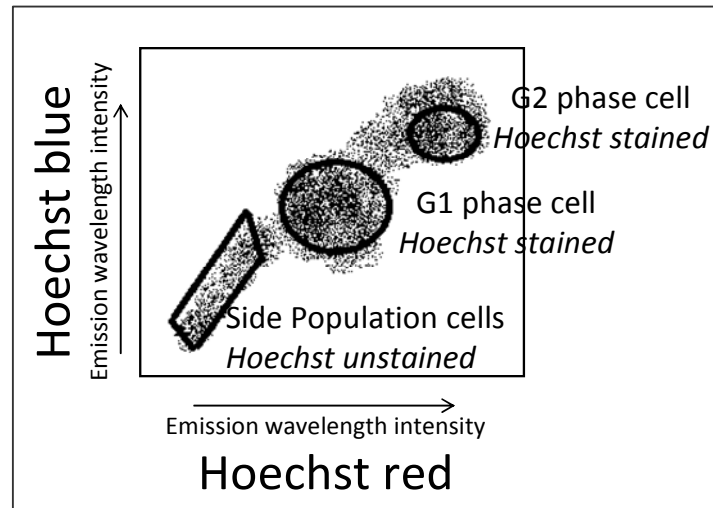


Figure 2: Schematic appearance of the side population fraction on flow cytometry. On the scheme are present G1 and G2 positive stained cell populations showing difference in DNA content. The side population of unstained population is on the side of the G1 cell population in the low dye content area. The scheme is interpreted from original protocol (Petritz, 2007).

After the methods described above had been discovered for haematopoietic tumour stem cells their potential was further extended for tumours of other origins. Side population cells possessing TICs properties were found in breast cancer, lung cancer, melanoma, and ovarian cancer (Alvi et al, 2003; Hsu et al, 2011; Hu et al, 2010; Mo et al, 2011).

In human colon cancer, Ricci-Vitiani identified the human colon tumour initiating cells as a $CD133^+$ subpopulation which initiated tumours in SCID-xenografts to a much higher degree when compared to the $CD133^-$ cell population (Ricci-Vitiani et al, 2007). In another tumour of epithelial origin, human breast carcinomas, a subpopulation of cells that were simultaneously $CD24^-$ and $CD44^+$ was shown in serial transplantation experiments to be enriched for tumour initiating cells (Phillips et al, 2006). In contrast, no tumours were induced by $CD24^+/CD44^+$ cells (Phillips et al, 2006). Tumour initiating cells were also found in the subset of $CD133^+$ cells in prostate adenocarcinomas, in the $CD24^-/CD44^+$ cell fraction in oesophageal cancer, and in the $CD133^+$ cells in lung cancer which possessed spherical growth and self-renewal potential (Bütöf et al; Tirino et al, 2008; Visvader & Lindeman, 2008). In contrast to the colon cancer studied by Ricci-Vitiani, $CD133^+$ human colorectal carcinoma cells did not show tumour initiating properties (Dittfeld et al, 2010). In glioblastoma the side population as well as $CD133^+$ marker were also shown to be able to identify tumour cells with tumour initiating cells properties (Bao et al, 2006; Fukaya et al, 2010).

In osteosarcoma and other tumours of mesenchymal origin, the usefulness of CD surface markers is doubtful. Mesenchymal normal stem cells can differentiate into multiple cell types including fibroblasts, chondrocytes, adipocytes, osteoblast (Jiang et al, 2002). Thus,

any of these cells may be produced in mesenchymal tumours, leading to a very inhomogeneous tumour content (Pautke et al, 2004). Moreover, the hierarchical organization in mesenchymal tissues is not well defined and no specific mesenchymal stem cell markers had been identified so far (Pevsner-Fischer et al, 2011). Nevertheless, in few studies on human osteosarcoma the CD133⁺ cell population was proposed to be specifically enriched in tumour initiating cells (Bütöf et al; Tirino et al, 2008; Visvader & Lindeman, 2008).

1.6.2. Genetic markers of stemness

Whereas cell surface markers are valuable tools to identify stem cells, they contribute little to the functional understanding of the pathways that regulate stem cell proliferation or fate. For this purpose, expressed genes such as transcription factors, cell cycle regulators or signalling proteins are of great interest.

In early embryogenesis stem cells pluripotency is maintained by a panel of “core transcription factors” such as Sox2, Oct3/4 and Nanog (Rodda et al, 2005).

Sox2 (sex determining region Y-box 2), a member of the Sox family of transcription factors (Seo et al, 2011), is expressed in the inner cell mass during embryonic development as well as being required later for the regulation of neural tissues development (Seo et al, 2011). Sox2 forms a trimeric complex with another transcription factor Oct3/4 in embryonic stem cells. Oct3/4 is a homeodomain transcription factor of the POU family (Boyer et al, 2005). Oct3/4 in conjugation with another “core transcription factor” Nanog is required in embryonic stem cells for the stable maintenance of pluripotency and is found only in the stem cell-rich inner cell mass (Boyer et al, 2005). In mesenchymal stem cells, as well as in embryonic stem cells, the Klf4 (Kruppel-like factor 4) transcription factor was found to indicate stem-like properties (Saulnier et al, 2011).

In vitro experiments have shown that forced expression of Sox2 and Oct3/4, in combination with Klf4 and c-myc, induces the reprogramming of adult fibroblast cells into cells with properties resembling pluripotent stem cells, creating the “induced pluripotent stem cells” (Takahashi & Yamanaka, 2006). The study of tumour initiating cells revealed that these transcription factors may have a function similar to that in normal stem cells. Thus, the genetic markers that are responsible for pluripotency in embryonic and multipotency in normal stem cells (Boyer et al, 2005) may be also important markers for maintenance of the tumour initiating cells.

In epithelial tumours such as ovarian cancer, colorectal cancer, breast cancer over-expression of Oct3/4, Nanog and Klf4 corresponds to the cells possessing tumour initiating cell properties (Gao et al, 2009).

For neural stem cells during central nervous system (CNS) development the presence of the protein marker Nestin was identified (Bauer et al, 2006). Nestin is an intermediate filament protein that is expressed not only during the early stages of development in the central nervous system (CNS), but also in the peripheral nervous system (PNS), as well as in pancreatic island precursor cells, myogenic cells and pluripotent progenitor cells capable to multilineage development (Bauer et al, 2006).

Over-expression of Sox2 was shown to maintain the self-renewal of osteosarcoma cells and leading to sarcosphere formation i.e. ability of cells to grow in non-attached 3-D clusters in growth medium under serum-free conditions, mimicking tumour growth (Basu-Roy et al, 2012b).

A recent study (Veselska et al, 2008) showed that the expression of Nestin in human primary osteosarcomas was correlated with CD133⁺ expression thereby occurring in cells with stem-like properties.

The other transcriptional regulator suggested to play a role in tumour initiating cells is Bmi1. This is a member of the polycomb family and was shown to be involved in the self-renewal of epithelial tumours such as hepatocellular carcinoma (Chiba et al, 2008). Recently, it was described that Bmi1 over-expression can inactivate the p53 gene through p14/ARF silencing leading to the reprogramming of terminally differentiated cells. (Spike & Wahl, 2011)

The network of regulation between stemness genes is shown in Figure 3. The network shows a strong interaction between the different embryonic transcription factors, suggesting the complexity of stem cell stemness regulation.

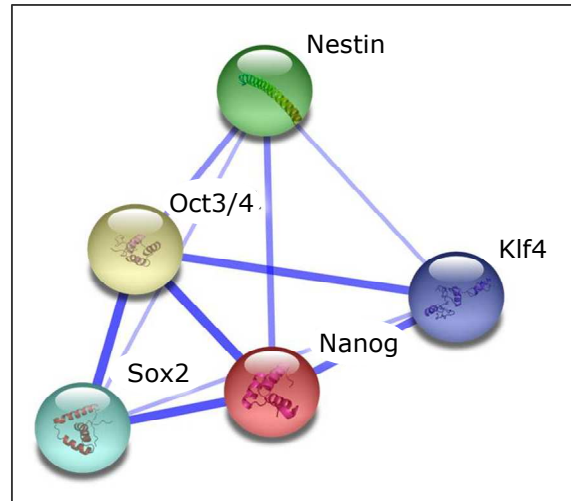


Figure 3: Network connections of transcription factors Nanog, Oct3/4, Sox2, Nestin and Klf4 involved in the self-renewal regulation of tumour initiating cells. The connections between transcription factors are shown by lines, the stronger the associations, the thicker the lines. (Generated with String 9.02 on-line proteomics tool).

1.7. The molecular characterisation of side population cells as potential tumour initiating cells

Side population (SP) cells (see 1.5.1.) were shown to express markers or stemness genes and induce tumours upon *in vivo* serial transplantation compared to the SP-depleted main population cells in tumours of mesenchymal origin, including osteosarcoma, chondrosarcoma and synovial sarcoma (Wu et al, 2007). Yang showed that the proportion of side population cells in primary human osteosarcoma cells varied between 4-10% (Yang et al, 2011). The side population cells had high tumorigenicity in *in vivo* limiting dilution transplantation experiment. The TD₅₀ for the side population cells isolated from primary human osteosarcoma was found to average around 1000 cells whereas for the SP-depleted main population cells the TD₅₀ was 50.000 cells (Yang et al, 2011). The side population cells with characteristics of TICs over-expressed Nanog and Oct3/4 stemness markers compared to the SP-depleted main population cells (Yang et al, 2011).

The side population cells identified in primary human ovarian cancer ascites cells expressed Oct3/4 stem cells markers and, after injecting under the kidney capsule in SCID mice, induced tumours whereas the SP-depleted main population cells did not (Hu et al, 2010).

The side population cells isolated from a human glioblastoma cell line were shown to induce tumours *in vivo* as well as to form spheres *in vitro* (Fukaya et al, 2010). The side

population cells were shown to express Nestin and differentiate into astrocytes and oligodendrocytes, and thus possess TICs-like properties (Fukaya et al, 2010).

To formally prove that side population cells are indeed functionally tumour initiating cells it would require a standard quantitative transplantation assay *in vivo* (Hewitt, 1953; Hewitt, 1958; Kallman et al, 1967). This method is very time consuming and expensive as it requires large numbers of recipient animals. One possible option would be to change from *in vivo* quantitative transplantation to an *in vitro* colony forming assay using the limiting dilution technique in 96 well plates (Traycoff et al, 1995). This method uses the principle of quantitative transplantation but the cell dilutions are put into 96 wells instead of being injected into animals, and clonal growth is observed in individual wells instead of tumour formation in mice.

1.8. The radioresistance of tumour initiating cells

There is no doubt that to achieve local tumour control after irradiation all tumour initiating cells (TICs) have to be sterilised. If only one tumour initiating cell is left after treatment a recurrence may occur (Baumann et al, 2009). It has been argued that tumour initiating cells are inherently more radioresistant, or due to their hypoxic niche may develop resistance and thus survive radiation therapy and regrow the tumour (Bütöf et al).

The response of tumour initiating cells to current cancer treatments has been investigated in many studies. It was shown that in different tumour types the tumour initiating cells show pronounced resistance to common chemotherapeutic agents compared to differentiated non-TICs (Gong et al, 2010; Hsu et al, 2011; Hu et al, 2010; Yang et al, 2011). This is probably due to the potential over-expression of ABC transporter proteins and/or detoxification enzymes (Chuthapisith, 2011). The resistance of the side population cells, i.e. potential TICs cells (section 1.7), to cisplatin chemotherapeutic compounds was shown in primary human ovarian cancer (Hu et al, 2010). In lung cancer cell lines it was shown that tumour initiating cells express stemness markers and were resistant to cisplatin treatment (Hsu et al, 2011). The side population cells isolated from primary osteosarcoma tumour also showed greater resistance to doxorubicin than SP-depleted main population cells (Yang et al, 2011).

Conflicting results are reported from studies investigating the response of tumour initiating cells to radiation (Brunner et al, 2012; Bütöf et al; Woodward & Bristow, 2009). It even was suggested that tumour initiating cells are generally more radioresistant than the non

tumourigenic majority of the tumour cells (Bao et al, 2006). Bütof described in a review the evidence for the poor survival of glioblastoma patients treated with radiotherapy if tumour cells expressed specific surface markers such as CD133⁺, in oesophageal carcinoma CD24⁻/CD44⁺, or in colorectal cancer CD133⁺ (Bütof et al; Visvader & Lindeman, 2008). A study on clonogenic survival after irradiation of cells derived from mammospheres formed from CD24⁻/CD44⁺ sorted TICs cells showed that the cells derived from mammospheres were more radioresistant compared to unselected cells derived from monolayer cultures (Phillips et al, 2006). However, in this study the radiosensitivity of tumour initiating cells was compared to the unsorted adherent cells that also contained tumour initiating cells at a lower percentage. This could mean that the difference in radiosensitivity was determined by the fraction of tumour initiating cells diluted in non tumour initiating cells rather than by their inherent radioresistance (Phillips et al, 2006). In a glioblastoma study it was speculated that CD133⁺ cells were more radioresistant than CD133⁻ cells due to higher radiation induced apoptosis of CD133⁻ cells. However, no evidence for a difference of the unlimited proliferative potential as the defining property of tumour initiating cells was investigated (Bao et al, 2006). Smit showed that CD24⁻/CD44⁺ tumour initiating cells derived from esophageal cancers were more resistant to irradiation than CD24⁺ and unsorted cell populations (Smit et al, 2013). In this experiment cell populations isolated from primary tumours by FACs sorting were recovered overnight, irradiated, and replated for assay of their clonogenic survival (Smit et al, 2013).

In contrast to the above, an *in vitro* study on a colorectal cancer cell line showed that CD133⁺ cells did not differ in radioresistance from CD133⁻ cells using the classical clonogenic survival assay for radiation doses up to 12Gy (Dittfeld et al, 2010).

Figure 4 shows a sketch by Berry (1961) which demonstrates how the TD₅₀ value of mouse lymphoma cells increases if cells were previously exposed to X-ray's, indicating that radiation inactivated tumour initiating cells.

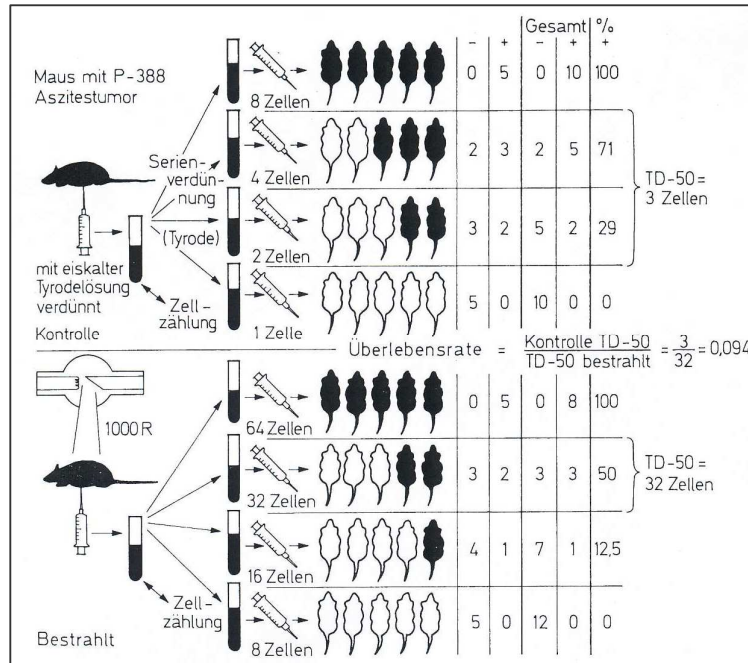


Figure 4: Results of the TD₅₀ quantification in *in vivo* transplantation of mouse lymphoma cells with and without radiation. TD₅₀ for control animals is found as 3 cells whereas the TD₅₀ for irradiated cells was 32 cells. This result is indicating inactivation of 90% of TICs by radiation, the survival fraction is 10% (Berry & Andrews, 1961).

From the clinical experience of radiation oncology we know that the radiation doses required for local control increases with increasing tumour volume (Halperin E.C. et al, 2008). This is also in line with the results of *in vivo* quantitative transplantation of 12 different tumours defined as mammary carcinoma, sarcoma and fibrosarcoma that show an inverse correlation between the logarithm of TD₅₀ values and the radiation dose required to control respective tumour TCD₅₀, i.e. dose of radiation required to achieve the local control in 50% of induced tumours (Figure 5) (Hill & Milas, 1989). This means, as fewer cells are required to induce a tumour in 50% of recipient mice, i.e. containing a larger proportion of tumour initiating cells, a higher dose is required to eliminate all tumour initiating cells and control that tumour (TCD₅₀) (Figure 5). These findings suggest that the proportion of tumour initiating cells is a very important determinant of tumour radioresistance.

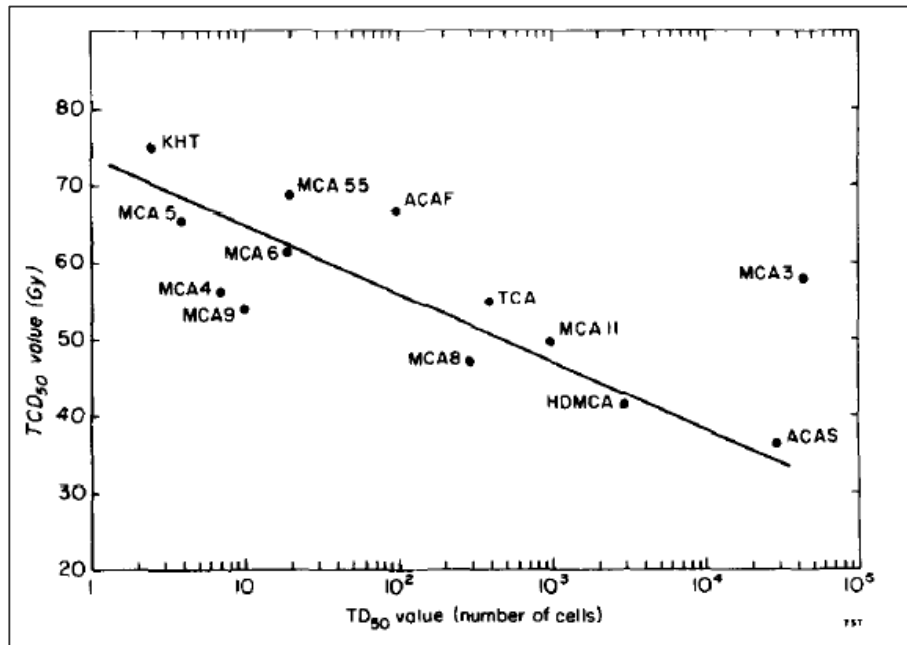


Figure 5: TCD₅₀ (Gy) values plotted against TD₅₀ values for 12 different tumours including mammary carcinomas (MCA 3-6, 8, 9, 11, 55), fibrosarcoma (KHT) and adenoacanthomas (ACAS-F). Significant negative correlation was shown between tumour local control dose (LDT₅₀) and log number of unirradiated cells required to initiate tumour *in vivo* in 50% of inoculation sites (TD₅₀) (Hill & Milas, 1989).

1.9. Clonogenic survival and DNA damage as the most important criterium of tumour radiosensitivity

Determination of tumour cell radiosensitivity *in vitro* has been correlated with tumour radiosensitivity (Deacon et al, 1984). Loss of proliferative ability after irradiation or any other cytotoxic treatment leads to the so called reproductive death (Hall, 2012). Such cells may still express their normal cell function or may differentiate in a normal way, they may even undergo a few cell divisions but they do not exhibit long term reproductive potential. The cells that survive radiation treatment and are able to proliferate indefinitely to repopulate a tumour *in vivo* and give rise to tumour relapse and metastasis or to form a cell colony *in vitro* (more than 50 cells) are defined as clonogenic cells (Hall, 2012). In 1956 the description of a new method of investigating unlimited proliferative potential *in vitro*, by studying the cell colony forming capacity of human cancer cells after irradiation in cell culture, was published by Puck and Marcus (Puck & Marcus, 1956). The authors produced the first radiation survival curve for HeLa cells after irradiation, and showed that HeLa cells were much more radiosensitive than previously assumed. Since then, the clonogenic survival assay or colony formation assay has been widely used in radiobiological studies as the “gold standard” for

cellular sensitivity testing, as it incorporates multiple modes of cell death as well as delayed growth arrest in the phenotype tested (Hall, 2012). The loss of clonogenic potential as a function of radiation dose is traditionally described by a cell survival curve plotted on a log-linear scale (log surviving fraction versus linear dose). Nowadays, the mathematical method of fitting the dose dependence of cell survival i.e. ability to form a colony is the linear-quadratic model that assumes two radiation hits are required for cell lethality. In this model the α component of the equation represents clonogenic cell inactivation in a linear manner by one lethal event per cell, and its probability of occurrence is proportional to the dose. The quadratic β component of cell death is induced by two sublethal events and therefore its probability is proportional to the square of the dose. Based on the linear-quadratic model the surviving fraction (S) is a function of a dose expressed with a following formula: $S = e^{(-\alpha D - \beta D^2)}$ (Hall, 2012).

During the last decades the clonogenic assay to determine survival of cells after radiation was developed not only for adherent colony forming cultures but also for cells suspended in semi-solid or viscous medium that show anchorage-independent growth (Franken et al, 2006). The clonogenic assay can be applied for cells from both normal tissue and from tumours. The clonogenic assay is widely used in a variety of studies with different types of cells not only to determine radiation sensitivity but also to determine sensitivity to chemotherapeutic drugs. One disadvantage of the clonogenic assay is that not all tumour cells with diffuse growth have a capacity to grow to form colonies. To overcome this problem, a method was developed to determine clonogenic survival after radiation using the limiting dilution technique in 96-well plates *in vitro* (Grenman et al, 1989). In an experiment the plating efficiency and clonogenic survival of squamous-cell carcinomas cell lines established directly from tumour tissues were compared in soft agar and in 96 well plates. The radiation clonogenic survival in agar was directly compared to the value obtained in 96 well plates and good correlation was found (Grenman et al, 1989).

DNA double strand breaks are considered to be the most critical lesions induced by radiation. Unrepaired damage of the chromatin structure can lead to severe consequences, such as cell death and insufficiently repaired may lead to loss of clonogenicity, deletions, mutations, genomic instability and malignant transformation.

The phosphorylation of histone H2AX at serine 139 (γ H2AX) is one of the earliest detectable reaction to DNA double strand breaks induced by ionising radiation (Rogakou et al, 1998). The site of DSBs recruits several additional proteins including the tumour suppressor p53-binding protein 1 (53BP1). Multiple copies of phosphorylated γ H2AX and

53BP1 co-localise around the point of a radiation-induced DNA double strand break forming a focus that can be detected by immunofluorescent reaction (Markova et al, 2007). Foci are detectable after irradiation and the amount of co-localised γ H2AX/53BP1 foci increases until it reaches a plateau 30 min after irradiation although this may vary between the cell lines. The number of nuclear γ H2AX/53BP1 foci increases with increasing dose of irradiation and decreases with time after irradiation due to repair of DNA double strand breaks (Markova et al, 2007). It is accepted that co-localised γ H2AX/53BP1 foci are a good indicator for radiation-induced DNA double strand breaks that increase detection specificity (Ward et al, 2003).

The mechanism of repair of DNA double strand breaks was reported to be biphasic with both a fast and a slow component (Iliakis et al, 2004). Two main pathways contribute to the repair of double strand breaks, non-homologous end-joining (NHEJ) and homologous recombination (HR). NHEJ is an error prone pathway that proceeds without a template and acts in all phases of cell cycle. HR is an error free pathway that requires a second undamaged homologous sequence as a template and therefore acts only in S/G2 phase of cell cycle (Brandsma & Gent, 2012).

Radiation induced and residual DNA double strand breaks are considered to be predictive factors of cellular radiation sensitivity. Some investigations have shown that residual (non-repaired) DNA double strand breaks indicate lethal chromatin damage and thus loss of clonogenic potential (Banath et al, 2010; Dikomey et al, 1998; Menegakis et al, 2009). On the contrary, other studies show a correlation between residual DNA double strand breaks and radiosensitivity in normal human cells but no correlation amongst different tumour cell lines (Yoshikawa et al, 2009), suggesting additional pathways after repair are inactivated in tumour cells. A candidate is p53, when mutated this may inhibit apoptosis, allowing non-repaired cells to divide.

1.10. Hypothesis:

The recurrence rate of osteosarcoma is high compared to the other childhood tumours, regardless of improvements in chemotherapy treatment strategy. There is increasing evidence for the existence of a small subset of tumour initiating cells (TICs), sharing some properties of normal stem cells in tumours. These cells are involved in chemotherapy resistance, repopulation of the tumour and giving rise to distant metastasis. However conflicting results have been published on the role of tumour initiating cells in the radiation response. There is no clear evidence whether these cells are inherently radioresistant or whether other factors influence their radiation response. **Thus, in the present study we hypothesise that the radiosensitivity of mouse osteosarcoma cell lines is determined by the inherent radioresistance of tumour initiating cells.**

To test this hypothesis we aim to:

- 1). Identify tumour initiating cells (TICs) in mouse osteosarcoma (MOS) cell lines and determine the TICs fraction in different MOS cell lines
- 2). Characterize the phenotypic characteristics of these potential tumour initiating cells
- 3). Measure the intrinsic radiosensitivity of tumour initiating cells from mouse osteosarcoma cell lines

II Materials

2.1. Equipment

Alpha Innotech ChemiImager System, Biozym, Hessisch Oldendorf, Germany
Cell counter, Beckman Coulter, Fullerton, USA
Cell scraper, Sarstedt. Inc. Newton, USA
Centrifuge Biofuge fresco, Heraeus Instruments, Osterode, Germany
Centrifuge Biofuge pico, Heraeus Instruments, Osterode, Germany
Centrifuge Eppendorf 5415R, Eppendorf, Hamburg, Germany
Centrifuge Fisherbrand Mini, Fisher Scientific, Schwerte, Germany
Centrifuge Rotanta 460R, Andreas Hettich, Tuttlingen, Germany
Centrifuge Rotina 420R, Andreas Hettich, Tuttlingen, Germany
Centrifuge Varifuge 3.0R, Heraeus Instruments, Osterode, Germany
Cs137 HWM-D 2000 machine, Wälischmiller Engineering, Markdorf, Germany
Dispenser Multipipette® plus, Eppendorf, Hamburg, Germany
Electrophoresis Cell, X-cell sure lock, Western blot system, Invitrogen, Darmstadt, Germany
Electrophoresis Gel system, Horizontal Midi Gels, PEQLAB, Erlangen, Germany
Electrophoresis Power Pac Basic, Bio-Rad Laboratories, Munich, Germany
Electrophoresis Transfer Blot, Bio-Rad Laboratories, Munich, Germany
Freezer -180 °, The Air Liquide, Dusseldorf, Germany
Freezer -20°C , Liebherr, Ehingen(Donau), Germany
Freezer -80 °C, New Brunswick, Nürtingen, Germany
Heating block, Thermomixer comfort 1.5 ml, Eppendorf, Hamburg, Germany
Heating block, Thermomixer comfort 2ml, Eppendorf, Hamburg, Germany
Incubator for bacterial plates, Kendro Products Laboratory, Hanau, Germany
Incubator, Sanyo, Bad Nenndorf, Germany
Isovolt 340, X-ray cabinet, 230kV, GE, Ahrensburg, Germany
LSR II flow cytometer BD, San Jose, CA, USA
Magnet plate, NeoLab, Heidelberg, Germany
Magnets stirrer, NeoLab, Heidelberg, Germany
Microscope Axioplan 2, Carl Zeiss, Jena, Germany
Microscope Axiovert 135, Carl Zeiss, Jena, Germany
Microscope KEYENCE BZ-9000 series, Keyence, Frankfurt, Germany
Microwave Privileg 1034HGD, Otto, Hamburg, Germany

MoFlow cell sorter, Dako Cytomation, Carpinteria, USA
Mr. Frosty freezing container, Thermo scientific, Darmstadt, Germany
Multiple plate reader, TECAN Infinity M200, Tecan, Crailsheim, Germany
pH meter, Schott instruments, Mainz, Germany
Pipettes 10, 20, 100, 200, 1000 μ l, Eppendorf, Hamburg, Germany
Power supply, Model 200/2.0 Bio-Rad Laboratories, Munich, Germany
Shaker Incubator for bacterial cultures, Innova 4430, New Brunswick Scientific, Edison, USA
Shaker, GFL, Segnitz, Germany
Sonicator B12, Branson, Ultrasonic, Danbury, USA
SpeedVac Concentrator, Univapo 100H, UniEquip, München, Germany
StepOne, Applied Biosystems, Darmstadt, Germany
Sterile laminar flow work bench, BDK Luft und Reinraumtechnik, Sonnenbühl-Genkingen, Germany
Vacuum Concentrator plus, Eppendorf, Hamburg, Germany
Vortexer, Heidolph Instruments, Schwabach, Germany
Water Bath, GFL, Segnitz, Germany

2.2. *Consumables*

Blotting paper, Biometra, Gottingen, Germany
Cell culture dishes, 10cm, Nunc, Rhein, Germany
Cell culture flasks T125, T75, T25, Nunc, Rhein, Germany
Cell Culture plates multi – wells, Falcon Blue Max BD Biosciences, Heidelberg, Germany
Combs, PEQLAB, Erlangen, Germany
Cover slips, VWR, Darmstadt, Germany
Cryogenic vials, VWR, Darmstadt, Germany
Gel cassettes 1.5 mm Invitrogen, Darmstadt, Germany
Glass slides SuperFrost® 76 x 26 mm, Carl Roth, Karlsruhe, Germany
Membrane Western Amersham™ 0,45 μ m Hybond™ GE Healthcare, Munich, Germany
Needles, single use Ø 0.60, 0.90mm, Sterican®, B.Braun, Melsungen, Germany
Optical Adhesive Film, MicroAmp , RQ-PCR, Applied Biosystems, Darmstadt, Germany
Parafilm® Carl Roth, Karlsruhe, Germany
PCR plate 96-well, AB gene, Rhein, Germany
Pipette tips Graduated Filter Tips, TipOne Starlab, Ahrensburg, Germany
Reaction tubes 1.5 ml, 2.0ml, Eppendorf, Hamburg, Germany
Reaction tubes 15ml, 50ml, Falcon Blue Max BD Biosciences, Heidelberg, Germany

Syringe filter sterile, 0.2µm cellulose acetate membrane, VWR, Darmstadt, Germany
Syringe, single-use 1ml (50ml) Henke-Sass-Wolf, Tuttlingen, Germany
Tube with Cell Strainer Cap, 35µm Nylon mesh filter, Falcon Blue Max BD Biosciences, Heidelberg, Germany

2.3. *Molecular weight standards*

DNA ladder 1 Kb Plus, Life Technologies, Carlsbad, California, U.S
DNA molecular weight marker VIII, Roche, Mannheim, Germany
Prestained Protein-Marker V, Peqlab, Erlangen, Germany

2.4. *Reagents and chemicals*

5x First Strand Buffer, Invitrogen, Darmstadt, Germany
Agarose LE for gel electrophoresis, Biozym, Hessisch Oldendorf, Germany
Albumin from bovine serum (BSA), Sigma-Aldrich, Steinheim, Germany
Ampicillin, Sigma, Steinheim, Germany
Ampuwa® water, Fresenius, Germany
APS (Ammonium persulfate), Sigma-Aldrich, Steinheim, Germany
Bacto Trypton, BD, Pont de Claix, France
Bacto Yeast extract, BD, Pont de Claix, France
Bis-acrylamide ProtoGel 30 % (w/v), National diagnostics, Atlanta, USA
Boric Acid, Merck, Darmstadt, Germany
DMEM 1g/l Glucose, Gibco/Invitrogen, Karlsruhe, Germany
DMSO (Dimethylsulfoxid), Sigma-Aldrich, Steinheim, Germany
EDTA (Ethylenediaminetetraacetic acid), Sigma-Aldrich, Steinheim, Germany
Ethanol, Merck, Darmstadt, Germany
EtBr (Ethidium bromide), Merck, Darmstadt, Germany
Fetal Calf Serum Gold (FCS), PAA Laboratories GmbH, Cölbe, Germany
Glycerol, Applichem, Darmstadt, Germany
Glycin, Merck, Darmstadt, Germany
HCl, 1 mol/l (1 N), Merck, Darmstadt, Germany
Hoechst 33342, Merck, Darmstadt, Germany
Isoflurane CP, Pharma, Germany
Isopropanol, Merck, Darmstadt, Germany

Loading DNA dye 6x, Fermentas, Thermo scientific, Darmstadt, Germany
Low fat Milk, Cycofin, Zeven, Germany
Methanol, Merck, Darmstadt, Germany
NaAc, Applichem, Darmstadt, Germany
NaCl, Applichem, Darmstadt, Germany
NaOH, Applichem, Darmstadt, Germany
OligodT primers, Invitrogen, Darmstadt, Germany
Opti-MEM medium, Gibco Darmstadt, Germany
Paraformaldehyde, Merck, Darmstadt, Germany
PBS (Phosphate buffered saline), Invitrogen, Darmstadt, Germany
Ponceau, Sigma-Aldrich, Steinheim, Germany
Protease inhibitor cocktail tablets, Roche Diagnostics, Mannheim, Germany
Puromycin, CalBiochem, Darmstadt, Germany
Random primers, Promega. Mannheim, Germany
Reverse transcriptase SuperScript® II, Invitrogen, Darmstadt, Germany
RIPA (Radioimmunoprecipitation assay) buffer, Thermo Scientific, Rhein, Germany
RNase OUT, Invitrogen, Darmstadt, Germany
Running buffer 10X SDS-PAGE, Rotiphorese, Carl Roth, Karlsruhe, Germany
SDS (Sodium dodecyl sulphate)10 % (w/v) solution, Bio-Rad Laboratories, Munich, Germany
Stripping buffer, Thermo Scientific, Rhein, Germany
SYBR Green Master Mix 2x, Applied Biosystems, Darmstadt, Germany
TEMED (Tetramethylethylenediamine), Applichem, Darmstadt, Germany
Tris, Applichem, Darmstadt, Germany
Trypsin, Invitrogen, Darmstadt, Germany
Tween 20, Sigma-Aldrich, Steinheim, Germany
Vectashield, Linaris, Wertheim, Germany
Verapamil, Sigma-Aldrich, Steinheim, Germany
 β -mercaptoethanol, Sigma-Aldrich, Steinheim, Germany

2.5. *Commercially available kits*

BCA Protein Assay, Pierce®, Rhein, Germany
Chemiluminescent Detection Reagents, GE Healthcare Life Sciences ECL Plus western blotting, Munich, Germany
Lipofectamin 2000, Life Technology, Invitrogen, Darmstadt, Germany

MTT, Roche Diagnostics, Mannheim, Germany

RNeasy Plus Micro Kit, Qiagen, Hilden, Germany

2.6. *Antibodies*

Antibody	Dilution
53BP1, polyclonal, rabbit, NB 100-305, Novus Biological, CO, USA	1:500
Alexxa488 anti rabbit, Lot. 659082, Invitrogen, Oregon, USA	1:1000
Anti mouse IgG, HRP conjugated, CalBiochem, Darmstadt, Germany	1:5000
Anti rabbit IgG, HRP conjugated, CalBiochem, Darmstadt, Germany	1:5000
Bmi1, monoclonal, mouse, NG1923488, Millipore, Schwalbach, Deutschland	1:500
Cy3 anti mouse, No. 515-165-003, Jackson Immunoresearch, West Grove, USA	1:1000
p53(FL-393), polyclonal, rabbit, Lot. D2705, Santa Cruz, Heidelberg, Germany	1:1000
Sox2, monoclonal, rabbit, No. 3579, Cell Signaling technology, Frankfurt am Main, Germany	1:500
Tubulin, monoclonal, mouse, Lot. T 5168, Sigma-Aldrich, Steinheim, Germany	1:60.000
γ H2AX, monoclonal, mouse, Lot. 2064512, Millipore, Schwalbach, Deutschland	1:1000

2.7. *Restriction enzyme*

ScaI, 20.000units/1ml, New England Biolabs, Frankfurt am Main, Germany

2.8. *Bacteria*

Top 10 E.Coli, Life Technology, Invitrogen, Darmstadt, Germany

2.9. *Plasmids and reference DNA*

Pooled mouse embryonic cDNA (kindly provided by Dr. M. Rosemann, Institute of Radiation Biology at Helmholtz Center Munich)

pCAG-tdTomato vector system (kind gift from Dr Ingo Burtscher, Institute of Stem Cells Research at Helmholtz Center Munich)

2.10. Established cell lines

HeLa (human epithelial cervix carcinoma), ATCC, Wesel, Germany

2.11. Buffers and solutions

<p>Laemmli buffer (50ml)</p> <p>20ml 10% SDS 5 ml β-mercaptoethanol 10ml Glycerol 10ml H₂O (Ampuwa) 5ml 1M Tris, pH 6.8 0.005g Bromphenol blue (0.01%)</p>
<p>Separating gel (15 %) for SDS-PAGE (10 ml)</p> <p>3.75ml 30 % (w/v) acrylamide/bis 2.5ml 1.5 M Tris (pH 8.8) 100μl 10% (w/v) SDS 3.6ml H₂O Ampuwa 50μl 10 % (w/v) APS 5μl TEMED</p>
<p>Stacking gel (4%) for SDS-PAGE (5ml)</p> <p>500μl 30 % (w/v) acrylamide/bis 1.26ml 0.5M Tris (pH 6.8) 50μl 10% (w/v) SDS 3.18ml H₂O (Ampuwa) 25μl 10% (w/v) APS 5μl TEMED</p>
<p>Western Blot Transfer buffer (10X)</p> <p>31.2g Tris base 144g Glycin pH 8.3</p>
<p>Western Blot Transfer buffer (1X)</p> <p>100ml 10x transfer buffer 20% (v/v) MeOH Up to 1000ml H₂O (Ampuwa)</p>

<p>T-TBS (10x)</p> <p>24.2g Trizma base 80g NaCl Dissolve in 1000ml H₂O (Ampuwa) pH adjustment to pH 7.6 + 10ml Tween 20</p>
<p>LB media (pH 7.5)</p> <p>10g Bacto-Tryptone 5g Yeast extract 10g NaCl</p>
<p>LB Agar (pH 7.0)</p> <p>10g Bacto-Tryptone 5g Yeast extract 10g NaCl 15g bacterial Agar</p>
<p>TBE buffer 5x (pH 8.3)</p> <p>89mM Tris 89 mM Boric Acid 2 mM EDTA</p>
<p>Western Blot: Blocking solution</p> <p>100 ml PBS 5g low fat Milk</p>
<p>Immunofluorescent reaction: Blocking solution</p> <p>100 ml PBS 1g BSA 0.15g Glycin</p>

III Methods

3.1. Establishment of Mouse Osteosarcoma (MOS) cell lines

The murine osteosarcoma (MOS) cell lines used for these studies were initially developed by Dr. M. Rosemann Helmholtz Zentrum Munich from bone tumours which arose in mice after the injection of a bone seeking α -emitter (Th^{227}). The primary osteosarcomas were dissected under sterile conditions, cut into pieces of $\sim 2\text{mm}$ \varnothing and placed into cell culture dishes with growth medium. During 14 days of incubation at 37°C and 5% CO_2 adherent cells started to grow out of the tumour fragments. Primary cultures were single cell cloned by limiting dilution in 96 well plates. Thirteen MOS cell lines were developed from 13 separate tumours (Figure 6). The MOS cell lines were shown to be tumorigenic by the formation of osteosarcoma tumour after the subcutaneous injection of MOS cell suspensions into syngenic mice. All of the developed tumours were histologically confirmed to be differentiated osteosarcomas.

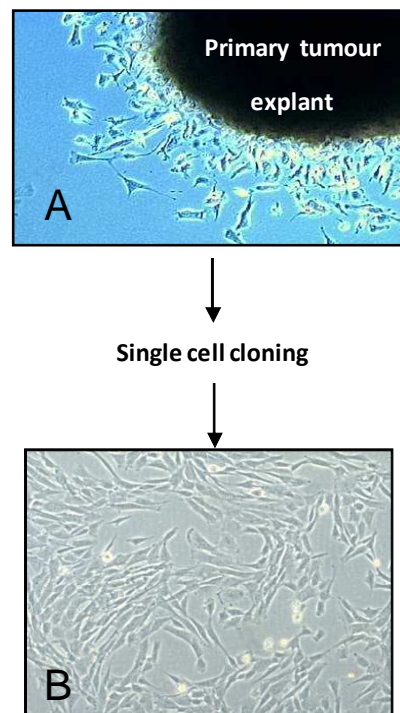


Figure 6: Development of MOS cell line. A: Primary tumour explant with outgrowing cells after 14 days in cell culture. B: Morphology of established single cell cloned MOS cell line grown in monolayer and imaged under phase-contrast at magnification 10x. The phenotype consists of polygonal elongated cells and fibroblast-like spindle cells.

3.2. *Growth inhibition of MOS cell lines after ionising irradiation*

Differences in the radiation response of the thirteen available MOS cell lines have been previously shown by radiation - induced growth inhibition experiments (Dr. M. Rosemann, Bahar Sanli-Bonazzi). Results are shown in Figure 7, with growth inhibition after 2Gy treatment relative to 0Gy control cells growth on the X-axis versus growth inhibition after 8Gy treatment relative to 0Gy control cells growth on the Y-axis. From thirteen cell lines tested two relatively radioresistant and two relatively radiosensitive were selected for the present study (Figure 7). The selection of these cells was based on the MOS cells growth inhibition after 2Gy i.e. the standard dose of radiation per fraction used in radiotherapy treatment. MOS-S-184 and MOS-S-1403 were defined as the relatively radiosensitive cell lines as the $D_{50\%}$, i.e. dose to inhibit growth of half of the irradiated cells, for these cells was found to be less than 2Gy (Figure 7). MOS-R-306 and MOS-R-1929 were selected as relatively radioresistant cells as no growth inhibition was observed after 2Gy (Figure 7). $D_{50\%}$ for MOS-R-306 was found to be more than 2Gy and less than 8Gy whereas $D_{50\%}$ for MOS-R-1929 was found to be more than 8Gy.

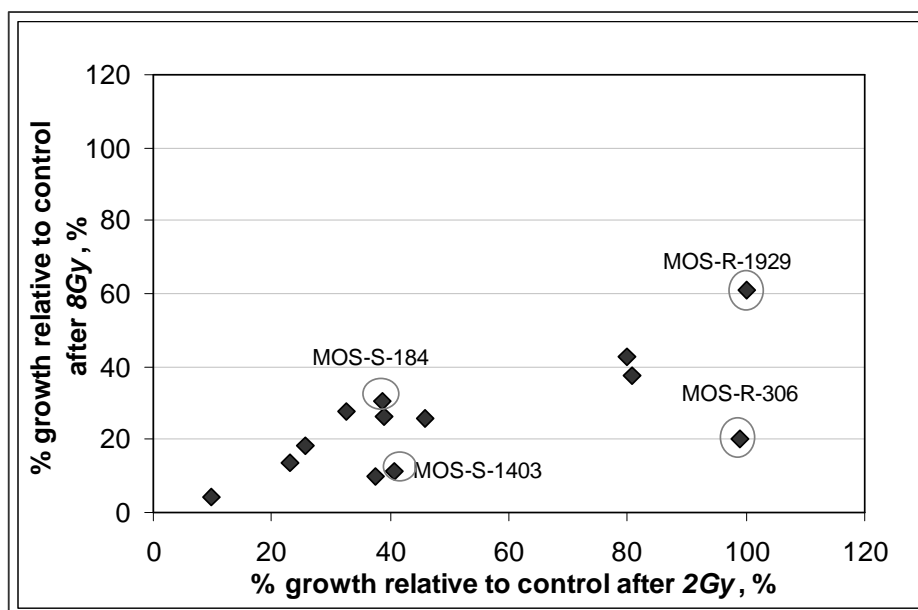


Figure 7: MOS cell lines growth inhibition after 2Gy and 8Gy of gamma irradiation. The percent of cell growth after 2Gy irradiation relative to 0Gy control cell growth is plotted on x-axis versus the percent of cell growth after 8Gy irradiation relative to 0Gy control cell growth plotted on y-axis. The four marked cell lines that were selected for the current investigation are shown. MOS-S-184 and MOS-S-1403 are relative radiosensitive as $D_{50\%}$ is less than 2Gy. MOS-R-306 and MOS-R-1929 are relatively radioresistant as $D_{50\%}$ is more than 2Gy. Data interpreted from the original data provided by Dr. M. Rosemann and B. Sanli-Bonazzi.

3.3. MOS cell line cultivation and liquid nitrogen freezing

The selected MOS cell lines were maintained in T75 cell culture flasks in Dulbecco's Modified Eagle Medium (DMEM) supplemented with 1g/l Glucose and 10% Fetal Calf Serum (growth medium) at 37°C and 5%CO₂. Upon reaching approximately 80% confluence the cells were passaged by subculture at a ratio of 1:3. For passaging, monolayers were washed with 5ml PBS and 1ml of 0.05% Trypsin- EDTA (1X) was added. Trypsin activity was stopped by adding 5ml of growth medium and cells were counted with a Coulter Counter, diluted and transferred into a new cell culture flask with fresh medium. For the study cell passage ranged from 10 to 16.

MOS cells were frozen down as a backup periodically. Cells at the exponential phase of growth (80% confluence) were washed with 5ml PBS, dissociated with 1ml 0.05% Trypsin-EDTA (1X) and the reaction stopped with 5ml growth medium. Cells were counted and the cell suspension was centrifuged at 1000rpm for 5 minutes. The cell pellet was resuspended to a concentration of 1×10^6 cells per 1ml in growth medium supplemented with 10% DMSO. The resuspended cells were transferred into cryogenic vial and stored at -80°C in a Mr.Frosty freezing container for 24h and than transferred to -177°C in liquid nitrogen for long term storage.

3.4. Irradiation of MOS cell lines

For all experiments that involved irradiation of cells the HWM-D 2000 Cs¹³⁷ γ -source was used. Irradiation facilities were provided by the Research Unit Medical Radiation Physics and Diagnostics at Helmholtz Zentrum Munich. The HWM-D 2000 contained Cs¹³⁷ with an activity of 2x74TBq (1983). Dose calibration i.e. air kerma rate on 30.04.13 was 0.49Gy per minute. It had a circular shielded irradiation chamber which is 10cm in height and 33cm in diameter. The time for irradiation was varied to provide the required dose. Cells were irradiated as adherent cell culture in flasks at room temperature. Control non-irradiated cells were simultaneously sham irradiated (0Gy) by placing cells outside the lead shielding of the irradiation chamber.

3.5. *Analysis and sorting of MOS side population cells*

The side population assay was used to identify the tumour initiating cells present in the cultured MOS cell lines.

3.5.1. *Hoechst 33342 staining*

One day prior to staining the MOS cells were passaged as described above. For the staining to avoid the loss of potentially loosely attached side population (SP) cells the growth medium was collected in 50ml Falcon tubes. The monolayer was washed with PBS, and the PBS also collected. Adherent cells were dissociated with 1ml 0.05% Trypsin-EDTA and the reaction was stopped and loose adherent cells recovered by adding the pooled medium plus the PBS wash solution. The cell number was counted with a Coulter Counter. Total number of cells was calculated by multiplying the volume of the cell suspension in ml by the number of cells counted per ml. Cells were centrifuged at 1000rpm for 5 minutes. The cell pellet was resuspended in fresh growth medium to achieve 1×10^6 cells per ml. The cell suspension was mixed gently. For the negative control half of the final cell suspension was separated into a fresh 50ml Falcon tube. An aqueous solution of Hoechst 33342 dye was added to both test and control at a concentration of $5 \mu\text{g}$ per 1 ml of cell suspension. The ABC inhibitor Verapamil was added to the negative control sample at a final concentration of $50 \mu\text{M}$ in order to provide a negative control with inactive efflux pump. The cells were incubated for 90 minutes at 37°C with one intermediate gentle cell agitation. After incubation the labelled cells were centrifuged at 1000rpm for 5 minutes at 4°C and resuspended in ice cold PBS to a concentration of 2×10^6 cells per ml. The cells were kept on ice prior to analysis. Directly before the analysis an aqueous solution of Propidium Iodine (PI) at a concentration of $2 \mu\text{g}$ per ml of cell suspension was added to identify dead cells. The FACS analysis of labelled cells was done within 1-2 hours after Hoechst 33342 staining. Immediately prior to the FACS analysis and sorting the cell suspensions were filtered through a sterile $32 \mu\text{m}$ Ø nylon mesh strainer to obtain a single cell suspension without clumped cells.

3.5.2. Flow cytometry analysis and Fluorescence Activated Cell Sorting (FACS)

To identify and/or sort the side population (SP) based on Hoechst 33342 uptake the Hoechst 33342 labelled cells were analysed using a MoFlow (collaboration with Dr. Joachim W. Ellwart, Cell sorter-Service, Institute of Molecular Immunology, Helmholtz Zentrum Munich). A total of at least 50.000 cells was analysed by side and forward scattering. The scheme for Hoechst 33342 labelled cell gating is shown in Figure 8. The Hoechst 33342 labelled cells were excited at 355nm (JDSU Xcyte, 355nm-100mW-100MHz, Nd:YAG UV Laser). The emission fluorescence of Hoechst 33342 was detected at 440/30nm (Hoechst33342-Blue) and 670/40nm (Hoechst33342-Red) filters. PI was excited at 488nm (Coherent Sapphire, 488nm-200mW, CDRH Laser) with the emission fluorescence detected at 610/20nm filter. The flow cytometry data were analysed with FlowJo and Winmdi version 2.8.

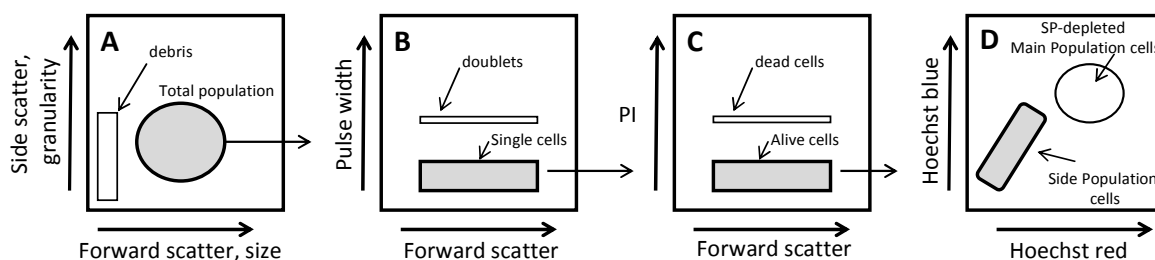


Figure 8: Scheme of Hoechst33342 labelled cells gating strategy. A: total cell population is defined by forward and side scattering, debris is gated out. B: Doublets are gated out as increased pulse width. C: Dead cells are gated out as PI positive stained cells. D: The side population is defined as a low Hoechst 33342 red/blue tailed population after gating out debris, doublets and dead cells.

3.5.3. Isolation of side population cells by Fluorescence Activated Cell Sorting (FACS)

During the FACS separation side population (SP) cells were collected into 2ml eppendorf tube which contained 0.5ml growth medium. Simultaneously with the collection of SP cells, equal number of the SP-depleted main population cells was collected into a separate 2ml eppendorf tube. Cell doublets, debris and dead cells were excluded by gating out (Figure 8). Figure 9 illustrates the FACS profile of MOS-R-1929 cells during cell sorting. The accuracy of the cell separation was measured by re-analysing the two sorted cell populations. After the

two fractions of cells were initially separated, an aliquot of each was run through the MoFlow again. Results of this are presented in section 4.1.3.

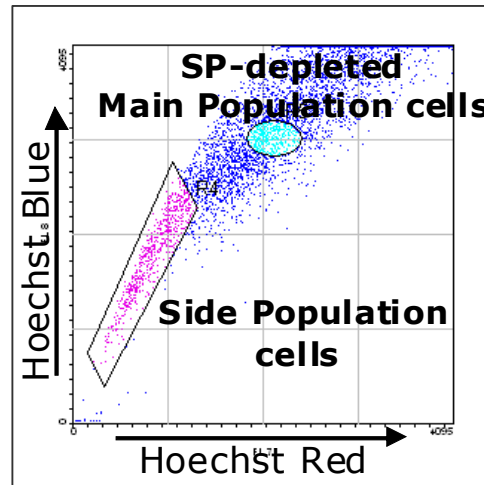


Figure 9: FACS profile of MOS-R-1929 cells. Dot plot represents the Hoechst 33342 stained population of MOS-R-1929 cells. Cells marked with polygon represent the side population cell fraction; whereas cells marked with ellipse represent the SP-depleted main population cell fraction. Vertical axis is the Hoechst blue fluorescence. Horizontal axis is the Hoechst red fluorescence.

3.6. Semi-quantitative RT-PCR analysis of target genes expression

The gene amplification was analysed by semi-quantitative RT-PCR reaction. The detection of specific amplicon production was based on the accumulation of SYBR green fluorescent dye bound to double stranded DNA during the semi-quantitative RT-PCR reaction. The difference in gene expression between samples was calculated by relative quantification using the $2^{-\Delta\Delta Ct}$ method (section 3.6.6.) (Livak & Schmittgen, 2001).

3.6.1. *Total RNA extraction*

Unsorted MOS cell lines or cultured SP and SP-depleted MP cell populations were collected at selected time points with a cell scraper. Cells were rinsed in 4°C PBS and centrifuged at 1000rpm for 5 minutes. The pellet was either kept on ice or frozen down at -20°C for later extraction. RNA was extracted using the RNeasy plus micro kit following the manufacture's protocol. Cell pellets were lysed in 350µl lysis buffer contained 1% β-Mercaptoethanol to prevent oxidation. To shear genomic DNA the lysate was pipetted up and down several times using a 1000µl pipett tip. To eliminate genomic DNA (gDNA) the cell lysate was run through

a gDNA elimination column and the RNA-containing flow through was precipitated with 70% ethanol. RNA was bound to the RNeasy minElute Spin Column matrix and was washed according to the manufacture's protocol and RNA was eluted with 15µl of elute buffer. Total RNA extract was stored at -20°C for short-term and at -80°C for longer storage. RNase free tubes and solutions provided with the kit were used.

3.6.2. *Quantification of nucleic acids*

RNA yield and purity were determined by UV-spectrophotometer measurement with the TECAN microplate reader using the DNA/RNA nanoquant plate. The absorption of nucleic acid at OD260 and of proteins at OD280 was recorded for each sample. An OD260 absorption equal to 1 is correlated to a concentration of approximately 40µg RNA per ml, or 50µg DNA per ml. The ratio A260/280 was determined since this ratio allows the estimation of nucleic acid purity. The A260/280 ratio for a pure RNA samples is about 2.0 whereas the A260/280 ratio for a pure DNA sample is about 1.8.

3.6.3. *cDNA synthesis (Reverse transcription) of total RNA*

To perform the semi-quantitative RT-PCR we used 1 µg of total RNA from each sample for reverse transcription (RT) into cDNA. The reaction was performed in a 20µl final volume. 1µg of RNA was adjusted to an 8µl volume with RNase free water (Ampuwa). Then 1.5µl of OligodT and 1.5µl of Random Primers were added (Table 1) and incubated for 2 minutes at 70°C, followed by incubation at room temperature for 10 minutes. Then 9 µl of the reverse transcription mix (Table 2) was added to the RNA template and the RT primers mix and incubated at 42°C for 1 hour, followed by a 5 minute denaturation at 95°C.

<i>Table 1: RNA template and RT primers reaction (1 reaction)</i>	
1 µg RNA dilution in 8 µl Ampuwa	8 µl
Random Primers (500µg/ml)	1.5 µl
OligodT(0.5 µg/µl)	1.5 µl
<i>Total volume</i>	<i>11 µl</i>

Table 2: Reverse transcription mix (1 reaction)	
DTT (0.1M)	2 μ l
10mM dNTP (10mM)	1 μ l
5x First Strand Buffer	4 μ l
RnaseOut (40U/ μ l)	1 μ l
Superscript II (200U/ μ l)	1 μ l
Total volume	9 μl

Newly synthesised cDNA was stored at -20°C prior analysis.

3.6.4. Semi-quantitative RT-PCR primers

The primers for the six potential stem cell related mouse genes and the housekeeping mouse gene TBP are listed in Table 3. They were designed using the on-line tool at www.genescript.com with the default specifications. All PCR products were designed to span one or more introns to avoid amplification of genomic DNA with predicted annealing temperature 60°C.

Table 3: semi-qRT-PCR mouse primer pairs.		
<u>Target gene</u>	<u>Forward primer</u>	<u>Reverse primer</u>
Sox2	5'CCC ACC TAC AGC ATG TCC TA 3'	5'GTG GGA GGA AGA GGT AAC CA 3'
Oct3/4	5' GAT CAC TCA CAT CGC CAA TC 3'	5' CGC CGG TTA CAG AAC CAT 3'
Nanog	5'AAC CTG AGC TAT AAG CAG GTT AAG A 3'	5'TGA ATC AGA CCA TTG CTA GTC TTC 3'
Bmil	5'GTC AGC TGA TGC TGC CAA T 3'	5'CCT CTT CTC CTC ATC TGC AA 3'
Nestin	5'CAA CTG GCA CAC CTC AAG AT 3'	5'GTG TCT GCA AGC GAG AGT TC 3'
Klf4	5'GCT GAA CAG CAG GGA CTG T 3'	5'TGG CAT GAG CTC TTG ATA ATG 3'
Mouse TBP	5'CCTT CGT GCA AGA AAT GCT GA 3'	5'CAG TTG TCC GTG GCT CTC TT 3'

3.6.5. Semi-quantitative RT-PCR reaction

Semi-quantitative RT-PCR was performed using the StepOne™ Real-Time PCR System from Life Technologies in a 20µl final reaction volume in 96 well plates. Each reaction was composed with 1µl (unsorted MOS cell lines) or 4µl (SP and SP-depleted MP cells) of synthesised cDNA template and 19µl or 16µl of semi-qRT-PCR master mix respectively (Table 4). For the control of unspecific amplification a non template control was used. For the control of possible amplification of contaminating mouse genomic DNA an aliquot of mouse total DNA (450ng/µl) was added to a separate reaction for each target gene. cDNA transcribed from mouse embryonic mRNA was used as the positive control of the specific amplification of each target gene.

<i>Table 4: semi-quantitative RT-PCR master mix.</i>		
	Unsorted MOS cells	SP and SP-depleted MP MOS cells
2x SYBR® Green Master Mix	10µl	
Primer pair: reverse primer (final concentration 5pmol/µl) plus forward primer (final concentration 5pmol/µl)	1.5µl	
H ₂ O	7,5µl	4.5µl
template	1µl	4 µl
<i>Total volume</i>	<i>20µl</i>	<i>20µl</i>

Samples were tested in two technical replicates. All pipetting steps were performed on ice. Reaction plates were gently mixed and spun down before starting the semi-quantitative RT-PCR reaction. Thermal cycler conditions are listed in Table 5 and identical for all primer pairs.

<i>Table 5: semi-quantitative RT-PCR thermal cyclers condition.</i>		
Step I (Denaturation stage)	95°C	10 minutes
Step II (Cycling stage) (40 cycles)	95°C	15 seconds
	60°C	1 minute
Step III (melting curve analysis)	95°C	15 seconds
	60°C	1 minute
	+0.3°C (gradual increase of the reaction temperature till it reaches 95°C)	
	95°C	15 seconds

3.6.6. Analysis of semi-quantitative RT-PCR amplifications

The positive amplification of the target or housekeeping gene mRNA in the sample was determined by detecting the accumulation of the SYBR Green fluorescent signal above the background level. The amplification threshold was set above the background fluorescence level within the exponential phase of fluorescence accumulation of amplification curve (Figure 10).

The Cycle Threshold (Ct) was determined as an interception between the threshold and the fluorescent amplification curve. The Ct value for each analysed gene was determined as the mean from the 2 technical replicates. For the control of the gene specific PCR product amplification the Melt (dissociation) Curve was analysed for each amplicon (Figure 11). The quality of the PCR products was qualitatively determined by loading 10µl onto 3% agarose gels (see 3.11.4).

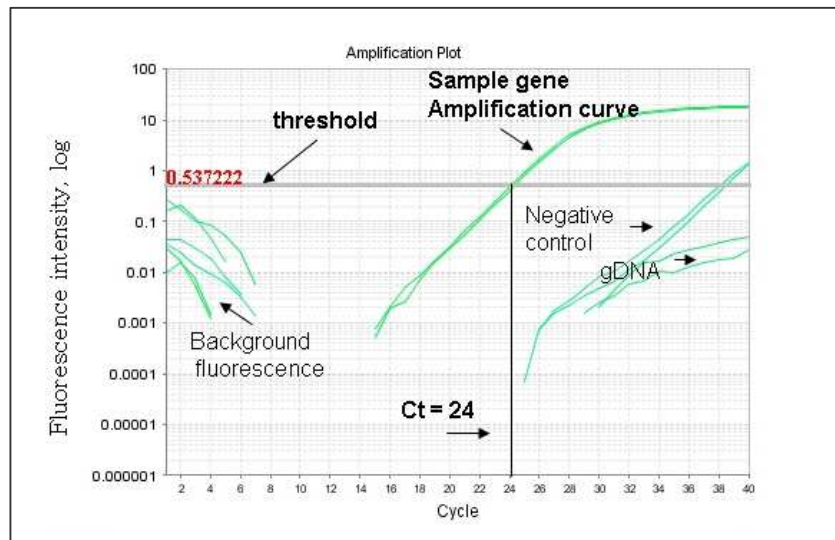


Figure 10: Graphical representation of the semi-quantitative RT-PCR data. In the figure is shown a sample from a gene amplification curve. The threshold is set at 0.54 within the exponential phase of amplification curve. The Ct value is found to be at 24th cycle as interception between the threshold and amplification curve. There is no specific amplification of negative control or genomic DNA (gDNA).

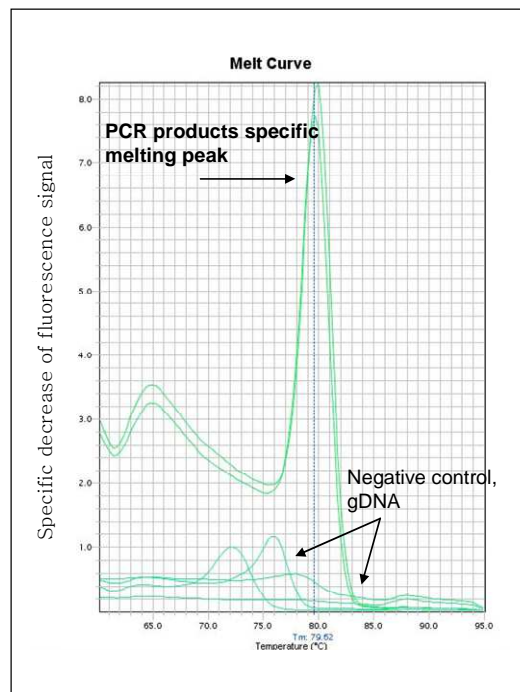


Figure 11: Graphical representation of the Melt Curve. In the figure is shown semi-quantitative RT-PCR product specific melting peak. There are no specific melting peaks in the negative control or genomic DNA (gDNA).

The fold changes in target gene expression between the side population and the SP-depleted main population cells, irradiated and non-irradiated cells or between the unsorted MOS cell

lines were calculated using the $2^{-\Delta\Delta Ct}$ method as was described before in the literature (Livak & Schmittgen, 2001). At first the expression level of the target gene was normalized to that of the housekeeping TBP gene expression for every sample analysed (ΔCt) (Table 6). Any difference in expression level between the normalised target gene in the sample of interest (eg.: treated cells) relative to the expression level of the normalized target gene in the relative sample (eg.: control cells) or relative to the target gene index (i.e. averaged expression level of the normalized target gene of samples used in the evaluation analysis) was calculated as $\Delta\Delta Ct$ (Table 6). The fold change in gene expression of the sample of interest (i.e. treated cells) normalised to TBP and relative to relative sample (i.e. control cells) was calculated by expressing an exponentially related $\Delta\Delta Ct$ value into linear related value (Table 6). Statistical evaluations were done with One-way ANOVA with Sidak's, and Dunnett's tests using GraphPad Prism version 6 for Windows.

Table 6: $2^{-\Delta\Delta Ct}$ equations.	
1). Normalization of RT-PCR relative amount of target gene to that of housekeeping gene	$\Delta Ct^{\text{treated, x}} = Ct^{\text{treated, x}} - Ct^{\text{treated, TBP}}$ $\Delta Ct^{\text{control, x}} = Ct^{\text{control, x}} - Ct^{\text{control, TBP}}$
Where,	<p style="text-align: center;">Ct-threshold cycle Δ - difference</p> <p>treated, x – expression of gene x in treated sample treated, TBP – expression of housekeeping gene TBP in treated sample</p> <p>control, x – expression of gene x in control sample control, TBP – expression of housekeeping gene TBP in control sample</p>
2). Difference between tested samples ($\Delta\Delta Ct$)	$\Delta\Delta Ct^{\text{treated, x}} = (\Delta Ct^{\text{treated, x}} - \Delta Ct^{\text{control, x}})$
The exponentially related log Ct value are converted into linear related value	$\text{Log}(2)_{\text{Fold change}} = \Delta\Delta Ct^{\text{treated, x}}$
3). Fold change in target gene normalized to TBP and relative to control	$\text{Fold change} = 2^{-\Delta\Delta Ct^{\text{(treated, x)}}$

3.7. Proliferation activity (MTT assay)

To analyse the proliferation activity in the side population (SP) and the SP-depleted main population cells the mitochondrial metabolic activity (MTT assay) of intact cells was tested. The cells were seeded into 24 well plates at defined cell concentrations. One well was left blank for each plate tested to provide a background value. After 4 days maintenance in culture metabolic activity of viable cells was measured with the MTT assay (following the manufacture's protocol). Medium was replaced with 100µl of fresh medium supplemented with 10 µl MTT labelling reagent. The formation of water insoluble purple formazan salt crystals was observed during of an incubation for 4 hours at 37°C. 100µl of solubilisation solution was added to each well and processed incubation at 37°C overnight. Solubilised formazan was quantified the next day spectrophotometrically with TECAN microplate reader with absorption at 595nm and reference absorption at 651nm. Samples optical density (OD) values were subtracted from the blank result and normalized per 1000 plated cells.

3.8. Protein immunoblotting (Western Blot analysis)

3.8.1. *Total protein extraction*

For the protein extractions unsorted MOS cells and control untreated HeLa cells were used. The cells were plated in T25 flasks at a concentration of 5×10^6 cells. At 80% of confluence unsorted MOS cells were irradiated with a range of doses of γ -irradiation. Unirradiated control cells were sham irradiated by keeping shielding in place. After irradiation the cells were incubated for 2 hours at 37°C. For the collection of proteins cells were washed with ice cold 2ml PBS and lysed with ice cold lysis buffer (RIPA Buffer supplied with complete mini protease inhibitor cocktail) directly in the flask. To avoid loss of material after the addition of lysis buffer the cells were physically removed from the flask surface with a scraper, collected to a 1.5ml eppendorf tube, held on ice and sonicated. Prior to further analysis the protein extracts were stored at -20°C.

3.8.2. Protein concentration measurement

Protein concentrations were measured using the BCA protein assay kit using BSA (albumin standard) as the standard. The protein extracts were thawed on ice. For each sample to be analysed 10 μ l of protein extract were mixed with 90 μ l water (Ampuwa). For the standard curve an albumin standard (BSA) was prepared in dilutions shown in Table 7.

Table 7: Standard curve dilutions.

BSA (Albumin standard) (stock 1mg/1ml)	Lysis buffer, μl	H2O (Ampuwa), μl
0	10	90
5 μ l	10	85
10 μ l	10	80
20 μ l	10	70
40 μ l	10	50
60 μ l	10	30
80 μ l	10	10

For every standard curve dilution and every sample 2ml of the reagent solution supplied with the kit were added. Vials were covered with parafilm to avoid evaporation of the reaction mixture. Reactions were carried out for 15 minutes at 60°C in a waterbath followed by a colorimetric measurement of the resulting fluorochrom. For each sample 200 μ l of the reaction solution was pipetted into 96 well plates in quadruplicate. The absorbance at 565nm was measured with a TECAN microplate reader. The standard curve was plotted in an excel program (Microsoft Office Word 2003) using a linear regression curve fit. Unknown protein concentrations were corrected for the background signal and the concentration calculated from the linear regression equation.

3.8.3. Sample preparation for loading into SDS electrophoresis gels

The protein extracts were thawed on ice. For every sample to be studied 20 μ g of total protein extract was used. Every sample was mixed with 2x Laemmli buffer (1:1 ratio) and heated for 5 minutes at 95°C. Samples were kept on ice prior loading into gels.

3.8.4. SDS-PAGE (polyacrylamide) gel preparation

For the size separation of proteins the samples were separated on a 15% polyacrylamide gel. The recipe for the preparation of one gel is listed in Table 8. Gels were cast into manufactured cassettes. In brief, all solutions for the separating gel were mixed in 50ml Falcon tube. TEMED and APS were added right before pouring the gel into the gel-casting cassette. Each cassette was loaded with ~8.3ml of the separating gel. On top of the separating gel 3ml isopropanol was pipetted. Polymerization was allowed for ~30 minutes at room temperature. After the isopropanol was decanted a stacking gel was layered on top of the set separating gel (the recipe is shown in Table 8). A well-forming comb (1.5 mm 10 well) was inserted into the staking gel for sample pocket formation. Polymerization was allowed for ~30 minutes at room temperature.

Table 8: Polyacrylamide gel (15%) recipe.

Gel type Compounds	Separating	Stacking
40% Acrylamid/Bis	3.75ml	0.5ml
0.5M Tris (pH 6.8)	-	1.26ml
1.5M Tris (pH 8.8)	2.5ml	-
10% SDS	100µl	50µl
H ₂ O (Ampuwa)	3.6ml	3.18ml
APS (10% w/v)	50µl	25µl
TEMED	5µl	5µl
Total volume	10ml	5ml

3.8.5. Electrophoretic separation of proteins

Gel-casting cassettes with polymerized gels were inserted into the gel electrophoresis chamber. The chamber was filled with running buffer and placed into a box filled with ice. Protein molecular weight marker (7µl) and up to 40µl of each sample were loaded into the wells. Electrophoresis was performed in two steps: a first run at 100V for 10-15 minutes to load proteins onto the separation gel followed by an increased voltage to 140-150V for 1.5-2 hours to separate proteins. Each run was done in two technical replicates.

3.8.6. *Transfer of separated proteins*

Transfer of the separated proteins was done in wet conditions (tank blot). Gels were taken from the gel-casting cassettes and rinsed with transfer buffer. The gel and a pre-soaked nitrocellulose membrane were placed in between two pieces of blotting paper, two sponges, wetted (ensuring no air bubbles) and loaded into a supported cassette. This “sandwich” was clamped together and placed into the transfer chamber filled with transfer buffer and containing a magnet stirrer with the blotting membrane toward the positive charge. The transfer chamber was placed on a magnet stirrer plate in a box filled with ice. Transfer was done at 100V for ~2 hours. After completing the transfer the separated proteins on the membrane were detected with rapid reversible Ponceaus S staining and documented.

3.8.7. *Antibody detection of target protein*

The membrane with transferred proteins was cut into pieces corresponding to the protein size to be detected. These membrane pieces were placed in a box containing blocking solution and incubated for 1 hour at 37°C in a water bath under continuous shaking, followed by 2x rinsing in T-TBS. Antibodies were diluted in 3% BSA/T-TBS in dilutions shown in section 2.6. Membranes were incubated with the antibodies at 4°C overnight with continuous gentle agitation, followed by 2 times 5 minute washes with T-TBS under shaking condition. HRP conjugated secondary antibodies were applied according to species used to generate the primary antibody (section 2.6) and incubated at room temperature for 1 hour. Excess secondary antibody was removed by 2x 5 minute washes with T-TBS under shaking condition.

3.8.8. *Detection of immunoblot signals*

A commercially available western blotting chemiluminescent detection kit (GE, Healthcare Life Sciences) was used to detect bound antibody. The staining solution for detection was prepared according to the manufacture’s protocol. Western blot nitrocellulose membranes were incubated in 4ml of staining solution for 5 minutes at room temperature and the chemiluminescent signal was immediately detected and documented with the Alpha Innotech ChemiImager system.

3.8.9. *Stripping and re-probing*

For re-probing, the western blot membranes were stripped using a commercially available stripping buffer. Western blot membranes were incubated for 20 minutes at room temperature with stripping buffer and washed 2x 5 minutes with T-TBS with gentle agitation. Antibody detection and development were performed as described above.

Quantification of the detected proteins was done with ImageQuant 5.2 software and normalised to tubulin protein level.

Statistical evaluations were done with One-way ANOVA with Sidak's, and Dunnett's tests using GraphPad Prism version 6 for Windows.

3.9. *Clonogenic assay*

3.9.1. *Serial dilution growth assay of side population and SP-depleted main population cells (clonogenic potential)*

To determine the number of clonogenic cells present in the side population (SP) and the SP-depleted MP cells the serial dilution technique was used. After the cells were separated into SP and SP-depleted MP fractions and counted with a Coulter Counter the SP and the SP-depleted MP cells were plated into 96 well plates at concentrations ranging from 1 to 8 cells per well plus a control with 100 cells per well. Each sample was tested in 24 individual wells. 2-fold serial dilutions from 8 to 1 cell, from 6 to 1.5 cells and from 5 to 1.25 cells were prepared in advance. Plated cells were maintained at 37°C for 10 days. Wells with growing cells were counted as positive wells if more than 50 cells were present in the well. Wells were examined by eye under phase contrast microscopy at low-power magnification (10X). The ratio of positive wells to negative wells was calculated.

3.9.2. *Clonogenic cell survival after irradiation assay (limiting dilution technique)*

To analyse the clonogenic cell survival after irradiation of unsorted MOS cells, and the SP and the SP-depleted MP cell the clonogenic survival assay was performed using the limiting

dilution technique in 96 well plates. The conventional clonogenic survival assay could not be performed because MOS cell do not grow in distinct colonies.

Unsorted cells were harvested with 0.05% Trypsin- EDTA(1X). Suspension of cells was allowed to stand for 5-7 minutes to sediment clumps of cells. Supernatant was removed and centrifuged at 600rpm for 5 minutes. Cells were washed with 5ml PBS and resuspended in 10ml DMEM medium supplemented with 10% FCS. In the case of freshly sorted side and SP-depleted main populations the cells were processed without additional cell culturing after sorting. Prepared cells were counted with Coulter Counter.

The limiting dilution density for MOS cell lines to obtain around 60% of positive wells (defined as a well with >50 growing cells) in 96 wells was determined prior the main experiments. Numbers of MOS cells giving this dilution are listed in Table 9. For the different MOS cell lines the control cell concentration to obtain 60% of wells with growing cells was different, representing the variation in plating efficiency difference between cell lines.

MOS-R-1929	6 cells /well
MOS-R306	6 cells /well
MOS-S-184	6 cells /well
MOS-S-1403	18 cells /well
side population cells	6 cells /well
SP-depleted main population cells	60 cells /well

For radiation treatment the number of cells was increased relative to the radiation dose applied and the expected cell plating rates to compensate for the reduced plating efficiency of cells after irradiation. Setup for the MOS cells clonogenic assay after ionising irradiation using limiting dilution technique in 96 well plates is shown in Table 10. The setup for the experiment where SP and SP-depleted MP cells were analysed is listed in Table 11.

Cells were plated in different cell concentrations in 96 well plates and incubated at 37°C for 1 hour. After incubation the cells were irradiated with various doses of γ -irradiation and allowed to grow at 37°C for 10 days. For semi-automated high throughput detection of wells with growing cells, cells were stained with EtBr. This is a UV fluorescent dye that strongly binds to the DNA and thus allows cells detection with the TECAN microplate reader. For this the plates were washed with PBS, permeabilised with 80% Ethanol for 1 hour at 4°C, washed with PBS two times, stained with EtBr staining solution (1 μ g per 1ml of PBS) and incubated

in the dark for 1 hour. After washing off the EtBr staining solution with PBS, the optical density (OD) values were measured with the TECAN microplate reader with excitation at 256nm and emission at 600nm. The correlation between the optical density values and growing cells was validated by counting growing cells in 96 wells by eye with subsequent staining of the same plate with EtBr. The threshold for detection of growing of more than 50 cells in the well was determined at optical density (OD) equal to 30. The values below threshold were considered as wells containing no growing cells.

Table 10: Limiting dilution assay experimental setup for clonogenic survival of MOS cell lines after exposure to ionising irradiation.

MOS-R-1929, MOS-R-306, MOS-S-184		MOS-S-1403	
Plating density of cells per well in 96 well plate to give 60% positive wells	Irradiation dose, Gy	Plating density of cells per well in 96 well plate to give 60% positive wells	Irradiation dose, Gy
6	Control (0)	18	Control (0)
6	0,5	18	0,5
15	1	45	1
30	2	90	2
60	4	180	4
120	8	360	8

Table 11: Limiting dilution assay experimental setup for clonogenic survival of side and SP-depleted main populations after exposure to ionising irradiation.

side population cells		SP-depleted main population cells	
Plating density of cells per well in 96 well plate to give 60% positive wells	Irradiation dose, Gy	Plating density of cells per well in 96 well plate to give 60% positive wells	Irradiation dose, Gy
6	Control (0)	60	Control (0)
6	0,5	60	0,5
15	1	120	1
30	2	300	2
60	4	600	4
120	8	1200	8

To determine the clonogenic cell survival after radiation the plating efficiencies and survival fractions after different radiation doses were analysed.

Plating efficiency (PE) of plated cells of each tested cell line or cell population was calculated using the Poisson distribution according to the formulas listed in Table 12. For the PE calculations the frequency of wells that did not contain growing cells was counted.

Table 12: Formulas to calculated Plating Efficiency (PE) of plated cells in 96 well plates relative to wells that produced no growing cells according to Poisson distribution.	
Poisson distribution	$F_0 = \frac{f_c^n \times e^{-f_c}}{n!}$ $F_0 = e^{-f_c}$ $f_c = -\ln(F_0)$
Where,	<p>F₀ is frequency of wells without growing cells</p> <p>f_c is average number of clonogenic cells</p> <p>n is the expected number of colonies (number of cells giving a positive well), here is 0</p> <p>e is base of the natural logarithm</p>
<p>Sample derivation of PE from the Poisson distribution.</p> <p>Example: Calculation of PE in control MOS-R-1929 cells, where 6 cells per well gave 60% positive wells.</p>	$PE = \frac{-\ln(F_0)}{f_p}$ $PE = \frac{-\ln(0.4)}{6} = 0.15$
Where,	<p>F₀ is frequency of wells receiving no growing cells) (no plated cells), here is 0.4 (or 40%)</p> <p>f_p average number of cells plated per well in the experiment</p> <p>PE is plating efficiency</p> <p>6 is number of plated cells per well</p>

PE efficiency was calculated for each cell line or cell population and for each radiation dose applied. Survival fraction of irradiated cells was calculated as following:

$$SF_{D_x} = \frac{PE_{D_x}}{PE_c}$$

where,

SF – survival fraction at given dose

D_x – given dose

PE – plating efficiency

c – control (0Gy)

As the $PE_c \gg PE_{D_x}$ so the SF will be lower than 1 if cell survival reduced by radiation. Survival fractions were plotted as a function of radiation dose on a logarithmic scale and were fitted to a linear-quadratic (LQ) model according to the following formula:

$$SF = e^{-(\alpha D + \beta D^2)}$$

where,

SF is a survival fraction at given dose

e is a base of the natural logarithm

D is a given dose

α is a linear component

β is a quadratic component

For plotting as a linear-log plot the above formula can be derived as follows:

$$\log_e(SF) = -(\alpha D + \beta D^2)$$

The α and β components can thus be directly compared between different cell survival curves. Also from the LQ fitted survival curves for tested cell lines and cell populations the median lethal dose LD_{50} , LD_{10} and survival fraction at a dose of 2Gy (SF2) are available. LD_{50} is the dose that is required for killing half of the clonogenic cells. LD_{10} is the dose that kills 90% of the available clonogenic cell. As 2Gy is the standard fractionation dose in conventional radiation therapy the SF at 2 Gy (SF2) was calculated from the LQ equation as the anti-natural logarithm. LD_{50} (dose, Gy at SF 50% or 0.5) was calculated according to formulas listed in Table 13.

Table 13: Formulas to calculated radiation dose required to kill half of the clonogenic cells (LD_{50}).
$SF(0.5) = e^{-(\alpha D_{LD50} + \beta D_{LD50}^2)}$
$\log_{10}(0.5) = -(\alpha D_{LD50} + \beta D_{LD50}^2)$
$-0.3 = -(\alpha D_{LD50} + \beta D_{LD50}^2)$
$0.3 + \alpha D_{LD50} + \beta D_{LD50}^2 = 0$
$D_{LD50} = \frac{-\alpha + \sqrt{\alpha^2 + 4\beta \times 0.3}}{2 \times \beta}$
<p>Where,</p> <p>SF(0.5) is a survival fraction = 50%</p> <p>e is a base of the natural logarithm</p> <p>D_{LD50} is a radiation dose to give SF = 50%</p> <p>α is a linear component</p> <p>β is a quadratic component</p>

LD_{10} (dose, Gy at SF 10% or 0.1) was calculating using the same principle.

Statistical evaluations were done with One-way ANOVA with Sidak's, Holm-Sidak's and Tukey's tests using GraphPad Prism version 6 for Windows.

3.10. Immunofluorescent detection of DNA double stand breaks (DSBs) after irradiation (γ H2AX and 53BP1 foci)

3.10.1. Immunofluorescent staining of γ H2AX and 53BP1 foci

To analyse DNA double strand break repair and repair kinetics after irradiation the presence of co-localised γ H2AX and 53BP1 in DNA break repair foci were detected.

One day prior to irradiation MOS cells were seeded onto sterile glass slides at a density of 150.000 cells per slide and cultured under standard conditions. The next day cells were irradiated at room temperature using different doses followed by incubation at 37°C 5% CO₂ (Table 14).

<i>Table 14: DNA DSBs dynamics and kinetics experimental setup.</i>			
Dynamics of DNA DSBs		Kinetics of DNA DSBs repair	
Dose, Gy	Incubation, min	Dose, Gy	Incubation, min
0Gy	90	0Gy	90
1Gy		1Gy	240
2Gy		1Gy	420
			1400

After incubation the adherent cells were rinsed with PBS for 5 minutes at room temperature and fixed with 2% paraformaldehyde in PBS for 15 minutes at room temperature. At this stage slides were either stained immediately or stored at 4°C in the fixative solution. Cells were washed with PBS for 5 minutes at room temperature. For permeabilization slides were incubated with 1% Triton X100 in PBS 3 times for 5 minutes and washed with PBS two times for 5 minutes, both under shaking condition at room temperature. Nonspecific antibody binding was blocked with 1% BSA, 0.15% Glycerol in PBS blocking solution for 1 hour in a humid chamber at 37°C. Primary antibodies were applied overnight at 4°C in a humid chamber with a concentration of mouse monoclonal anti- γ -H2AX of 1:1000 and of rabbit polyclonal anti-53BP1 of 1:500 diluted in blocking solution. The following day washing steps were used to remove the primary antibodies. Slides were washed with PBS for 5 minutes, 0.15% Triton X100/PBS for 10 minutes and with PBS for 5 minutes. Finally, slides were washed with 0.01% Tween 20/PBS 2 times 5 minutes and with PBS for 5 minutes. All wash steps were done at room temperature under gentle shaking condition. Before the secondary fluorescent labelled antibodies were applied the slides were re-blocked with blocking solution for 30 minutes in humid chamber at room temperature. Secondary antibodies were diluted in blocking solution. For Alexa 488 anti-rabbit a dilution of 1:1000 and for Cy3 anti-mouse of 1:1000 was used (section 2.6). Incubation with secondary antibodies was done at room temperature in a humid chamber for 1 hour. Slides were washed with 0.15% Triton X100/PBS 2 times 5 minutes, followed by a wash with PBS for 5 minutes. Finally the slides were washed with 0.01% Tween 20/PBS 2 times 5 minutes followed by a wash with PBS for 5 minutes. All wash steps were done at room temperature under shaking condition. Cell nuclei were counterstained with 5 μ l/ml Hoechst 33342 in PBS for 2 minutes in the dark followed by a wash with PBS 5 minutes 2 times at room temperature in the dark. For better visualisation of the nuclei the cells were dehydrated by rinsing in Ethanol solutions with increasing concentration (70%, 80% and 100% Ethanol). After the slides were dried, they were mounted

with Vectashield and coverslips. Slides with labelled cells were stored at -20°C prior to analysis.

3.10.2. Analysis of γ H2AX and 53BP1 foci

γ H2AX and 53BP1 foci were counted manually by eye using fluorescence microscope (KEYENCE BZ-9000). Images of stained cells were taken using a fluorescence microscope (KEYENCE BZ-9000). Images were taken under 40X fold magnification and analysed with BZ-II Analyser Keyence. For the analysis only foci with co-localised γ H2AX and 53BP1 signals were scored. For each experiment 1-2 slides and at least 100 cells were counted. For the dose-response of radiation-induced DNA DSBs the mean number of foci and the standard deviations of scored foci were plotted in a linear mode vs. the radiation dose. For the kinetics of radiation-induced DNA DSBs repair foci, the mean number of foci and the standard deviations of scored foci were plotted in an exponential decay mode as a percentage of foci repaired during the time, relative to the foci present at the 90 minutes after irradiation. The $T_{1/2}$ of repair was calculated from exponential decay quantity as following:

$N(t) = N_0 \times e^{-\lambda t}$
$\frac{N(t)}{N_0} = N(t_{1/2}) = 0,5 = e^{-\lambda t_{1/2}}$
$\ln(0.5) = -\lambda t_{1/2}$
$t_{1/2} = \frac{\ln(0.5)}{-\lambda}$
where: N(t) is the value at the time t $N_0 = N(0)$ is the initial value λ is the decay rate constant e is the natural logarithm $t_{1/2}$ is repair time after which the value is reduced to 50% of the initial value (0.5)

Statistical evaluations were done with Student's t test and One-way ANOVA with Sidak's and Dunnett's tests using GraphPad Prism version 6 for Windows.

3.11. *In vivo osteosarcoma mouse model*

3.11.1. Mammalian plasmid for expression of red fluorescence protein (RFP) *tdTomato*

The pCAG-tdTomato vector system for the expression of red fluorescence protein was the kind gift from Dr Ingo Bartscher from Institute of Stem Cells Research at Helmholtz Center Munich. The vector map is shown in Figure 12. The plasmid is 7887 bps in length. RFP *tdTomato* emits light in the visible red spectrum (excitation at 554nm, emission at 581nm). Expression of the *tdTomato* protein is driven by the chicken beta actin promoter. The plasmid carries ampicillin resistance and puromycin resistance genes for selection in bacteria and mammalian cells respectively. The plasmid can be linearized using the single *ScaI* restriction site for optimal delivery and integration into the cell genome.

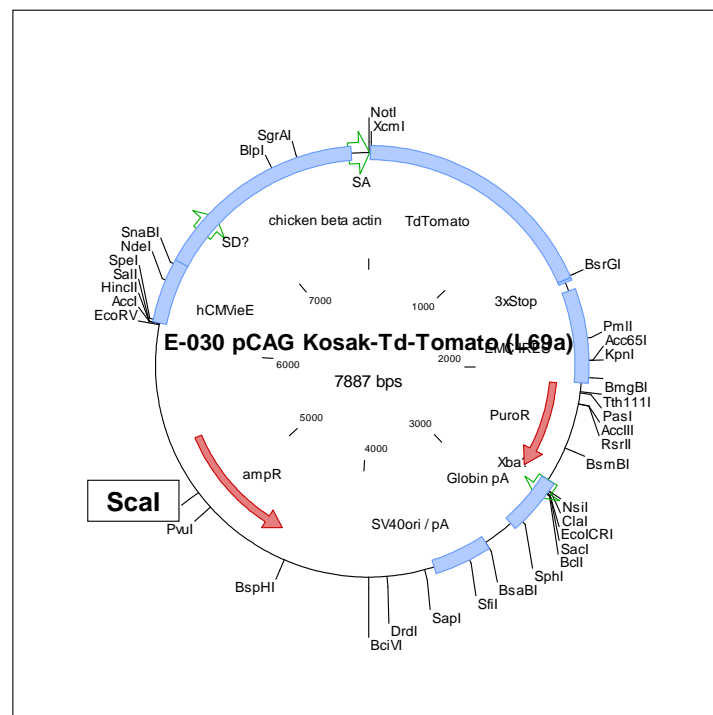


Figure 12: Map of mammalian plasmid pCAG Kosak-td-Tomato. (Map and construct were provided by Dr Ingo Bartscher). The single *ScaI* site is indicated in bold font.

3.11.2. Plasmid amplification

The pCAG-tdTomato plasmid was grown in the commercially available chemically competent TOP10 E.Coli stain (Invitrogene). One vial of E.Coli were mixed with 3µg of the pCAG-tdTomato plasmid, incubated on ice for 15 minutes and heat shock transformed for 1 minutes at 42°C followed by an incubation on ice for 5 minutes. Transformed bacteria were mixed with 150µl liquid bacterial medium (LB-medium) and incubated for 30 minutes at 37°C under shaking condition to allow recovery of expression of ampicillin resistance. After incubation 125µl of bacterial suspension was plated onto solid bacterial medium (LB-medium supplemented with bacterial agar and 100µg per ml ampicillin) in a Petri dish and incubated overnight at 37°C. The next day bacterial colonies showing resistance to ampicillin were picked and cultured in 250ml liquid bacteria medium with 100µg per ml ampicillin for 24 hours at 37°C under constant shaking. Bacterial cultures were harvested and collected at 4000g for 15 minutes at 4°C. Plasmid DNA was purified from the E.Coli with the QiaGen plasmid purification kit following the manufacture's protocol. The plasmid pellet was dissolved in 500µl of H₂O (Ampuwa) in 2ml eppendorf tube and precipitated in presence of 50µl 3MNaAc and 1450ml 100% Ethanol. The plasmid DNA was recovered by centrifugation for 10 minutes at 15.000 rpm at 4°C. The pellet was washed with 70% Ethanol and centrifuged for 5 minutes at 15.000 rpm at 4°C and resuspended with Ampuwa water. Resuspension was done overnight at 4°C without mechanical pellet dissociation. Plasmid DNA yield was measured by spectrophotometer measurement with the TECAN microplate reader in the DNA/RNA nanoquant plate as described in section 3.6.2. The concentration of plasmid DNA was calculated from the OD₂₆₀ and the ratio of A₂₆₀/280 determined. Plasmid DNA was stored at -20°C prior further analysis.

3.11.3. Digestion of plasmid DNA and fragment analysis

The pCAG-tdTomato plasmid was linearized using the ScaI restriction enzyme. This digestion does not influence any important genes (Figure 12). ScaI digestion was performed following the manufacture's protocol with provided buffer where 6µg of plasmid DNA were mixed with 2µl of restriction enzyme as shown in Table 15. Digestion was performed at 37°C for 2 hours.

<i>Table 15: DNA digestion mix.</i>	
Buffer 3 10x	4 μ l
Restriction enzyme (ScaI) 20.000Units/ml	2 μ l
Plasmid DNA (3 μ g/ μ l)	2 μ l
Water (Ampuwa)	32 μ l
<i>Total volume</i>	<i>40μl</i>

Gel electrophoresis for the control of sufficient plasmid DNA digestion was performed as described below (section 3.11.4.). Digested plasmid DNA was stored at -20°C prior to transfection into MOS cells.

3.11.4. Gel electrophoresis of plasmid DNA

The quality of the plasmid DNA was determined by loading 5 μ l of the linearized plasmid DNA onto 1.5% agarose gel. The gel was prepared using 1.5g Agarose added into 100ml 1xTBE electrophoresis buffer under continuous stirring. The agarose solution was boiled in a microwave oven to allow the agarose to melt completely. Once the agarose solution cooled down to about 60°C, 8 μ l of ethidium bromide solution from a stock solution of 10mg/ml was added to the agarose whilst continuously mixing. A 1.5mm well-comb was positioned into the clean gel casts and the molten agarose solution was then poured into the plastic gel form containing a comb. When the gel was completely solidified (approximately 30-40 min at room temperature) the comb was carefully removed and the gel placed in the electrophoresis tank. 1x TBE electrophoresis buffer was added to cover the gel. The samples and a DNA length marker were each mixed with 3 μ l loading DNA dye and loaded into the wells. After 1 hour of electrophoresis at 90V the location of the DNA within the gel was photographed under UV-light-illumination using the Alpha Innotech ChemiImagertm system.

3.11.5. Transfection of MOS cells with pCAG-tdTomato

Lipofectamine[®] 2000 Transfection Reagent kit was used to transfect exponentially growing MOS cells with the fluorescent dye-expressing plasmid following the manufacture's protocol. MOS cells were plated one day prior transfection in 6-well plates at a concentration of

400.000 cell per well. On the day of transfection the linearized plasmid DNA-lipid complex was prepared (Table 16).

<i>Table 16: Plasmid DNA-lipid complex (for 6 well).</i>	
<i>Compound</i>	<i>Amount</i>
Linear plasmid DNA	4 µg
	+
Opti-MEM [®] Reduced Serum Medium	250 µl
Lipofectamine [®] 2000	10 µl
	+
Opti-MEM [®] Reduced Serum Medium	250 µl

4 µl of ScaI linearized plasmid DNA (1µg/µl) was diluted in 250 µl Opti-MEM[®] Reduced Serum Medium. Lipofectamine[®] 2000 reagent was mixed with Opti-MEM[®] Reduced Serum Medium and let stand for 5 minutes at room temperature. Diluted plasmid DNA was mixed with diluted Lipofectamine[®] 2000 reagent and mixed gently. The mixture was incubated for 20 minutes at room temperature. For the transfection 500 µl of linearized plasmid DNA-lipid complex was applied to the cells.

Cells were incubated at 37°C for 2-3 days. Cells were observed under the fluorescence microscope with the excitation at 554nm and the emission at 581nm. At this time a transfection efficiency ~40% was observed.

3.11.6. Stable integration of pCAG-tdTomato into the MOS genome

To select for a stable transfection of the pCAG-tdTomato the expression plasmid carries a puromycin selection marker. Puromycin is an antibiotic leading to protein synthesis inhibition and is toxic for eukaryotic cells unless they carry a puromycin resistance gene. MOS cells cultures, where the transfection of the cells had reached an efficiency ~ 40%, were considered for selection for stable intergration. MOS cells were cultured under puromycin selection by adding the antibiotic in growth medium at a concentration of 5µg per 1ml. Growth medium containing puromycin was replaced every second day. After three weeks of culture most of the surviving cells were expressing red fluorescent protein.

3.11.7. Single cell cloning of MOS cells stably expressing the red fluorescence protein

MOS cells were single cell cloned in 96 well plates after puromycin antibiotic selection. Growing cells were washed and trypsinized. The cell suspension was let stand for 5 minutes to allow cell clumps to sink. The tubes were centrifuged at 600 rpm for 5 minutes and the cell pellet was washed with PBS and resuspend in medium. The cells were counted with a Coulter Counter and were seeded in 96 well plates at a concentration of 0,5 cell per well in growth medium without the presence of any antibiotic since the plasmid was stably integrated into the genome. For each cell line several plates were seeded. Cells were incubated for at least 10 days at 37°C. Expressing clones were checked regularly for red fluorescence. Expressing colonies that comprised at least 50 cells were considered for further analysis. Colonies were further maintained in cell culture without the puromycin pressure and expanded. At every intermediate step a portion of cells was frozen down as a backup at -80°C.

3.11.8. Experimental animals

F2BALB/c/C3H mice were used for the transplantation experiments. All animal experiments were conducted under standard regulations of the HMGU animal protection officer.

3.11.9. In vivo injection of pCAG-tdTomato MOS cells into mice

The MOS-R-306 cell line expressing CAG-tdTomato was chosen for a pilot study of the *in vivo* formation and visualization of labelled tumour. For each injection solution of one million cells in 200µl of PBS per injection was prepared. Cells were detached, pelleted and rinsed with sterile PBS. The cell pellet was resuspended in sterile PBS and the cell suspension kept on ice prior to injection. Three mice were used for the experiment. The area of the lower back, lateral to the spine was the site chosen for the injection. The place of injection was shaved and treated with 70% ethanol. The cell suspension was carefully injected subcutaneously. The development of tumours was followed daily until the growth size was suitable for fluorescence imaging. No tumours were allowed to grow to a size that impaired the animals' health.

3.11.10. *Epifluorescence imaging of tumour formation in vivo*

At approximately 12 days all three animals had developed at 5-10mm diameter tumour-like growth at the site of injection. Live *in vivo* imaging of transplanted “tumours” was made using epi-fluorescence imaging (collaboration with Institute of Biological and Medical Imaging, Helmholtz Center Munich). Mice were shaved and imaged under Isoflurane anaesthesia. The mouse torso was externally illuminated with light from a 554nm filter and the fluorescence emitted from the tumour was imaged non-invasively using a CDD camera fitted with a 581 nm filter.

3.11.11. *Histological examination*

Mice were sacrificed and the tumours at the injection site were removed for histological examination by the Department of Pathology at Helmholtz Center Munich. Hematoxylin/Eosin stained sections were evaluated by the Department of Pathology at Helmholtz Center Munich.

IV Results

4.1. Characterisation of MOS cell lines

4.1.1. The fraction of side population cells in MOS cell lines

In the four studied MOS cell lines the potential tumour initiating cells (TICs) were determined as the side population (SP) in flow cytometric analysis after staining with the fluorescent vital dye, Hoechst 33342. The side population fraction was defined as the fraction of Hoechst 33342 stained cells that formed a tail extending from the G_0/G_1 cells (see Figure 9). Figure 13 illustrates the profile of the flow cytometric analyses of the side population fraction and its validation by inhibiting with verapamil in the MOS-R-1929 cell line.

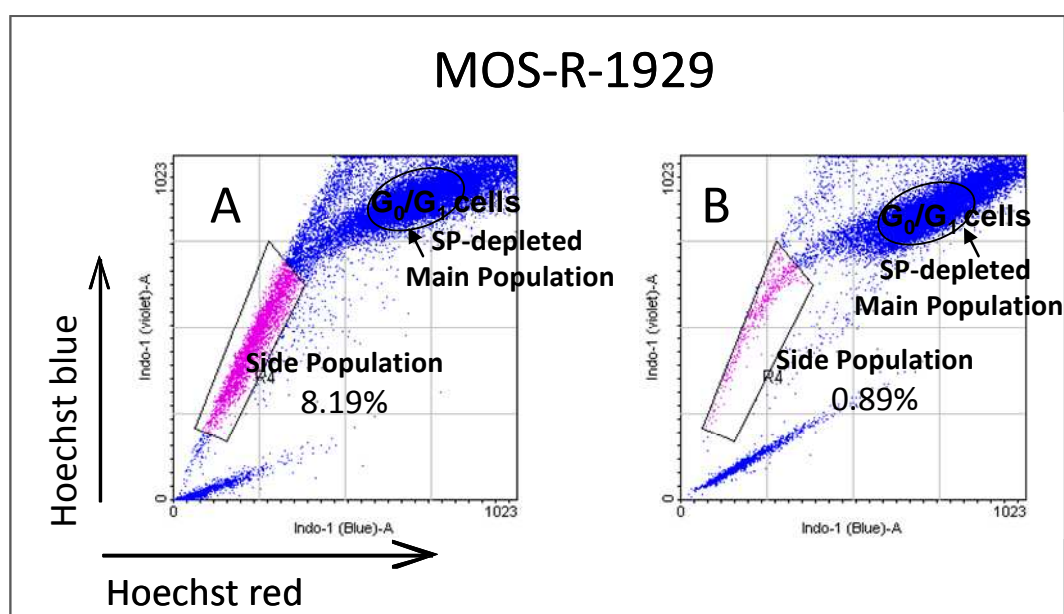


Figure 13: Flow cytometric analyses of MOS-R-1929 cell line. A: The dot plot represents the cells stained with Hoechst 33342 for 90 minutes at 37°C as described in section 3.5.1. Area marked with the polygon represents the side population fraction (SP). B: The dot plot represents the cells stained with Hoechst 33342 in presence of Verapamil at a final concentration of 50 μ M for 90 minutes at 37°C. Area marked with the polygon represents the remaining side population labelled cells due to inhibition of the efflux pump by Verapamil. The doublets and fragments and dead cells were gated out as described in section 3.5.2. Vertical axis is the Hoechst blue fluorescence. Horizontal axis is the Hoechst red fluorescence.

The four investigated cell lines had different side population fractions (Figure 14). The radiation resistant cell line (as shown in growth inhibition assay, Figure 7) MOS-R-1929 has a significantly higher proportion of the side population cells with an average of 15% compared to the radiation resistant MOS-R-306 (0.75%) and radiation sensitive MOS-S-184 (0.67%) and in MOS-S-1403 (0.14%) cell lines (Figure 14).

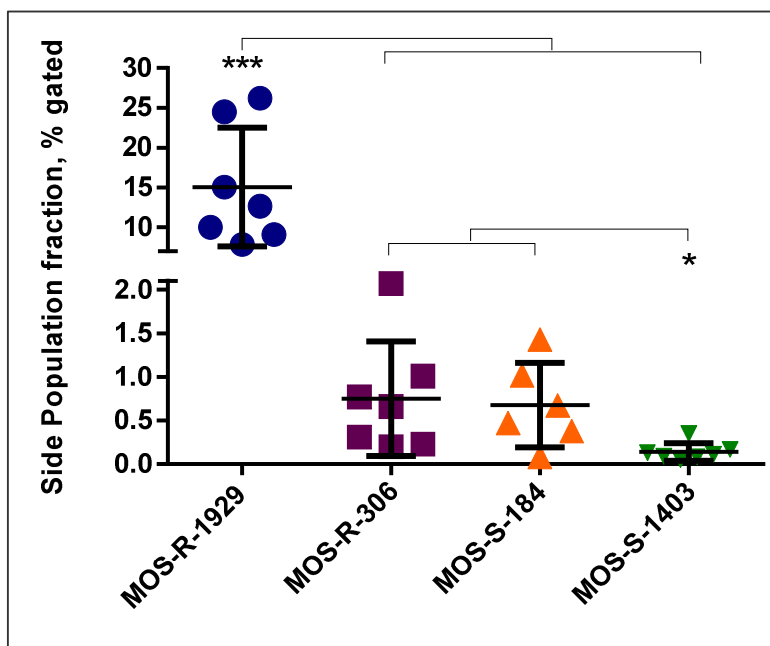


Figure 14: The side population fraction in the investigated MOS cell lines. Each point represents the side population fraction determined in an independent flow cytometric analysis. At least six independent experiments were conducted per cell line. The mean values and standard deviations are presented for each cell line. Statistical evaluation of difference between cell lines was done with unpaired Student's t test using GraphPad Prism version 6 for Windows. $p \leq 0.05$ (*), $p \leq 0.001$ (***)

The side population fraction was validated in all cell lines by blocking the multidrug resistance (Mdr) ATP-Binding Cassette (ABC) transporters efflux pump by Verapamil (Table 17).

Cell line	Without verapamil, % gated from total stained cells	With verapamil, % gated from total stained cells
MOS-R-1929	8.19	0.89
MOS-R-306	0.21	0.01
MOS-S-184	0.24	0.12
MOS-S-1403	0.1	0.05

4.1.2. Side population and SP-depleted main population cells from MOS-R-306 have different morphologies

The side population (SP) and SP-depleted main population (MP) cell populations were sorted from the MOS-R-306 cell line and grown in cell culture for 7 days under standard conditions. The SP cells formed spherical loosely attached cell clusters on top of spread-out cells which probably represented differentiated cells. The SP-depleted MP cells however grew in a monolayer of fibroblast-like spindle cells. No clusters were evident (Figure 15).

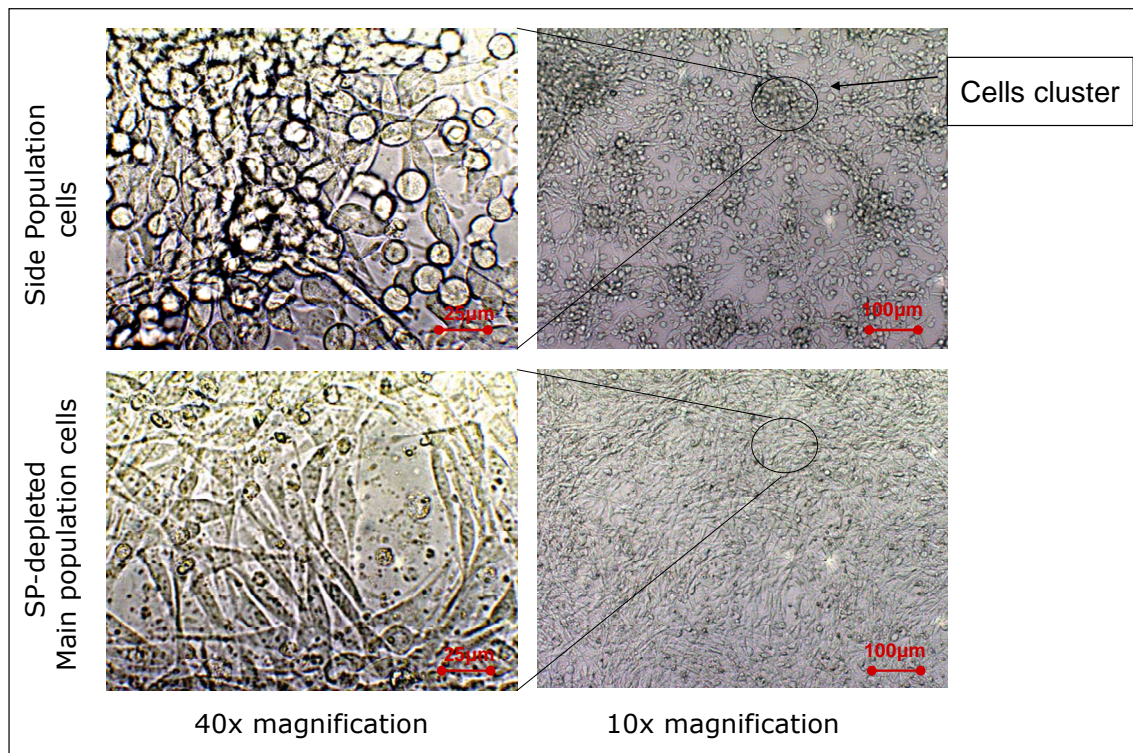


Figure 15: Cell morphology of the side population and SP-depleted main population cells from the MOS-R-306 cell line after 7 days cell culture. The side population cells are mainly rounded cells that grow on top of elongated spindle-like cells in cluster-like formations. The SP-depleted main population cells grow as a monolayer and are represented by polygonal and elongated spindle-like cells with few round cells. Images of growing cells were taken at low-power (10X) and high-power (40X) magnification.

4.1.3. Repopulation of side population and SP-depleted main population cells during growth of seeded SP cells and SP-depleted MP cells

The experiment was performed twice with MOS-R-1929 cells separated into the side population (SP) and the SP-depleted main population (SP-depleted MP) fractions. These were seeded and cultured under standard conditions for 1, 5 and 10 days. The other three cell lines were not suitable for this experiment due to their very low SP fractions. Flow cytometry profiles and results where the fractions of SP and SP-depleted MP in these cultured cells were determined are shown in Figure 16 and Table 18 respectively.

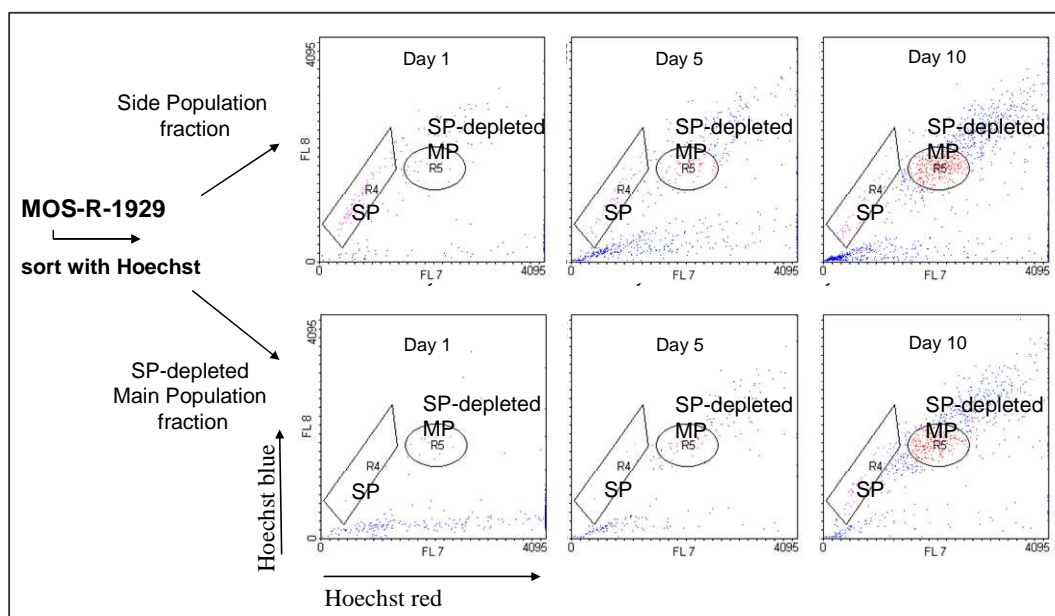


Figure 16: Repopulation of the SP and SP-depleted MP cells (flow cytometric analysis). Profiles represent regeneration of two populations of cells by the SP and the SP-depleted MP cells after separation and 1, 5 and 10 days maintenance in cell culture respectively. R4 polygon represents SP fraction of cells; R5 ellipse represents SP-depleted MP fraction of cells

Side population (SP) cells			SP-depleted main population cells		
Days in culture	SP cells fraction, % gated from all stained cells	SP-depleted MP cells fraction, % gated from all stained cells	Days in culture	SP cells fraction, % gated from all stained cells	SP-depleted MP cells fraction, % gated from all stained cells
1	28.05	5.28	1	0.34	3.02
5	7.07	10.19	5	2.27	16.36
10	4.31	29.02	10	5.98	27.66

The accuracy of the cell separation was measured at day 0 by re-analysing sorted cells (Figure 17).

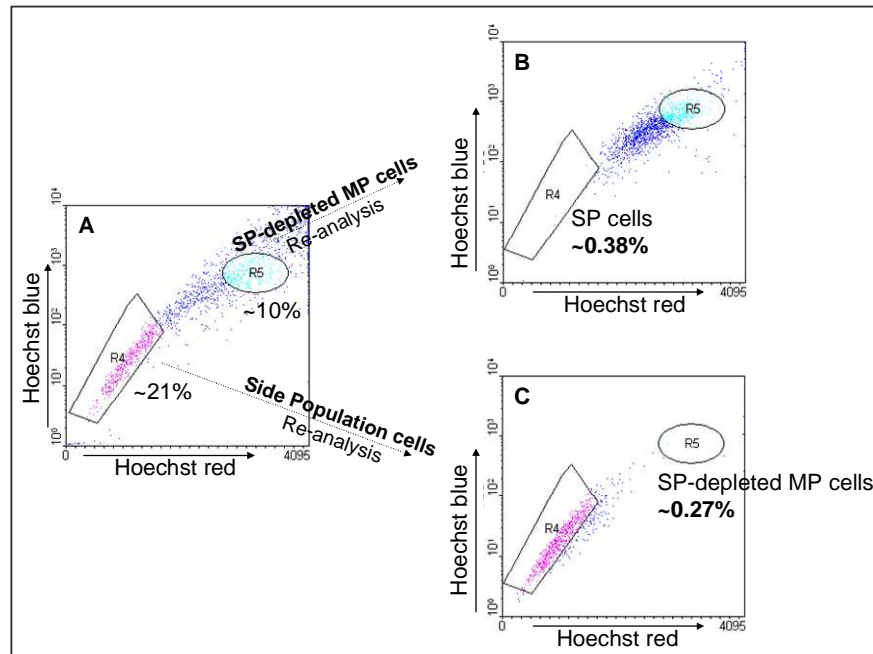


Figure 17: FACS profiles of re-analysed sorted SP and SP-depleted MP cells from MOS-R-1929. A: The dot plot represents the SP cells (R4 area) and the SP-depleted MP cells (R5 area) during primary FACS sorting of the unsorted cell population. B: The dot plot represents re-analysed SP-depleted MP cells directly after sorting. The purity of the sorting is more than 99% i.e. the SP fraction contamination is 0.38% C: The dot represents re-analysed SP cells directly after sorting. The purity of the sorting is more than 99% i.e. the SP-depleted MP fraction contamination is 0.27%.

In the SP cells that were cultured after FACS separation, the fraction of SP cells decreased whilst at the same time the fraction of SP-depleted MP cells increased. On the other hand, in the SP-depleted MP cells the SP fraction slowly increased. After 10 days in culture the original fraction of SP cells is almost restored in both SP cultured and SP-depleted MP cultured cells. This re-establishment of the ratio of SP and non-SP (SP-depleted MP) cells found in the population before sorting suggests a dynamic exchange between the populations in both directions. SP cells differentiate to give rise to new non-SP cells as the SP-depleted MP can only have come from SP cells in such a short culture time. SP cells are possibly regenerated from SP-depleted MP cells as they reappear in culture of SP-depleted MP cells. It is also possible that they come from SP cells already present as over 10 days 1 cell may give rise to 1000 SP cells (Figure 17) (Figure 18 and Figure 19).

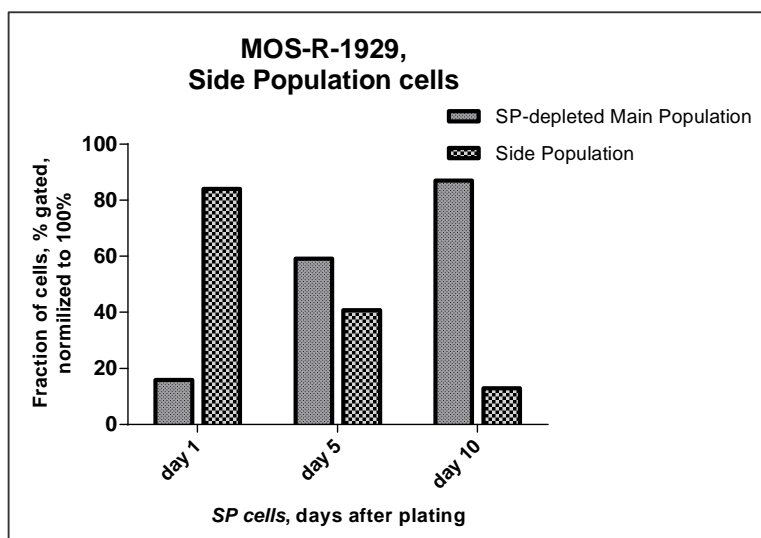


Figure 18: Change of the side population (SP) cells sorted from MOS-R-1929 during cell cultivation. The SP and the SP-depleted main population fractions of cells regenerated by SP are shown after FACS separation and 1, 5 and 10 days maintenance in cell culture under standard conditions. Fractions of cells presented as a percentage of cells after gating out the debris, doublets and dead cells from total stained cells and normalized to 100%.

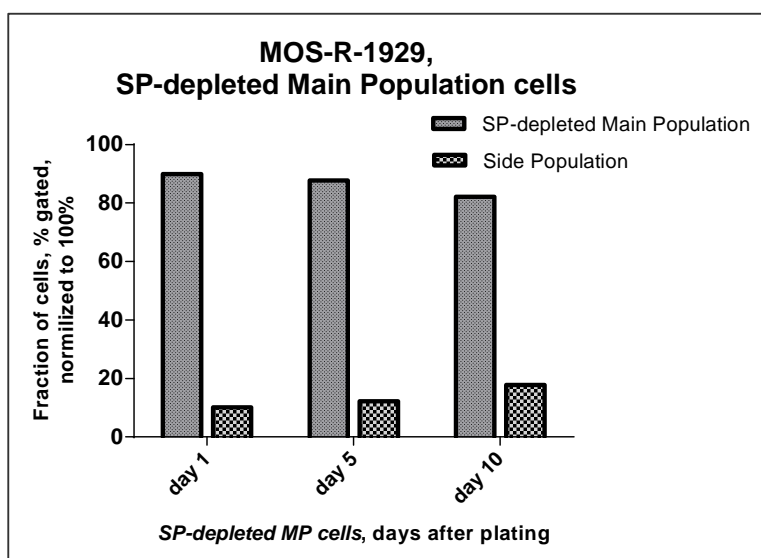


Figure 19: Change of the SP-depleted main population (SP-depleted MP) cells sorted from MOS-R-1929 during cell cultivation. The SP and the SP-depleted MP fractions of cells regenerated by SP-depleted MP cells are shown after FACS separation and 1, 5 and 10 days maintenance in cell culture under standard conditions. Fractions of cells presented as a percentage of cells after gating out the debris, doublets and dead cells from total stained cells and normalized to 100%.

In addition to the flow cytometric analysis of the side population and the SP-depleted MP cells they were analysed for the expression of mRNA markers that identify embryonic and adult normal stem cells (Figure 20). No detectable differences in expression of known stem

cell markers at any of the analysed time points were found in the SP cells separated from MOS-R-1929 (Figure 20).

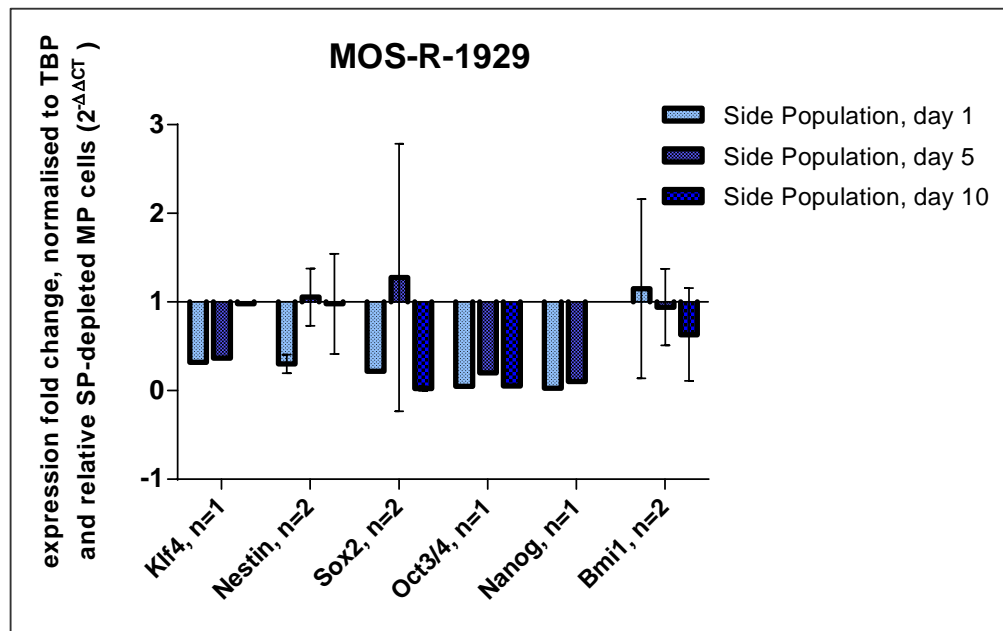


Figure 20: Semi-qRT-PCR expression of candidate stem cell marker genes changes of MOS-R-1929 side population (SP) cells during cell culture. During repopulation the SP and the SP-depleted main population cells were analysed for the expression of embryonic and adult stem cells markers. Histograms show expression fold change level of the side population cells normalised to mouse TBP and relative to representative SP-depleted main population cells. Mean values and standard deviations are shown. Statistical evaluation of difference between side population cells at different time points was done with one-way ANOVA with Sidak's test using GraphPad Prism version 6 for Windows.

4.1.4. Proliferation activity of cultured side population and SP-depleted main population cells (MTT assay)

Proliferation activity of the side population (SP) and the SP-depleted main population (SP-depleted MP) cell populations was analysed with the MTT assay. After the fluorescent Hoechst 33342-based separation of the SP and the SP-depleted MP cells, both populations were maintained in culture for four days. The ability of cells to metabolically reduce tetrazolin dye, MTT, to formazan was assayed. On Figure 21 the optical density values (OD) of MTT assay for the SP and the SP-depleted MP cells are presented. In this experimental design, the metabolic activity determined with MTT assay is taken to indicate oxygen consumption of these cell populations.

A significantly lower metabolic activity of the SP cells compared to the SP-depleted MP cell population was found between these cell populations separated from MOS-R-306 cells. This result supports the hypothesis of a slow proliferation and low oxygen consumption behaviour of stem cells. MOS-S-184 SP cells also showed a trend towards slower proliferation compared to SP-depleted MP cells (Figure 21). These observations indicate that the SP and the SP-depleted MP cells indeed may have different oxygen consumption or proliferate at different rates. At the same time MOS-R-1929 did not demonstrate such difference in mitochondrial metabolic activity. MOS-R-1929 side population cells exhibited trend towards higher proliferation rate (Figure 21).

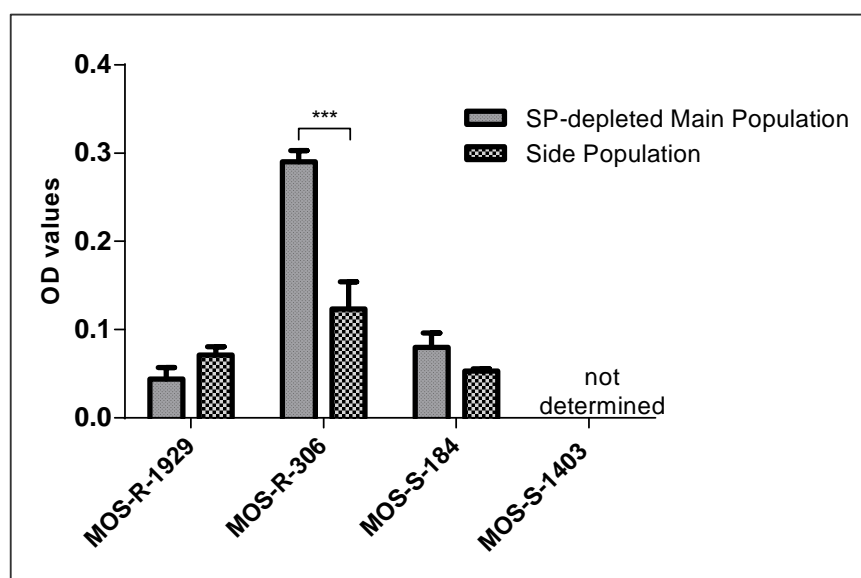


Figure 21: Cell proliferation rate of the side population (SP) and the SP-depleted main population cells of MOS cell lines. Proliferation was measured with the MTT assay. Histograms represent optical density (OD, 570nm), normalised per 1000 plated cells. Measurements were done 4 days after plating cells to achieve exponential phase of cells growth. Mean values and standard deviations are shown (n=2). MOS-S-184 represents mean value of 2 technical replicates. Statistical evaluation was done with 2way ANOVA with Sidak's test using GraphPad Prism version 6 for Windows. $p \leq 0.001$ (***).

The slightly higher or equal proliferation rate of the SP compared to the SP-depleted MP cells analysed from MOS-R-1929 may be due to the repopulation of the SP-depleted MP cells by SP cells at the time of analysis during cell culture as shown in Figure 18. On the other hand, MOS-R-306 and MOS-S-184 SP cells showed lower proliferation activity compared to the SP-depleted MP cells. The major difference between these three cell lines is a different abundance of the SP fraction in unsorted cells. The MOS-R-1929 contains the highest SP fraction (~15%) compared to the MOS-R-306 and MOS-S-184 (less than 1%). Thus, to

achieve the initial distribution the SP cells of these different cell lines require different time to get diluted by SP-depleted MP cells. This indicates that to analyse proliferation rate of these cell populations additional time points would be required and these results should be interpreted with caution, since these cell populations might differ in metabolic activity.

4.1.5. Clonogenicity of side population and SP-depleted main population cells

The side population (SP) cells were analysed for their clonogenicity in comparison to the SP-depleted main population (MP) cells. Clonogenic potential of the SP and the SP-depleted MP sorted MOS-R-1929, MOS-R-306 and MOS-S-184 cells was tested with the serial dilution clonogenicity assay in 96 well plates.

MOS-R-1929 showed distinct clonogenic potential of both sorted SP and sorted SP-depleted MP cell populations. MOS-R-1929 SP cells led to 50% of wells containing growing cells when only 2 cells were plated per well (Figure 22). On the contrary, to achieve the same 50% cell success rate with the SP-depleted MP cells more than 8 cells per well were required (Figure 22).

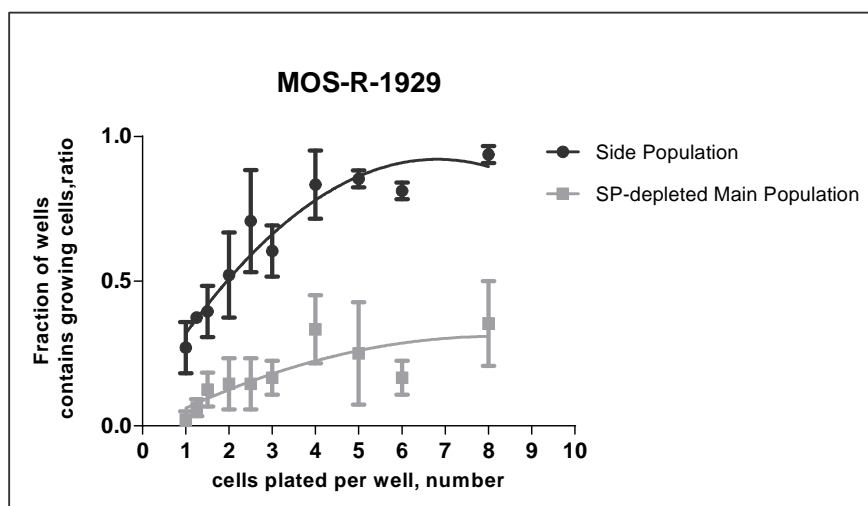


Figure 22: Serial dilution clonogenicity assay. The side population (SP) and the SP-depleted main population (SP-depleted MP) cells separated from MOS-R-1929 were plated in 96-well plate at different cell densities (cells range 1-8 and 100, 24 wells per each cell point.). At cell density as 100 cells per well all cell populations from all cell lines achieved growth in all 24 wells (data not shown). Experiment was performed right after sorting. Dot plots with trend lines are shown; error bars indicated standard deviations (n=2).

In the MOS-R-306 (Figure 23) and MOS-S-184 (Figure 24) cells the sorted SP cells did not show a large difference in clonogenicity to that of the SP-depleted MP cells. This may

indicate residual SP cells in the SP-depleted MP cells or more probably contamination of SP cells by non-SP cells due to the low SP fraction in these cell lines (Figure 14).

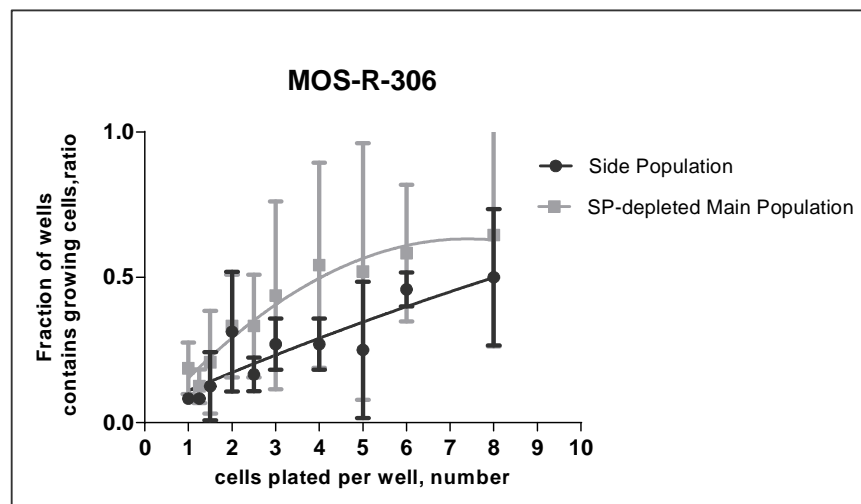


Figure 23: Serial dilution clonogenicity assay. The side population (SP) and the SP-depleted main population (SP-depleted MP) cells separated from MOS-R-306 were plated in 96-well plate at different cell densities (cells range 1-8 and 100, 24 wells per each cell point.). At cell density as 100 cells per well all cell populations from all cell lines achieved growth in all 24 wells (data not shown). Experiment was performed right after sorting. Dot plots with trend lines are shown; error bars indicated standard deviations (n=2).

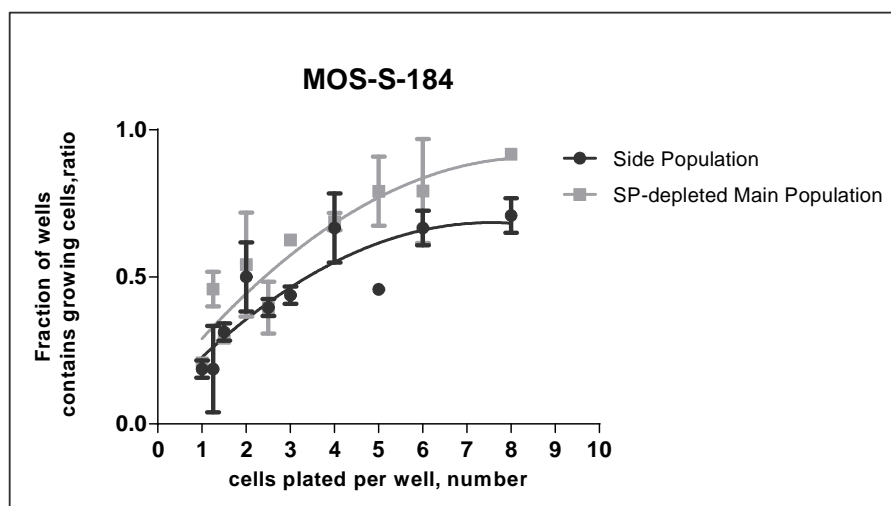


Figure 24: Serial dilution clonogenicity assay. The Side side population (SP) and the SP-depleted main population (SP-depleted MP) cells separated from MOS-S-184 were plated in 96-well plate at different cell densities (cells range 1-8 and 100, 24 wells per each cell point.). At cell density as 100 cells per well all cell populations from all cell lines achieved growth in all 24 wells (data not shown). Experiment was performed right after sorting. Dot plots with trend lines are shown; error bars indicated data from 2 technical replicates (n=1).

To determine the dilution where at least one cell was a clonogenic cell a Poisson distribution was used. The serial dilution is a random process and according to this the Poisson

distribution assumes that on average one clonogenic cell plated per well would lead to 63% of wells having at least one clonogenic cell and 37% of wells would be without any growing cells. The results are shown in Figure 25.

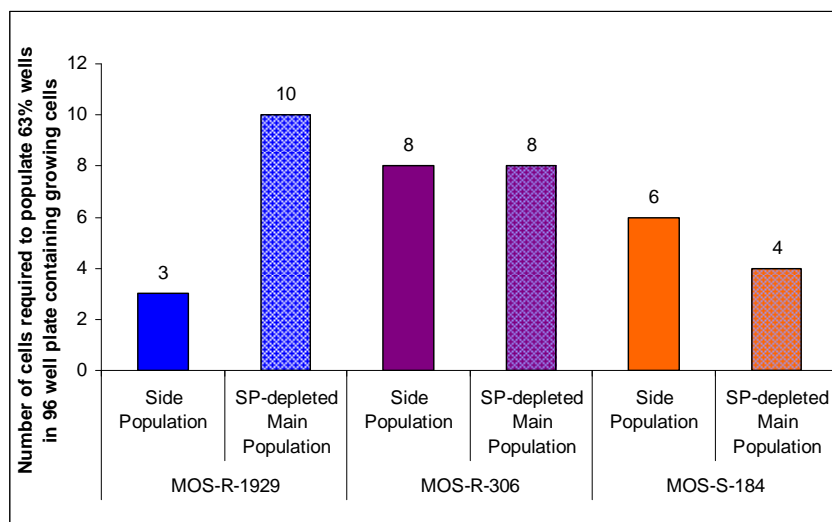


Figure 25: Clonogenic potential of side population (SP) and SP-depleted main population (SP-depleted MP) cells analysed with limiting dilution assay. On the figure the number of MOS-R-1929, MOS-R-306 and MOS-S-184 SP and SP-depleted MP cells seeded per well to populate 63% of wells with growing cells in 96-wells is shown. Mean values of at least 2 independent experiments (MOS-R-1929, MOS-R-306) and 1 independent experiment (MOS-S-184) are shown.

We observed that MOS-R-1929 SP cells required 3 cells to populate 63% wells with growing cells compared to the SP-depleted MP cells where more than 10 cells required to achieve the same results. This suggests the higher clonogenic potential of the MOS-R-1929 SP cells compared to SP-depleted MP cells.

4.1.6. *MOS cell line side population and SP-depleted main population cells differ in mRNA expression of markers present in embryonic and adult normal stem cells*

Embryonic and adult normal stem cells are both characterised by their expression of specific transcription factors involved in self-renewal and certain marker genes involved in early cell development. The side population (SP) cells sorted from MOS-R-1929 (Figure 27) and MOS-R-306 (Figure 26) were analysed for the expression of these genes to evaluate their identity as potential tumour initiating cells. After sorting, the SP and the SP-depleted main population (SP-depleted MP) cell populations were maintained in culture for 7 days. During this time cells recovered from sorting stress, and RNA was collected for the analysis.

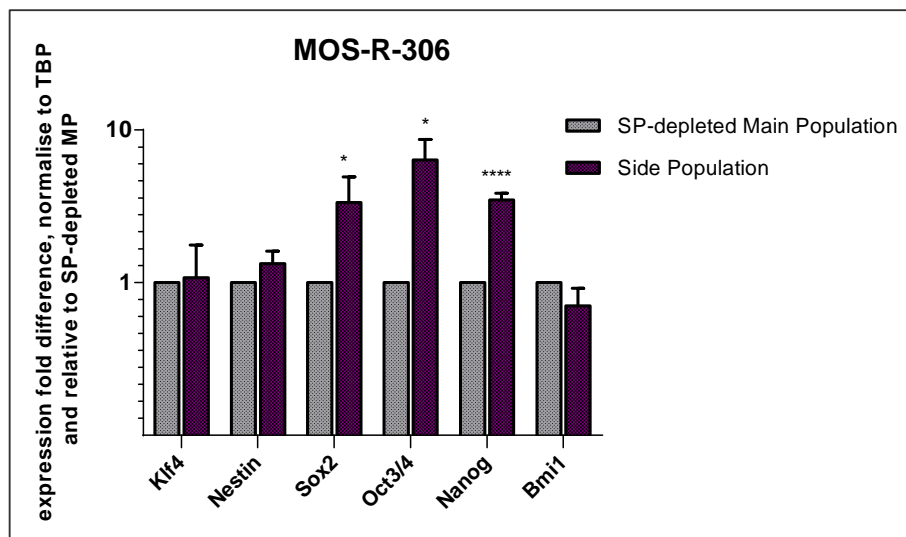


Figure 26: Semi-qRT-PCR expression analysis of candidate genes. Sorted MOS-R-306 side population (SP) and SP-depleted main population (SP-depleted MP) cells were analysed after 7 days in culture for the expression of embryonic and adult stem cells markers. The histograms show expression fold difference level of the SP cells normalised to TBP and relative to SP-depleted MP cells. Mean values and standard deviations are shown. At least 3 independent tests were performed, Oct3/4 only 2 experiments were done. Statistical evaluation of difference between SP and SP-depleted main population cells was done with 2way ANOVA with Sidak's test using GraphPad Prism version 6 for Windows. $p \leq 0.05$ (*), $p \leq 0.001$ (***)).

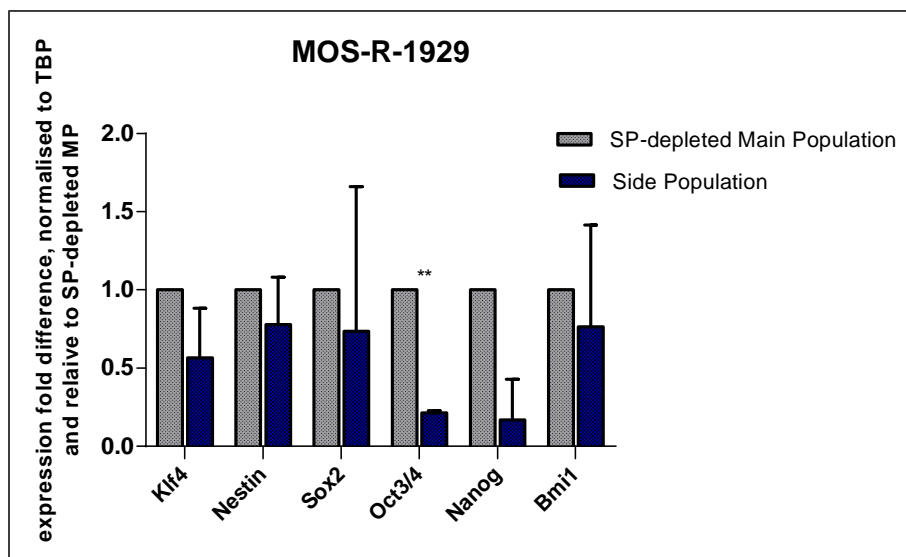


Figure 27: Semi-qRT-PCR expression analysis of candidate genes. Sorted MOS-R-1929 side population (SP) and SP-depleted main population (SP-depleted MP) cells were analysed after 7 days in culture for the expression of embryonic and adult stem cells markers. The histograms show expression fold difference level of the SP cells normalised to TBP and relative to representative SP-depleted MP cells. Mean values and standard deviations are shown. At least 3 independent tests were performed, Oct3/4 only 2 experiments were done. Statistical evaluation of difference between SP and SP-depleted main population cells was done with 2way ANOVA with Sidak's test using GraphPad Prism version 6 for Windows. $p \leq 0.01$ (**).

The SP cells sorted from MOS-R-306 showed a high level of expression of embryonic stem cells transcription factors Sox2, Oct3/4 and Nanog compared to SP-depleted MP cells. These findings support stem cells properties of MOS-R-306 SP cells. The SP cells sorted from MOS-R-306 did not show significant differences in expression of Klf4, Nestin or Bmi1, which are adult stem cells markers, when compared to the SP-depleted MP cells. The other tested cell line, MOS-R-1929, showed a trend to down-regulation of all markers in the SP cells compared to the SP-depleted MP cells with Oct3/4 being significantly down-regulated. Interestingly, when expression of “core transcription” factors was compared between MOS-R-306 SP and MOS-R-1929 SP cells no major difference in their expression was observed (Figure 28).

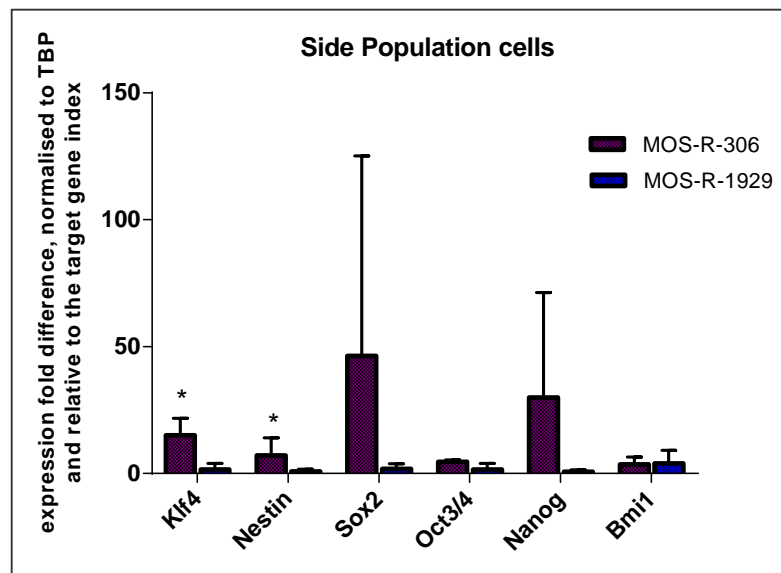


Figure 28: Semi-qRT-PCR expression analysis of candidate genes. The side population (SP) cells sorted from MOS-R-1929 and MOS-R-306 were analysed after 7 days in culture for the expression of embryonic and adult stem cells markers. Histograms show expression fold difference level of the SP normalised to TBP and relative to the target gene index. Mean values and standard deviations are shown. At least 3 independent tests were performed. Statistical evaluation of difference between cell lines was done with one-way ANOVA with Sidak’s test using GraphPad Prism version 6 for Windows. $p \leq 0.05$ (*).

Similar result was observed between MOS-R-306 SP-depleted MP and MOS-R-1929 SP-depleted MP cells (Figure 29).

On the other hand, the SP-depleted MP cells sorted from MOS-R-306 showed significant over-expression of adult stem cell marker Klf4 when compared to MOS-R-1929 SP-depleted MP cells (Figure 29). The similar over-expression was observed in MOS-R-306 SP cell compared to MOS-R-1929 SP cells (Figure 28). Together this may indicate that the side population cells origin may be heterogeneous.

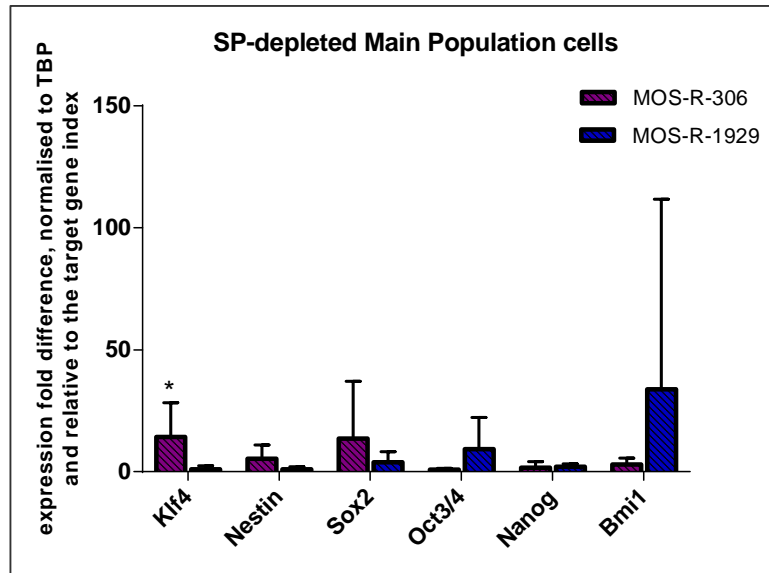


Figure 29: Semi-qRT-PCR expression analysis of candidate genes. The SP-depleted main population (SP-depleted MP) cells sorted from MOS-R-1929 and MOS-R-306 were analysed for the expression of embryonic and adult stem cells markers. Histograms show expression fold difference level of the SP depleted MP normalised to TBP and relative to the target gene index Mean values and standard deviations are shown. At least 3 independent tests were performed. Statistical evaluation of difference between cell lines was done with one-way ANOVA with Sidak's test using GraphPad Prism version 6 for Windows. $p \leq 0.05$ (*).

4.1.7. Correlation between the mRNA expression of markers present in embryonic and adult normal stem cells and the fraction of side population cells in unsorted MOS cell lines

Unsorted MOS cell lines were analysed for the expression of potential tumour initiating cells marker genes usually found in embryonic and adult stem cells in order to find out the potential correlation with their fraction of the SP cells.

We observed significant over-expression of both Sox2 (Figure 30) and Nanog (Figure 31) embryonic transcription factors in MOS-S-1403 compared to the other analysed MOS cell lines. This particular cell line does not contain many side population (SP) cells based on the flow cytometric analysis (SP fraction is ~0,2%), although it maintains continuous long-term proliferation during cell culture similar to the other MOS cell lines. Relative over-expression of Nanog compared to MOS-R-1929 and MOS-R-306 was also found in MOS-S-184 (Figure 31).

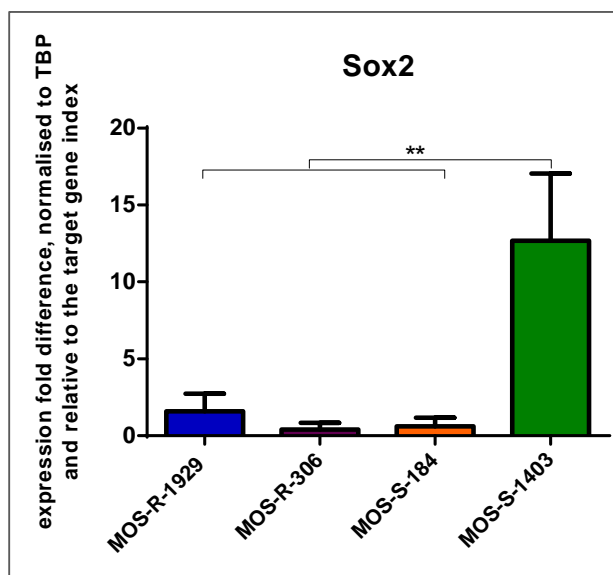


Figure 30: Semi-qRT-PCR expression profiles of expression of Sox2 in four MOS cell lines. The histograms show mRNA expression fold difference normalised to TBP and relative to the target gene index. Mean values and standard deviations are shown. At least 3 independent tests were performed. Statistical evaluation of difference between cell lines was done with one-way ANOVA with Tukey's test using GraphPad Prism version 6 for Windows. $p \leq 0.01$ (**).

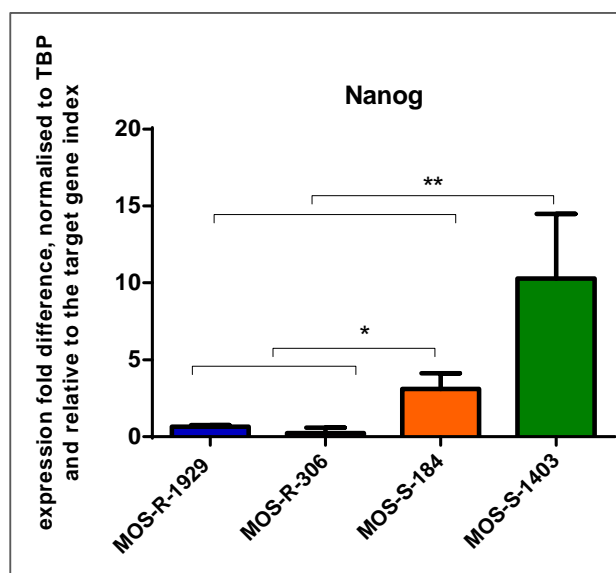


Figure 31: Semi-qRT-PCR expression profiles of expression of Nanog in four MOS cell lines. The histograms show mRNA expression fold difference normalised to TBP and relative to the target gene index. Mean values and standard deviations are shown. At least 3 independent tests were performed. Statistical evaluation of difference between cell lines was done with one-way ANOVA with Tukey's test using GraphPad Prism version 6 for Windows. $p \leq 0.01$ (**), $p \leq 0.05$ (*).

Differences in expression of the adult stem cells markers Bmi1 and Klf4 were not significant in the MOS cell lines (Figure 32 and Figure 33).

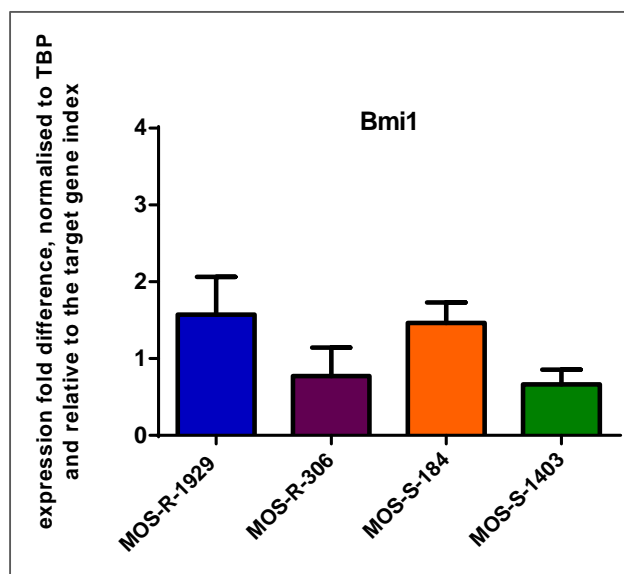


Figure 32: Semi-qRT-PCR expression profiles of expression of Bmi1 in four MOS cell lines. The histograms show mRNA expression fold difference normalised to TBP and relative to the target gene index. Mean values and standard deviations are shown. At least 3 independent tests were performed. Statistical evaluation of difference between cell lines was done with one-way ANOVA with Tukey's test using GraphPad Prism version 6 for Windows. No significant changes were detected.

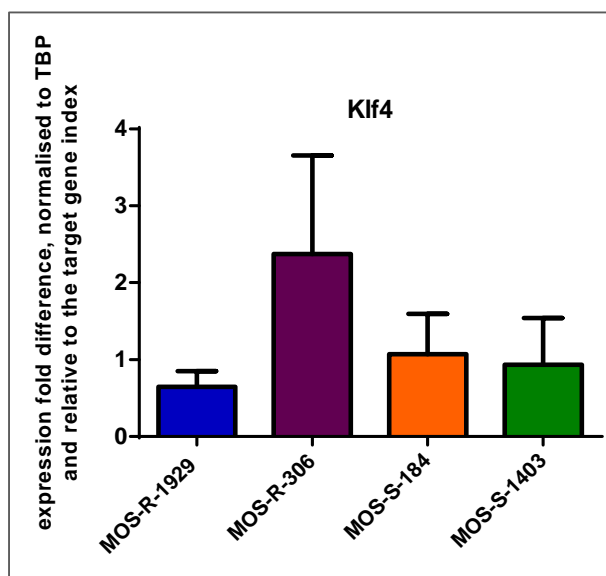


Figure 33: Semi-qRT-PCR expression profiles of expression of Klf4 in four MOS cell lines. The histograms show mRNA expression fold difference normalised to TBP and relative to the target gene index. Mean values and standard deviations are shown. At least 3 independent tests were performed. Statistical evaluation of difference between cell lines was done with one-way ANOVA with Tukey's test using GraphPad Prism for Windows. No significant changes were detected.

Another adult stem cell marker Nestin was found to be highly expressed in MOS-S-184 cells but to have relatively low expression in MOS-R-1929 cells (Figure 34).

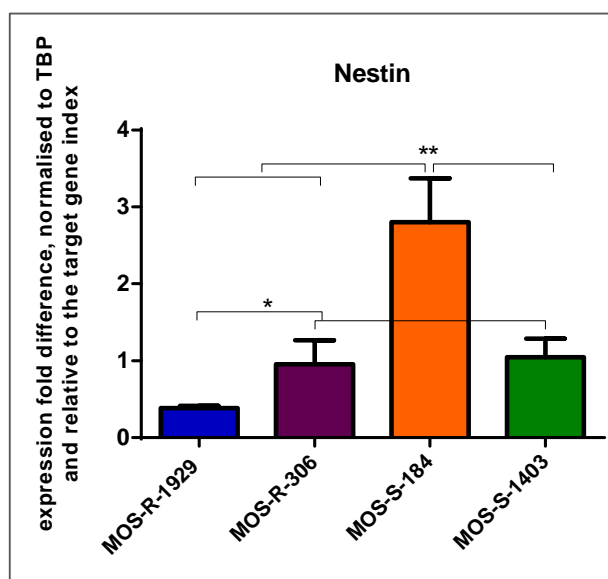


Figure 34: Semi-qRT-PCR expression profiles of expression of Nestin in four MOS cell lines. The histograms show mRNA expression fold difference normalised to TBP and relative to the target gene index. Mean values and standard deviations are shown. At least 3 independent tests were performed. Statistical evaluation of difference between cell lines was done with one-way ANOVA with Tukey's test using GraphPad Prism version 6 for Windows. $p \leq 0.01$ (**), $p \leq 0.05$ (*).

The analysed MOS cell lines did not show a correlation between expression of the stem cells markers Sox2, Nanog and Nestin and the size of the side population fraction of these cell lines (Figure 35), (Figure 36 and Figure 37).

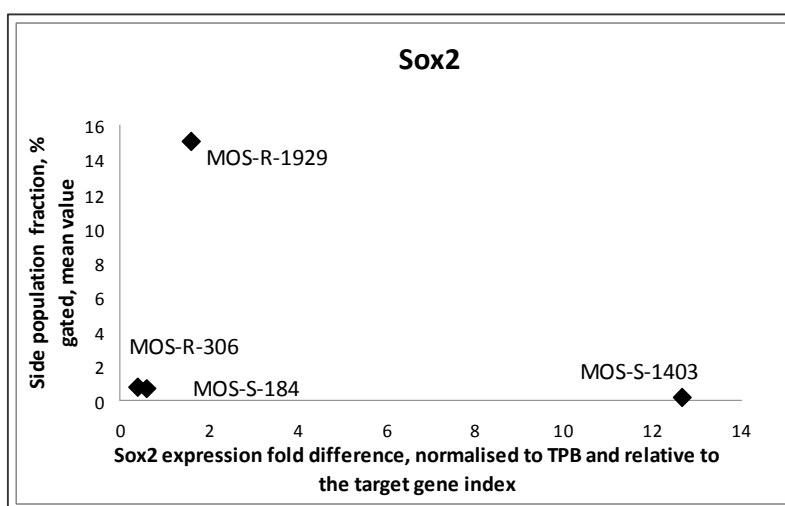


Figure 35: Correlation of the unsorted MOS cell lines side population (SP) fraction size and their expression of Sox2 stem cell marker. The vertical axis represents the side population fraction analysed with FACS, mean value from at least 6 independent experiments (Figure 14). Horizontal axis represents Sox2 expression fold difference between MOS cell lines, normalised to TBP and relative to the target gene index (Figure 30).

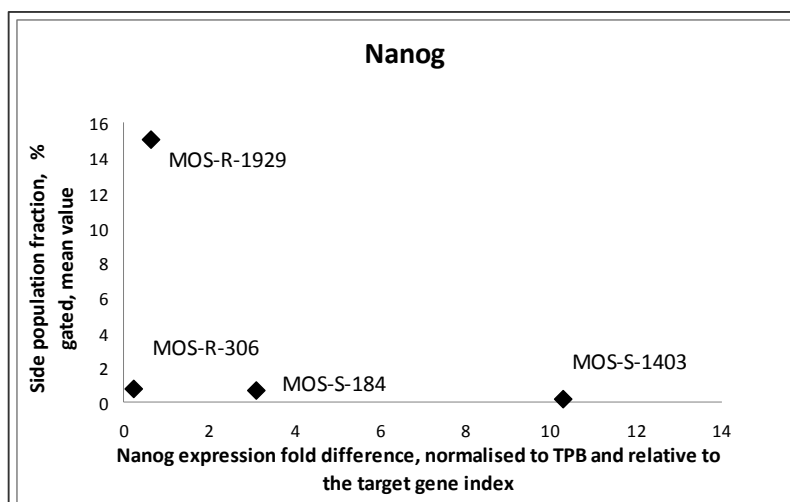


Figure 36: Correlation of the unsorted MOS cell lines side population (SP) fraction size and their expression of Nanog stem cell marker. The vertical axis represents the side population fraction analysed with FACS, mean value from at least 6 independent experiments (Figure 14). Horizontal axis represents Nanog expression fold difference between MOS cell lines, normalised to TBP and relative to the target gene index (Figure 31).

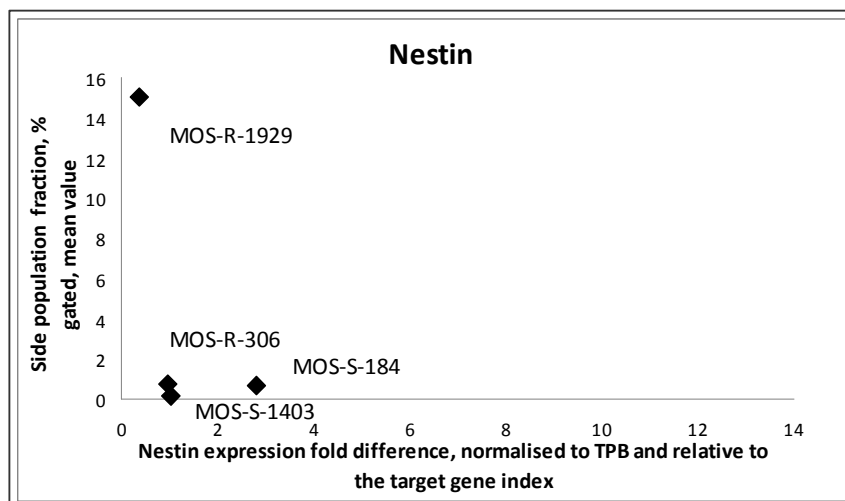
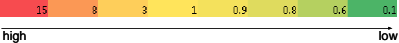


Figure 37: Correlation of the unsorted MOS cell lines side population (SP) fraction size and their expression of Nestin stem cell marker. The vertical axis represents the side population fraction analysed with FACS, mean value from at least 6 independent experiments (Figure 14). Horizontal axis represents Nestin expression fold difference between MOS cell lines, normalised to TBP and relative to the target gene index (Figure 34).

Expression of Sox2 and Nanog in MOS-R-1403 does not correlate with the SP cell numbers since the side population in this cell line is close to zero. A heat map of the stem cells markers expression and side population fractions is shown in Table 19 for all 4 MOS lines.

Table 19: Heat map of the stem cells marker expression fold difference (normalised to TBP and relative to the target gene index) and SP fraction of the MOS cells (mean values, %). Scale: . Scale:
 high low

	MOS-R-1929	MOS-R-306	MOS-S-184	MOS-S-1403
Sox2	1.6	0.4	0.6	12.7
Nanog	0.64	0.24	3.1	10.28
Bmi1	1.57	0.77	1.46	0.66
Klf4	0.64	2.37	1.07	0.93
Nestin	0.38	0.95	2.8	1.04
SP,%	15	0.75	0.67	0.14

4.1.8. Sox2 and Bmi1 protein expression in MOS cell lines

MOS cell lines were tested for Sox2 and Bmi1 protein expression. Proteins were collected for analysis during exponential cell growth phase in unsorted cells.

Detectable level of Sox2 protein was found on the immunoblot in MOS-S-1403. Yet MOS-R-1929, MOS-R-306 and MOS-S-184 did not show any detectable level of Sox2 expression (Figure 38).

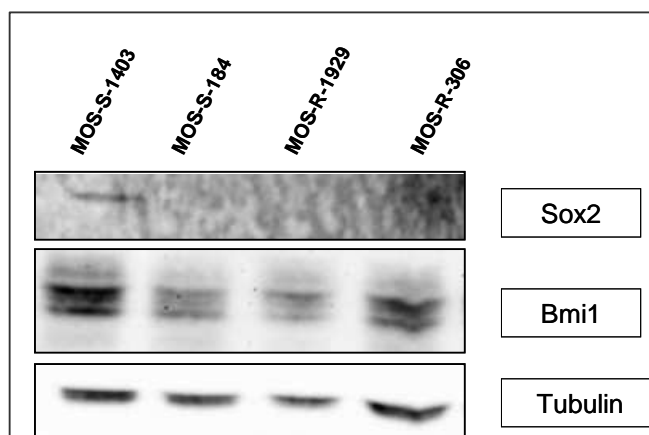


Figure 38: Western immunoblot analyses of Bmi1 (~35 kDa) and Sox2 (~34 kDa) protein expression of unsorted MOS cell lines. Bmi1 and Sox2 antibodies raised in different species were used to avoid cross reactivity. Tubulin (50 kDa) was used as a loading control.

Quantification of the Sox2 western blot protein level is shown in Figure 39.

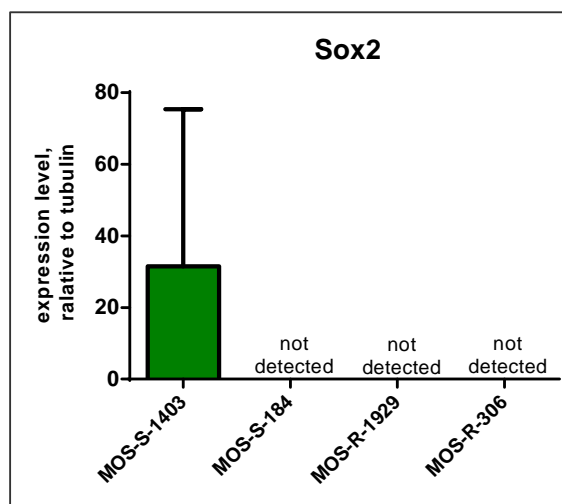


Figure 39: Sox2 quantification from the Western blot analysis. Histogram represents expression level relative to Tubulin. Mean value (n=2) and standard deviation are shown.

Protein expression of Bmi1 showed variations between experiments (Figure 40). A tendency to higher Bmi1 expression level in MOS-R-306, MOS-R-1929 and MOS-S-184 compared to the MOS-S-1403 was observed, but no significant differences were found (Figure 40).

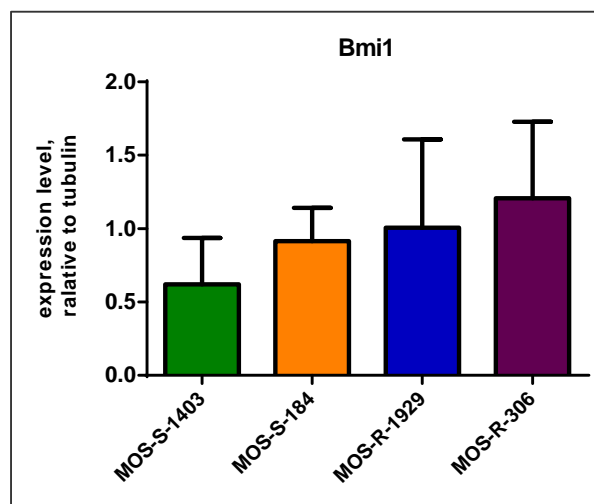


Figure 40: Bmi1 quantification from the Western blot analysis. Histograms represent expression level relative to Tubulin. Mean values (n=2) and standard deviations are shown. Statistical evaluation of difference between cell lines was done with one-way ANOVA with Sidak's test using GraphPad Prism version 6 for Windows. No significant changes were detected.

4.1.9. Overexpression of p53 protein in MOS-R-1929

From previous studies on MOS-R-1929 it was suspected that this cell line has a point mutation of the p53 gene, which leads to functional inactivation of the protein (Dr. Michael Rosemann, unpublished). In the present study, the protein level of p53 was analysed for all cell lines (Figure 41). Detectable p53 protein was found only in MOS-R-1929 cells, supporting previous findings that this cell line has a point mutation of p53 gene.

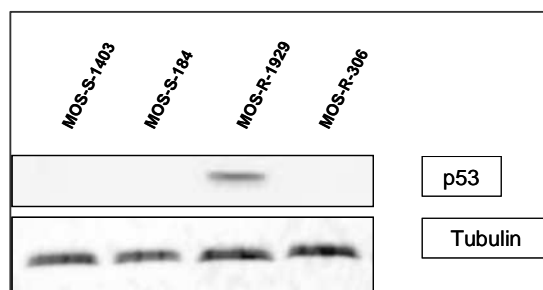


Figure 41: Western blot analysis of p53 (53 kDa) protein expression. Tubulin (50 kDa) was used as a loading control.

Quantification of the p53 western blot protein level is shown in Figure 42.

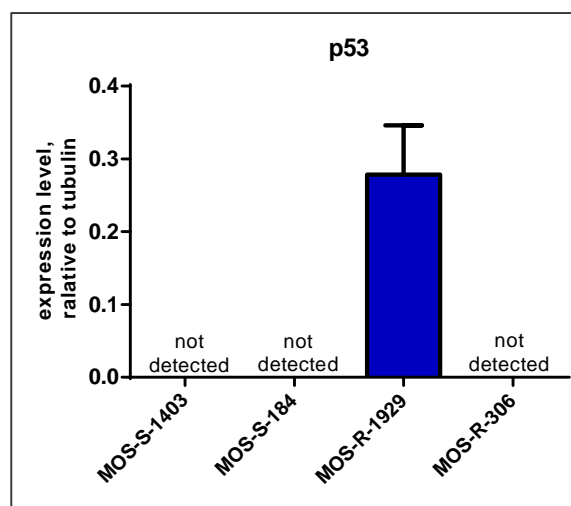


Figure 42: Western blot analysis of p53 (53 kDa) protein expression. Histogram represents quantification of p53 expression level relative to Tubulin. Mean value (n=3) and standard deviation are shown.

4.2. *Radiation sensitivity of MOS cell lines*

4.2.1. *Clonogenic survival of MOS cell lines*

The loss of reproductive potential of cell lines after ionising irradiation is normally tested with the clonogenic survival assay used as the “gold standard” method. As MOS cells do not form clearly distinguishable colonies we used an alternative method using limiting dilution with the endpoint being clonogenicity (Figure 43).

Of the four cell lines tested MOS-S-1403 and MOS-S-184 were more radiosensitive compared to MOS-R-306 and MOS-R-1929, both of which were relatively resistant to radiation. This difference is visible in the clonogenicity of the cell lines after 4Gy (p-value ≤ 0.01). After 8Gy the MOS-R-1929 cells show a significantly higher clonogenic potential compared to MOS-S-1403 (p-value ≤ 0.05). These data correspond well with the data of the side population fraction in MOS cell lines (Figure 14). MOS-R-1929 had on average 15% of TICs cells (Figure 14) whereas MOS-S-1403 did not contain as many SP cells (~0.14%). The other two tested cell lines MOS-R-306 and MOS-S-184 were comprised on average of less than 1% SP fraction cells (Figure 14).

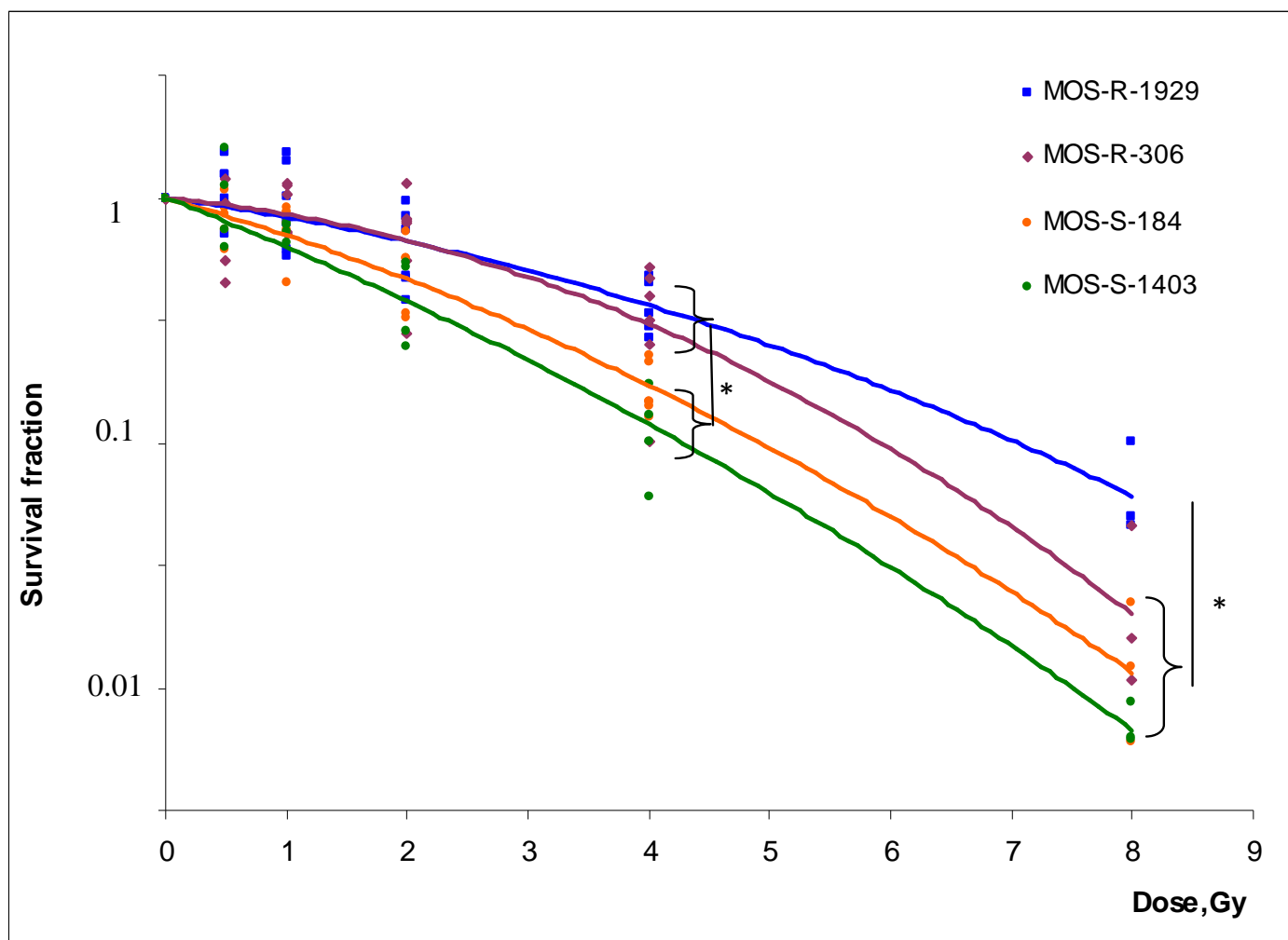


Figure 43: Limiting dilution assay of clonogenic survival. Cells were exposed to radiation and loss of clonogenicity assayed after 10 days. The data points are the individual results of at least 3 independent experiments. Survival fractions were fitted to the linear-quadratic function as $SF = \exp(-\alpha D - \beta D^2)$ as described in section 3.9.2. Results are shown in table 20. Statistical evaluation of difference between cell lines was done with one-way ANOVA with Tukey's and Holm-Sidak's tests. $p \leq 0.05$ (*)

Table 20: Clonogenic survival properties of MOS cell lines. α (alpha exponent value), β (beta exponent value) linear quadratic equation exponents of survival curves; LD ₅₀ and LD ₁₀ are cell inactivation doses in Gy; SF2 is a survival fraction at 2Gy.					
	α	β	LD ₅₀ (Gy)	D ₁₀ (Gy)	SF2
MOS-R-1929	0.07	0.01	3.02	7.04	0.66
MOS-R-306	0.05	0.02	2.68	5.50	0.65
MOS-S-184	0.14	0.01	1.83	4.91	0.46
MOS-S-1403	0.19	0.01	1.46	4.27	0.38

For the characterization of survival curves 4 different parameters were assessed. The alpha and beta terms i.e. the exponents of the linear quadratic equation, as well as LD₅₀ and D₁₀ i.e. the doses that inactivate 50% and 90% of the clonogenic cells respectively and the survival fraction after 2Gy of irradiation (SF2) (section 3.9.2.) are presented in Table 20. The alpha and beta values are considered to represent unreparable (α) and reparable (β) damage induced by radiation. The results show that the resistant and sensitive cell lines differ by more than two fold in their alpha exponents while the beta exponents are rather similar. The values of the alpha component for MOS-S-184 and even more prominent for MOS-S-1403 were found to be higher than for resistant cell lines. This suggests that the radiosensitivity of these cell lines may be due to accumulated non-reparable damage after irradiation, possibly by the insufficient repair of damage leading to residual chromosomal damage.

Sensitive and resistant cell lines also revealed differences in LD₅₀, which for MOS-S-1403 (1.46Gy) was half the dose of that for the resistant cell lines (~3Gy). LD₅₀ for MOS-S-184 was intermediate. The same observation was found for SF2, where MOS-S-1403 showed lower survival after 2Gy of radiation. The other sensitive cell lines, MOS-S-184, had not shown as prominent difference in LD₅₀ and SF2 values compared to resistant cell lines but was nevertheless lower in both LD₅₀ and LD₁₀ and SF2. High LD₁₀ values for resistant cell lines especially for MOS-R-1929 when compared for more radiosensitive MOS cell lines were found as well (Table 20).

We further compared the radiation sensitivity of MOS cell lines as LD₁₀ dose with their side population fractions. Figure 44 shows a direct correlation between the dose required to inactivate 90% of the cells and the side population fraction.

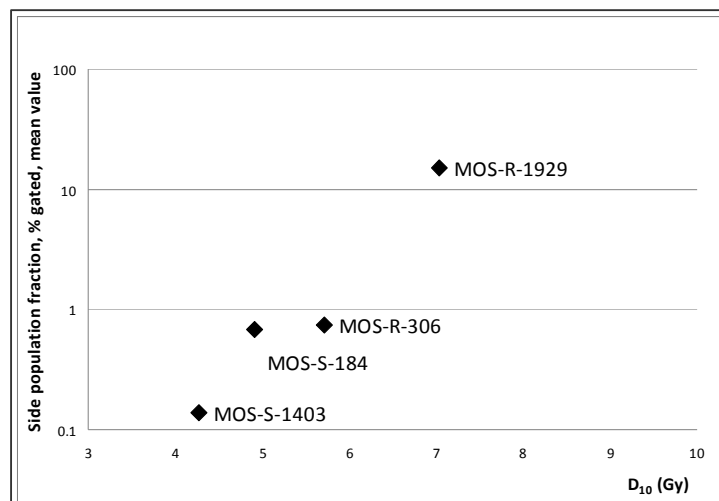


Figure 44: Clonogenic survival at D₁₀ comparison to the side population (SP) fraction in investigated MOS cell lines. Side population fraction represents mean value from at least 6 independent experiments (Figure 14). D₁₀ is a dose required to kill 90% of the cells calculated from linear quadratic fitted clonogenic survival curves (Table 20).

4.2.2. Comparison of the clonogenic survival after irradiation of side population and SP-depleted main population cells

The side population (SP) and the SP-depleted main population (SP-depleted MP) cell fractions were separated from MOS-R-1929, MOS-R-306 and MOS-S-184 cell culture based on the efflux of fluorescent Hoechst 33342 dye from the TIC cells. The radiation sensitivity of the separated cells was tested using the limiting dilution assay. The assay was performed immediately after sorting. For the SP-depleted MP cells, the number of plated cells was increased (10x) due to their reduced plating efficiency.

In the MOS-R-1929 cell line, the SP-depleted MP cells were significantly more radioresistant (at 8Gy $p \leq 0.05$) than the side population cells, contrary to our initial expectation that tumour initiating cells are radioresistant (Figure 45). The cell survival curve for unsorted MOS-R-1929 was placed between that of the SP and the SP-depleted MP cells (Figure 45).

The survival curves for the SP sorted cells from MOS-R-306 tested under identical conditions did not reveal a significantly higher radioresistance compared to the SP-depleted MP cells or to the unsorted cell population. The survival curves for MOS-R-306 are shown in Figure 46. The survival curve for MOS-S-184 SP cells shows greater sensitivity compared to MOS-S-184 unsorted and SP-depleted MP cells but as only one experiment was performed this result cannot be considered in the final evaluation (Figure 47).

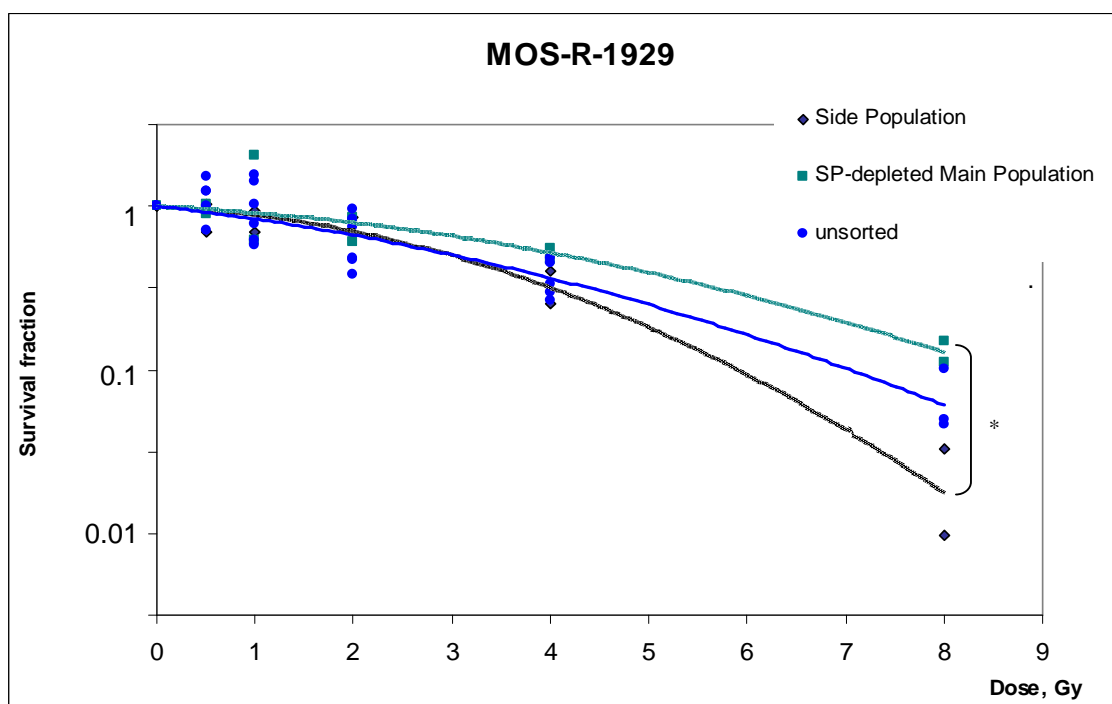


Figure 45: Limiting dilution assay of clonogenic survival for unsorted, SP and SP-depleted MP MOS-R-1929 cell line. Cells were exposed to radiation and clonogenicity assayed after 10 days. Survival fractions were fitted to the linear-quadratic function as $SF = \exp(-\alpha D - \beta D^2)$. The individual survival fractions from two independent experiments are shown ($n=2$). Statistical evaluation of difference between cell populations was done with one-way ANOVA with Turkey's test using GraphPad Prism version 6 for Windows. $p \leq 0.05$ (*).

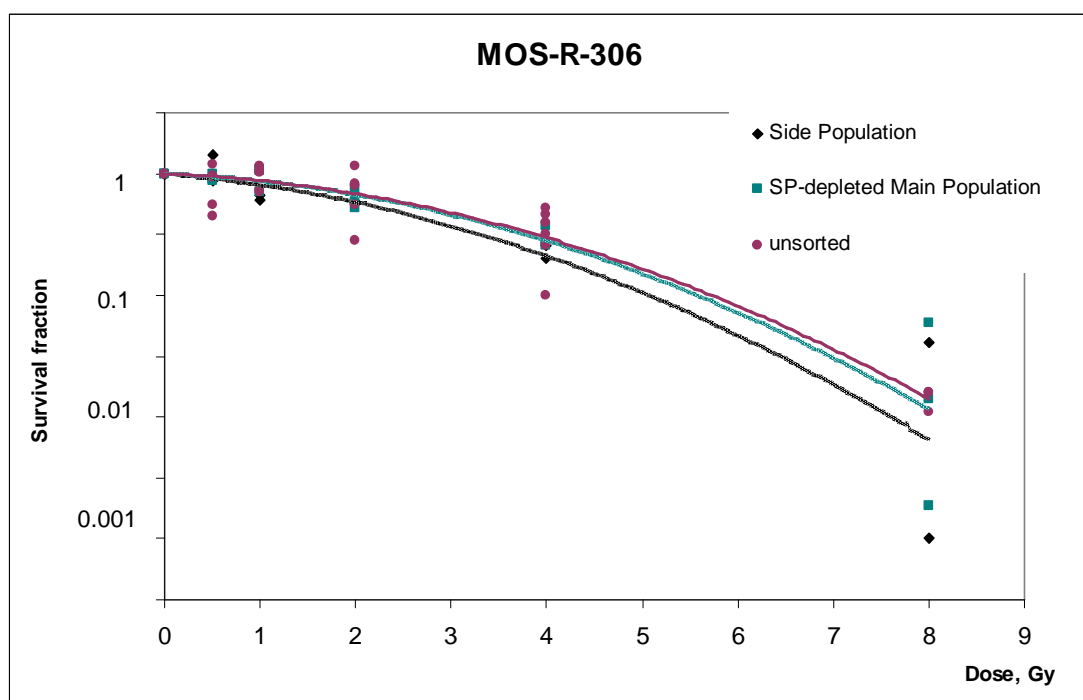


Figure 46: Limiting dilution assay of clonogenic survival for unsorted, SP and SP-depleted MP MOS-R-306 cell line. Cells were exposed to radiation and clonogenicity assayed after 10 days. Survival fractions were fitted to the linear-quadratic function as $SF = \exp(-\alpha D - \beta D^2)$. The individual survival fractions from two independent experiments are shown ($n=2$).

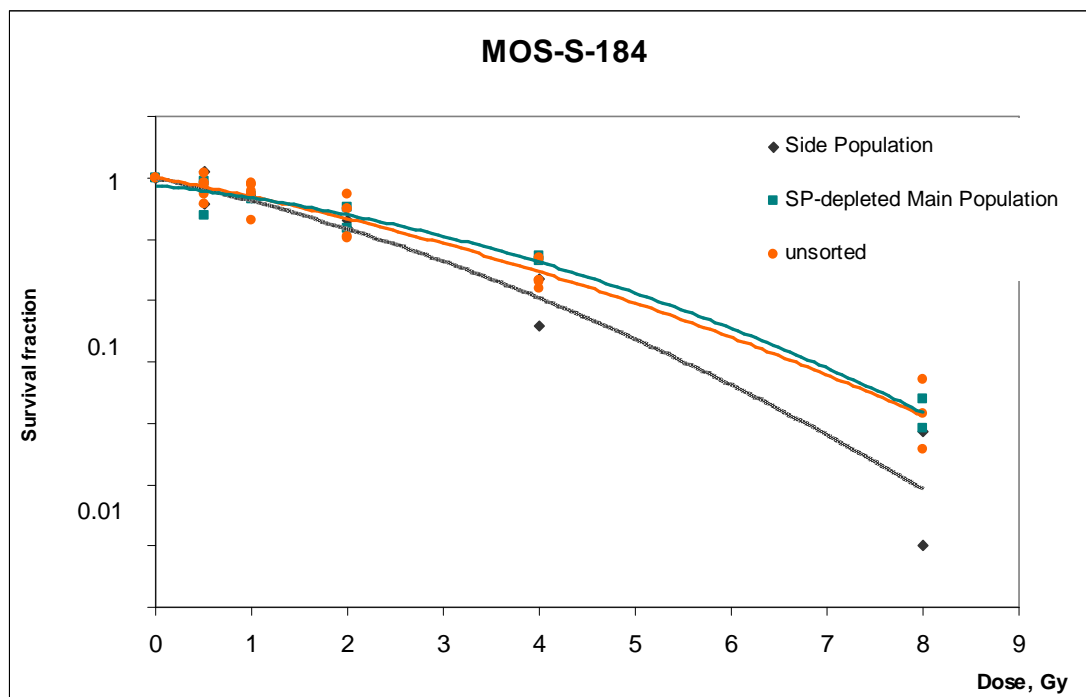


Figure 47: Limiting dilution assay of clonogenic survival for unsorted, SP and SP-depleted MP MOS-S-184 cell line. Cells were exposed to radiation and clonogenicity assayed after 10 days. Survival fractions were fitted to the linear-quadratic function as $SF = \exp(-\alpha D - \beta D^2)$. The individual survival fractions from two independent experiments are shown (two technical replicates, $n=1$).

The survival curves for the SP and the SP-depleted MP of MOS-R-1929 (Figure 45), MOS-R-306 (Figure 46) and MOS-S-184 (Figure 47) were also characterised for alpha and beta exponents, LD_{50} , LD_{10} and SF2 fraction (Table 21, Table 22, Table 23). Sorted SP and SP-depleted MP cell populations showed different alpha exponent while the beta exponent was found to be rather similar between the cell populations. This again may suggest a role of unrepaired DSBs damage influencing the cells radiosensitivity.

Table 21: Clonogenic survival properties of sorted MOS-R-1929 side population (SP) and MOS-R-1929 SP-depleted main population (SP-depleted MP) cells compared to unsorted cells. α (alpha exponent value), β (beta exponent value) linear quadratic equation exponents of survival curves; LD_{50} and LD_{10} are cell inactivation doses in Gy; SF2 is a survival fraction at 2Gy.					
	α	β	LD_{50} (Gy)	D_{10} (Gy)	SF2
MOS-R-1929	0.07	0.01	3.02	7.04	0.66
Side population	0.03	0.02	3.00	5.91	0.70
SP-depleted main population	0.03	0.01	3.99	8.35	0.77

MOS-R-1929 SP cells were characterized by a difference of 1.2 to 1.4 fold in their LD_{10} radiosensitivity compared to unsorted or SP-depleted MP cells respectively (Table 21). Also

SP-depleted MP cells showed slightly higher LD₅₀ and SF2 values compared to the unsorted and SP cells. MOS-R-306 SP cells showed slightly lower LD₅₀, LD₁₀ and SF2 values compared to SP-depleted MP and unsorted cell (Table 22). The same values were found to be slightly low for the MOS-S-184 SP cells compared to the unsorted and SP-depleted MP cells (Table 23).

Table 22: Clonogenic survival properties of sorted MOS-R-306 side population (SP) and MOS-R-306 SP-depleted main population (SP-depleted MP) cells compared to unsorted cells. α (alpha exponent value), β (beta exponent value) linear quadratic equation exponents of survival curves; LD ₅₀ and LD ₁₀ are cell inactivation doses in Gy; SF2 is a survival fraction at 2Gy.					
	α	β	LD ₅₀ (Gy)	D ₁₀ (Gy)	SF2
MOS-R-306	0.05	0.02	2.68	5.50	0.65
Side population	0.06	0.03	2.37	5.08	0.58
SP-depleted main population	0.03	0.03	2.81	5.59	0.67

Table 23: Clonogenic survival properties of sorted MOS-R-184 side population (SP) and MOS-S-184 SP-depleted main population (SP-depleted MP) cells compared to unsorted cells. α (alpha exponent value), β (beta exponent value) linear quadratic equation exponents of survival curves; LD ₅₀ and LD ₁₀ are cell inactivation doses in Gy; SF2 is a survival fraction at 2Gy.					
	α	β	LD ₅₀ (Gy)	D ₁₀ (Gy)	SF2
MOS-S-184	0.14	0.01	1.83	4.91	0.46
Side population	0.17	0.02	1.51	4.07	0.38
SP-depleted main population	0.08	0.02	2.38	5.44	0.58

4.2.3. Radiation-induced DNA double strand breaks after ionising irradiation in MOS cells

Detection of radiation-induced DNA double strand breaks (DSBs) was performed using immunofluorescent staining of DNA repair foci with the γ H2AX and 53BP1 antibodies in MOS-R-306, MOS-R-1929, MOS-S-184 and MOS-S-1403 cells. An example of stained cells is shown in Figure 48 where unirradiated, 1 and 2 Gy irradiated MOS-R-306 and MOS-S-184 cells are shown. For the evaluation of the radiation-induced DNA DSBs only double stained (yellow) signals were taken into account. Foci stained only for the phosphorylation of histone H2AX (γ H2AX) did not give reliable data due to the high background level of signals after single antibody staining which is in accordance with the literature (Markova et al, 2007) (Figure 48).

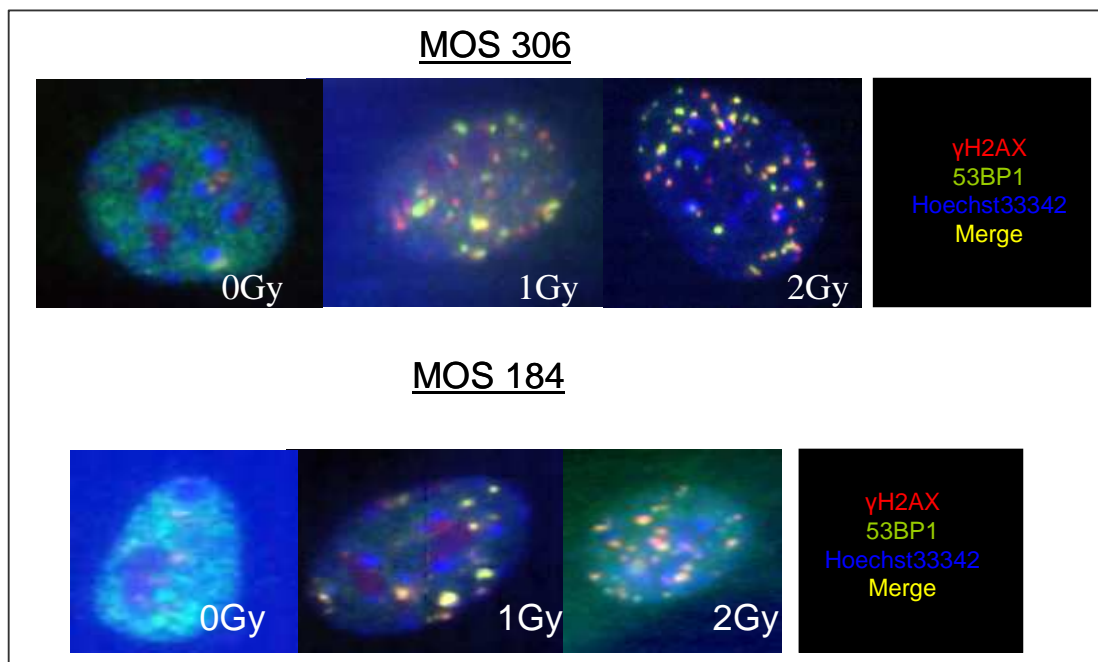


Figure 48: Representative images of MOS-R-306 and MOS-S-184 cells stained for γ H2AX and 53BP1 90 minutes after 1 and 2Gy of gamma irradiation. Colour code is blue: Hoechst 33342 staining, red: γ H2AX staining, green: 53BP1 staining, yellow: co-localization of γ H2AX and 53BP1 signals.

Co-localized γ H2AX and 53BP1 signals after induction of DNA DSBs were counted and plotted in a linear mode (Figure 49). All tested cell lines showed a dose dependent linear correlation between the number of DNA DSBs foci present at 90 minutes per cell and the radiation dose delivered.

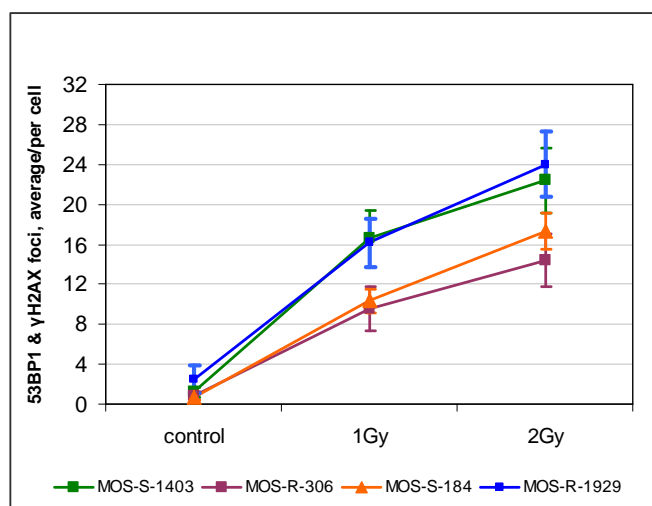


Figure 49: Dose dependent radiation-induced DNA DSBs (53BP1/ γ H2AX foci) analyzed 90 minutes after gamma irradiation. Mean values and standard deviations of 3 experiments are shown. At least 250 cells were counted for each dose point.

The difference in the radiation-induced DNA DSBs between MOS cell lines might have different reasons such as variations in chromatin structure or ploidy DNA content. Yet in the present study these was not analysed.

For the repair of DNA DSBs kinetics co-localized γ H2AX and 53BP1 signals at different times (90 minutes to 1440 minutes range) after 1Gy of γ -irradiation were counted and plotted using a log-linear scale, normalised to 100% at 90 minutes (Figure 50).

Two phases (fast and late slow) of repair were distinguished in three of the four MOS cell lines (MOS-R-306, MOS-S-184 and MOS-S-1403). The fast phase of repair was present between 90 minutes and 420 minutes after irradiation, whereas the slow phase of repair was present between 420 minutes and 1440 minutes after 1Gy of irradiation. In MOS-R-1929 no difference in the rate of reduction of the number of DNA DSBs foci between slow and fast phases of repair was found (Figure 50). Half repair times ($t_{1/2}$) of a foci regression were calculated for fast and slow repair for the MOS cell lines (Table 24). The calculations are shown in section 3.10.2.

Table 24: Half time ($t_{1/2}$) of repair of radiation-induced DNA DSBs in MOS cell lines. Mean values \pm standard deviations are present (n=3).		
	$t_{1/2}$, minutes (min)	
	fast phase of repair, min	slow phase of repair, min
MOS-R-1929	233 \pm 0.5	350 \pm 0.5
MOS-R-306	157 \pm 17	1050 \pm 350
MOS-S-184	140 \pm 0.5	1749 \pm 583
MOS-S-1403	157 \pm 17	875 \pm 525

The distribution of radiation-induced DNA DSBs after 1Gy 90 minutes is shown in a dot plot in Figure 51. The result is in accordance with previous data shown in Figure 49.

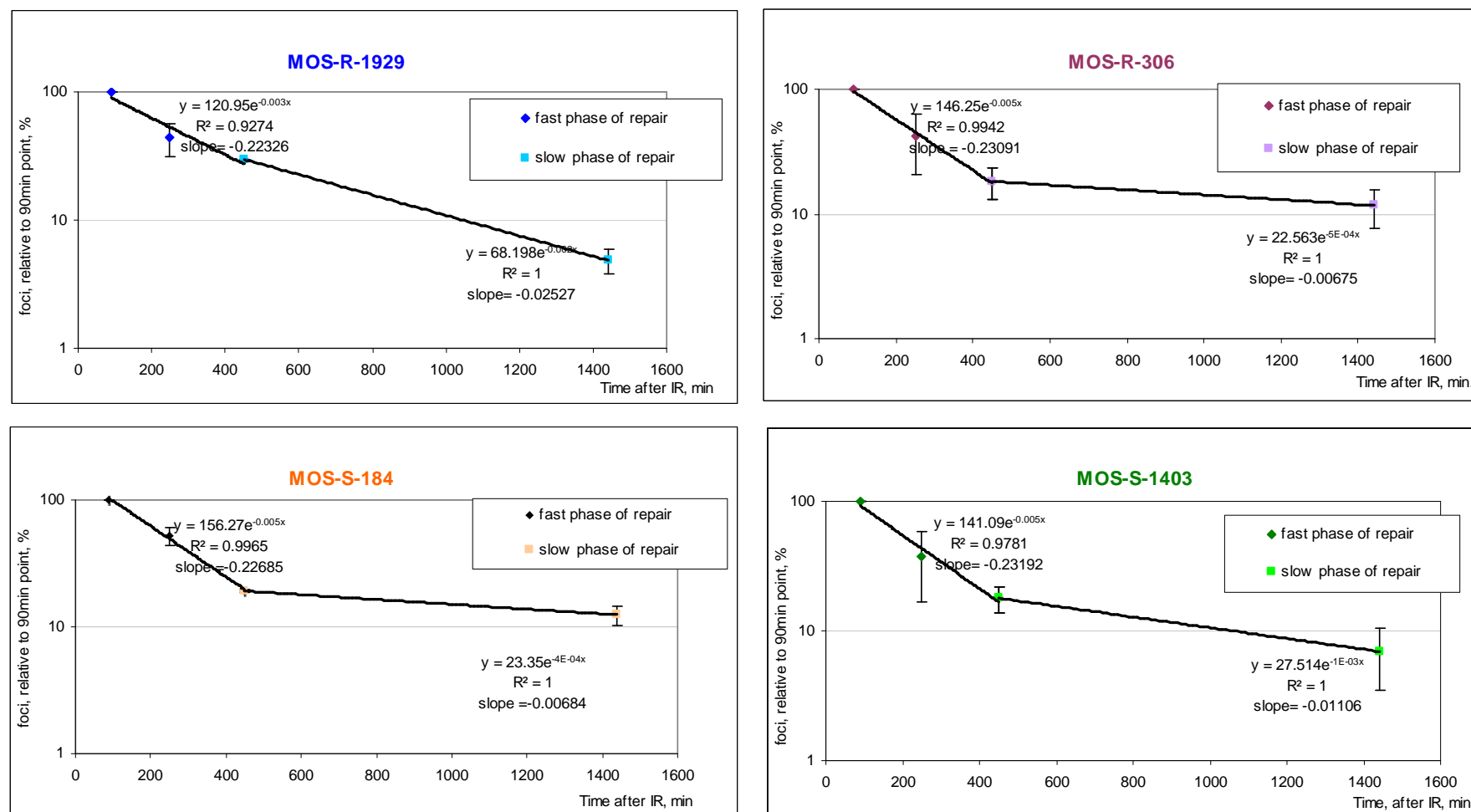


Figure 50: DNA DSBs repair kinetics in the 4 MOS cell lines. Radiation-induced DNA DSBs (53BP1/ γ H2AX foci) were analyzed between 90 and 1440 minutes after 1Gy of γ -irradiation. Mean values and standard deviations of 3 experiments are shown.

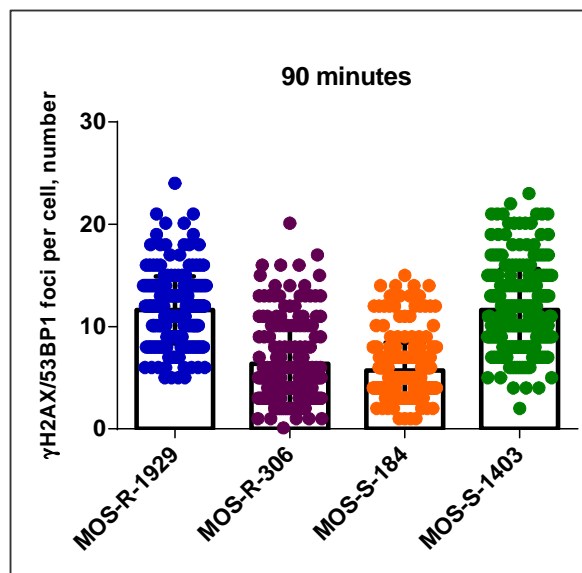


Figure 51: DNA DSBs radiation-induced foci remaining in individual cells 90 minutes after 1Gy of irradiation. Each dot represents one cell counted. At least 250 cells for each cell line are shown. Dots with equal number are over-lapping. Bars represent mean values and standard deviations.

The distribution of the residual unrepaired radiation-induced DNA DSBs damage after 1Gy 1440 minutes of repair time is shown in a dot plot Figure 52.

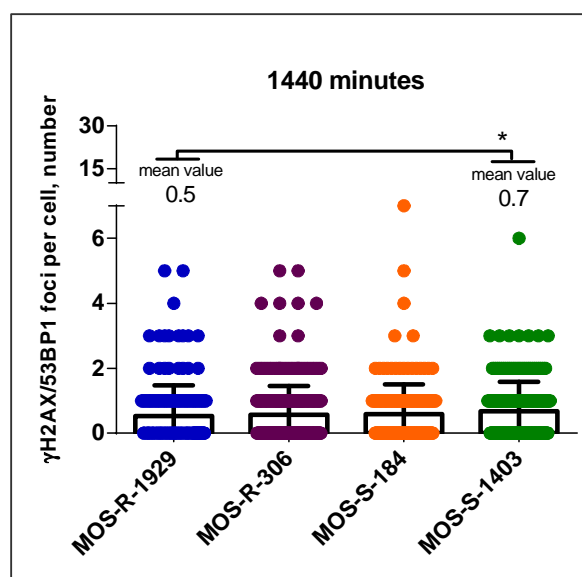


Figure 52: Residual DNA DSBs foci remaining in individual cells after 1440 minutes repair time after 1Gy of irradiation. Each dot represents one cell counted. At least 250 cells for each cell line are shown. Dots with equal number are over-lapping. Bars represent mean values and standard deviations. Statistical evaluation of difference between cell lines was done with nonparametric Mann-Whitney ranking test using GraphPad Prism version 6 for Windows. $p \leq 0.05$ (*).

MOS cell lines show a range of DNA DSBs repair rates (Table 24). We observe a slight correlation between the amount of residual unrepaired foci after radiation and the clonogenic survival curve in radiosensitive MOS-S-1403 compared to the more radioresistant MOS-R-1929 cell line (Figure 52, Table 25). There was no significant correlation between the number of unrepaired DNA DSBs and the α exponent (the low dose exponential slope) of the survival curve after 1440 minutes (24 hours) (Table 25, Figure 53).

Table 25: Slight correlation between radiosensitivity and unrepaired residual DNA DSBs and no correlation with the α exponent of the survival curve in 4 MOS cell lines.		
	α exponent	Unrepaired (residual) DSBs, mean per cell line
MOS-R-1929	0.07	0.5
MOS-R-306	0.05	0.6
MOS-S-184	0.14	0.6
MOS-S-1403	0.19	0.7

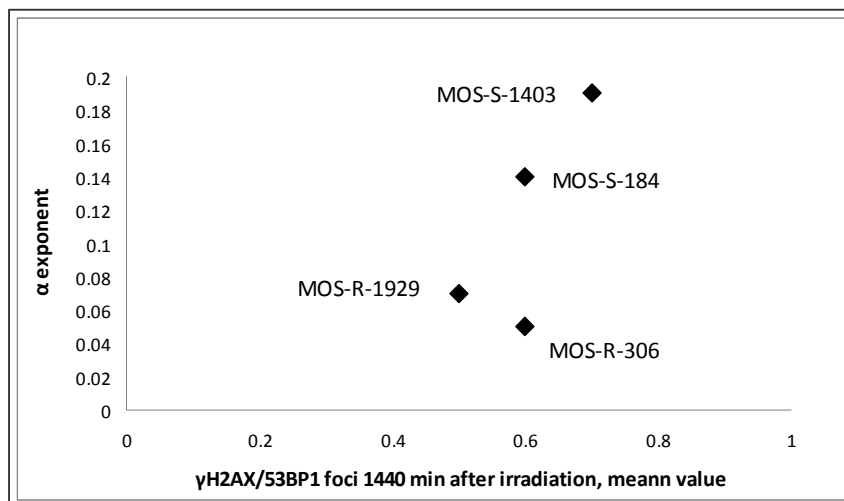


Figure 53: Comparison to the residual DNA DSBs foci after 1440 minutes repair time after 1Gy of irradiation (see Figure 52, Table 25) and the clonogenic curve α exponent (Table 20) of the MOS cell lines.

4.2.4. Change in the expression of stem cell markers after irradiation of MOS cell lines

The four MOS cell lines were tested for change in the expression of the selected embryonic and adult stem cell markers after ionising irradiation. Cells were irradiated at 4Gy of γ -irradiation and mRNA was collected after 2 hours of recovery at 37°C in incubator.

Significant up-regulation of Sox2 in all cell lines was found (Figure 54). MOS-S-1403 has a tendency for the up-regulation of Nanog (Figure 55), Bmi1 (Figure 57) and Klf4 (Figure 58) markers after irradiation, however changes were not significant.

The other cell lines did not show significant up or down regulation neither of Nanog (Figure 55), Nestin (Figure 56), Bmi1 (Figure 57) nor Klf4 (Figure 58) tested candidate markers.

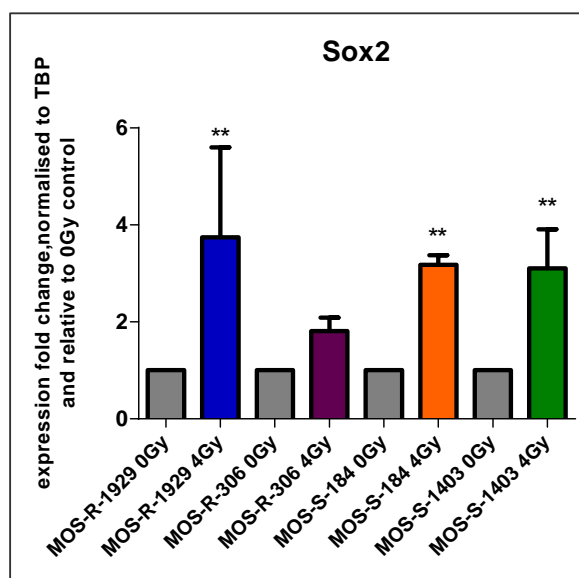


Figure 54: Semi-qRT-PCR analyse of candidate genes expression change after radiation. Four MOS cell lines were analysed for the change of expression of Sox2 (in 2 hours after 4Gy of γ -irradiation). Histograms show mRNA expression fold change level normalised to TBP and relative to unirradiated control (0Gy). Mean values and standard deviations are shown. At least 3 independent tests were performed. Statistical evaluation of difference between irradiated and control cells was done with one-way ANOVA with Sidak's test using GraphPad Prism version 6 for Windows. $p \leq 0.01$ (**).

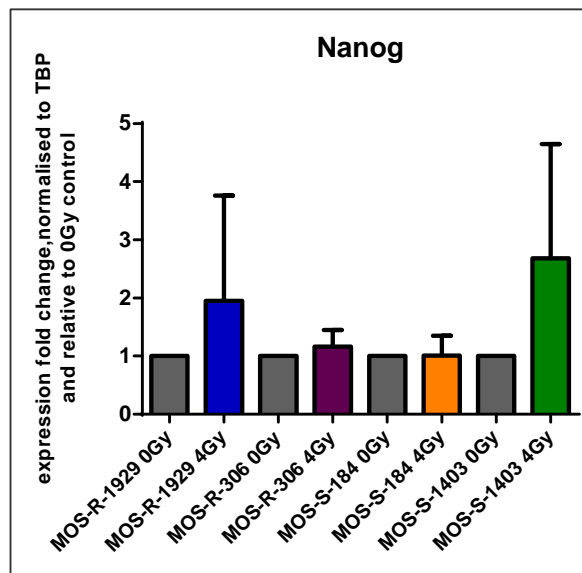


Figure 55: Semi-qRT-PCR analysis of candidate genes expression change after radiation. Four MOS cell lines were analysed for the change of expression of Nanog (in 2 hours after 4Gy of γ -irradiation). Histogram shows mRNA expression fold change level normalised to TBP and relative to unirradiated control (0Gy). Mean values and standard deviations are shown. At least 3 independent tests were performed. Statistical evaluation of difference between irradiated and control cells was done with one-way ANOVA with Sidak's test using GraphPad Prism version 6 for Windows. No significant changes were detected.

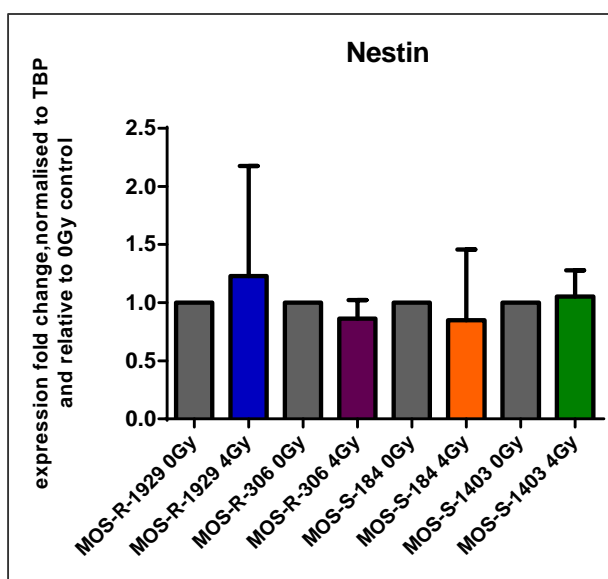


Figure 56: Semi-qRT-PCR analysis of candidate genes expression change after radiation. Four MOS cell lines were analysed for the change of expression of Nestin (in 2 hours after 4Gy of γ -irradiation). Histogram shows mRNA expression fold change level normalised to TBP and relative to unirradiated control (0Gy). Mean values and standard deviations are shown. At least 3 independent tests were performed. Statistical evaluation of difference between irradiated and control cells was done with one-way ANOVA with Sidak's test using GraphPad Prism version 6 for Windows. No significant changes were detected.

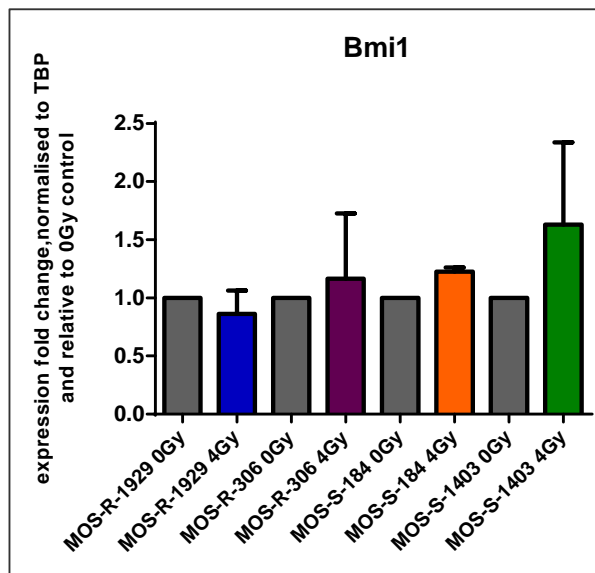


Figure 57: Semi-qRT-PCR analyse of candidate genes expression change after radiation. Four MOS cell lines were analysed for the change of expression of Bmi1 (in 2 hours after 4Gy of γ -irradiation). Histogram shows mRNA expression fold change level normalised to TBP and relative to unirradiated control (0Gy). Mean values and standard deviations are shown. At least 3 independent tests were performed. Statistical evaluation of difference between irradiated and control cells was done with one-way ANOVA with Sidak's test using GraphPad Prism version 6 for Windows. No significant changes were detected.

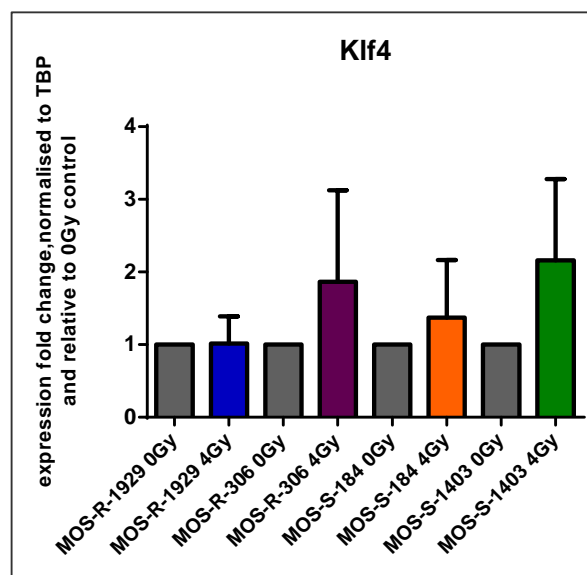


Figure 58: Semi-qRT-PCR analyse of candidate genes expression change after radiation. Four MOS cell lines were analysed for the change of expression of Klf4 (in 2 hours after 4Gy of γ -irradiation). Histogram shows mRNA expression fold change level normalised to TBP and relative to unirradiated control (0Gy). Mean values and standard deviations are shown. At least 3 independent tests were performed. Statistical evaluation of difference between irradiated and control cells was done with one-way ANOVA with Sidak's test using GraphPad Prism version 6 for Windows. No significant changes were detected.

4.2.5. Sox2 and Bmi1 expression change after irradiation in MOS cell lines (western blot)

Sox2 and Bmi1 expression changes were tested at the protein level (western blot). Protein samples were collected 2 hours after 4Gy of γ -irradiation. Detectable level of Sox2 protein was found in MOS-S-1403 (Figure 59); the other cell lines did not show detectable levels in either control or treated samples (Figure 59, Table 26). None of the MOS cell lines show Bmi1 expression change after irradiation (Figure 60).

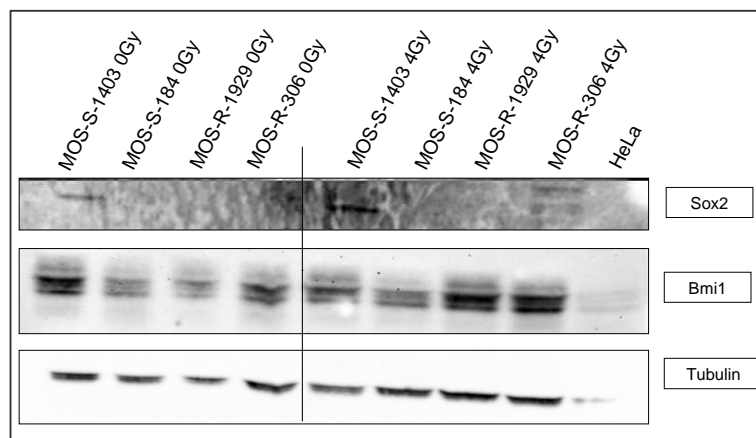


Figure 59: Bmi1 (~35 kDa) and Sox2 (~34 kDa) protein immunoblot analysis of MOS cell lines after irradiation. Bmi1 and Sox2 antibody belong to different species to avoid cross reactivity. Tubulin (50 kDa) was used as a loading control.

Table 26: Western blot Sox2 (n=1) and Bmi1 (n=3) protein levels ratio to Tubulin protein levels (mean value \pm standard deviation)			
treatment	MOS cell line	Sox2	Bmi1
Control (0Gy)	MOS-S-1403	0.08	0.56 \pm 0.36
	MOS-S-184	-	0.91 \pm 0.74
	MOS-R-1929	-	0.76 \pm 0.58
	MOS-R-306	-	0.89 \pm 0.59
Irradiated (4Gy)	MOS-S-1403	0.07	0.64 \pm 0.46
	MOS-S-184	-	0.75 \pm 0.48
	MOS-R-1929	-	0.69 \pm 0.41
	MOS-R-306	-	0.82 \pm 0.58

The quantification of the expression level change of Bmi1 is shown in Figure 60.

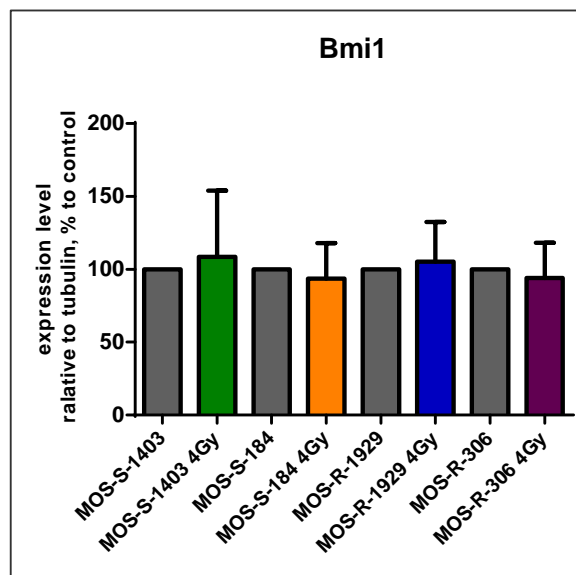


Figure 60: Quantification of Western blot analysis of Bmi1 expression expressed as a change after irradiation. Histograms represent expression levels normalised to Tubulin and expressed as a percentage of control (0Gy). Mean values and standard deviations are shown (n=3). Statistical evaluation was done with one-way ANOVA with Sidak's test using GraphPad Prism version 6 for Windows. No significant changes were detected.

4.3. Generation of an *in vivo* mouse osteosarcoma model

MOS-R-306 cells were stably transfected with pCAG-tdTomato red fluorescence protein (RFP). Stable transfected single cell clones were obtained by the limiting dilution techniques. In order to tell whether transfection have an influence on radiosensitivity, the influence of the pCAG-tdTomato transfection on the MOS cells characteristic properties was examined by analysis of radiation-induced DSBs in both untransfected and transfected cells. The result of this study is shown in Figure 61. There were no significant differences between analysed cells neither in unirradiated cell nor in 1Gy and 2Gy irradiated cells. For the *in vivo* pilot study, MOS-R-306 cells transfected with pCAG-tdTomato were injected subcutaneously into 3 syngenic mice. Work-flow is shown in Figure 62. At day 12 post injection tumour growth was observed in all mice and epi-fluorescent images were taken. In 2 of 3 cases tumour-like formations could be successfully visualised and in one case the tumour-like formation did not give any fluorescent signal. All growths were histologically examined (collaboration Institute of Pathology, Helmholtz Zentrum Munich). In the two cases were fluorescence was detected

tumours were proved to be osteosarcomas (Figure 63). In the one case where fluorescence was not detected tumour-like formation showed sign of inflammation.

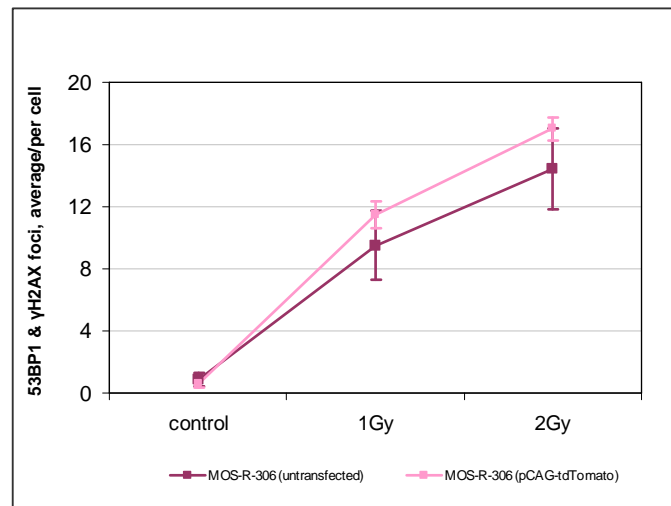


Figure 61: No difference in dose dependent increase of radiation-induced DNA DSBs (53BP1/γH2AX foci) between MOS-R-306 untransfected cells and MOS-R-306 transfected with RFP plasmid (MOS-R-306, pCAG-tdTomato) as analyzed 90 minutes after gamma irradiation. Mean values and standard deviations of 3 experiments (MOS-R-306, untransfected) and 2 technical replicates (MOS-R-306, pCAG-tdTomato) are shown. Statistical evaluation was done with unpaired t test using GraphPad Prism version 6 for Windows.

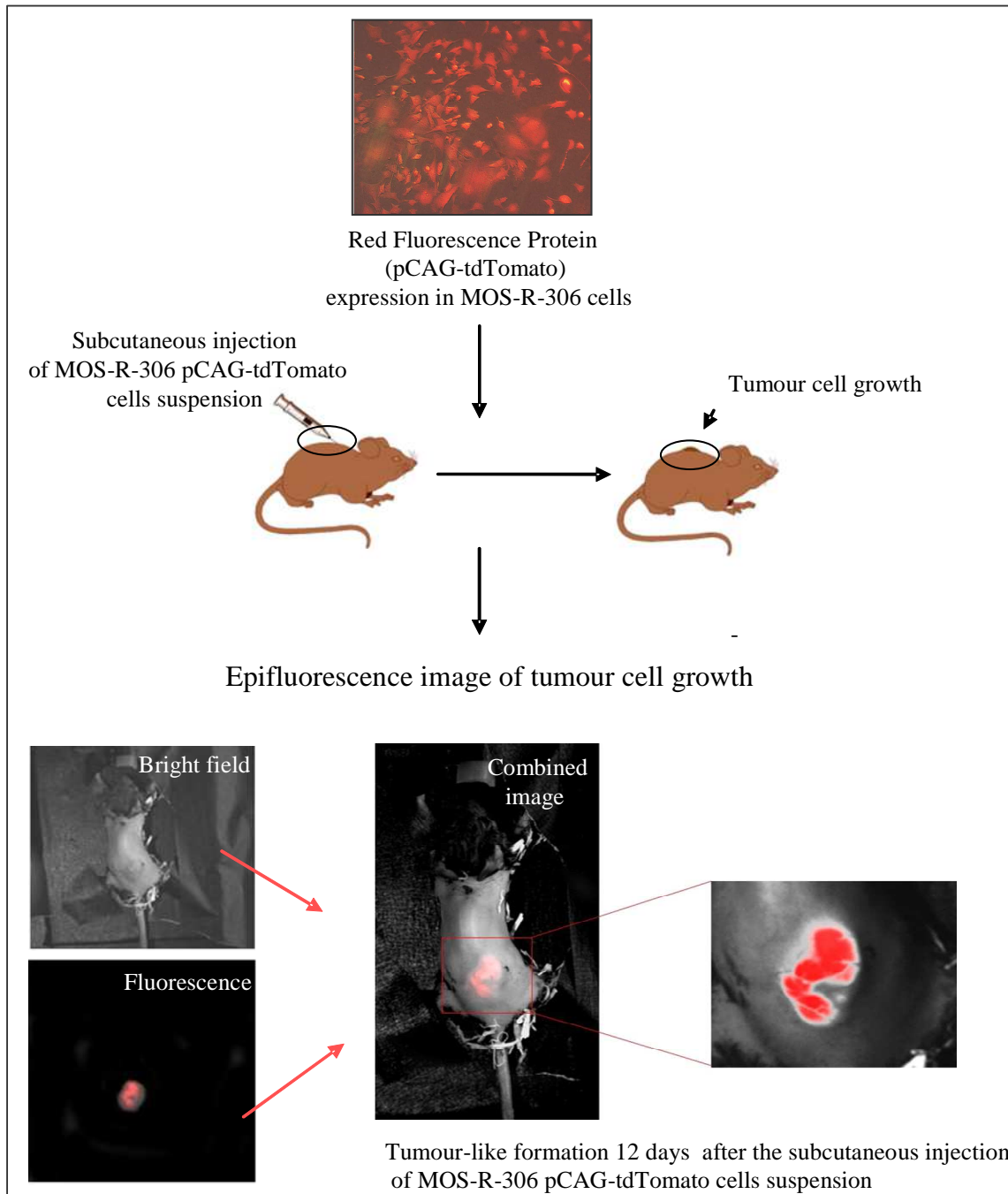


Figure 62: Work-flow of the pilot study of *in vivo* osteosarcoma mouse model. After transfected with pCAG-tdTomato (red fluorescent protein) MOS-R-306 were inoculated subcutaneously to mouse the tumour formation could be observed in 12 days. The tumour volume was recorded in anaesthetised alive animal using epi-fluorescent technique. The imaged tumour was pseudocoloured in red.

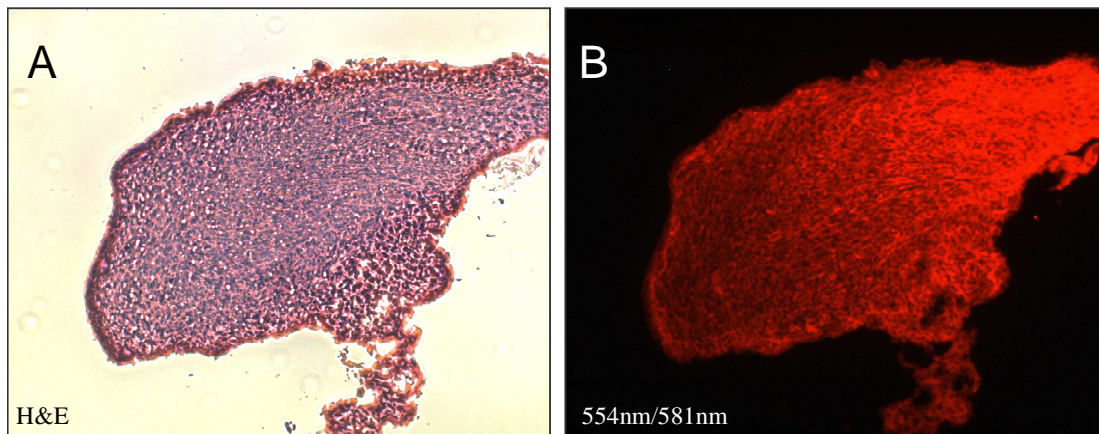


Figure 63: Images of osteosarcoma histology. A: Bright field image of osteosarcoma specimen stained with hematoxylin and eosin (H&E). Poorly differentiated cells (dark violet) and extracellular matrix (light pink) are present. B: Fluorescent image of the same osteosarcoma specimen with excitation at 554nm and detection with emission at 581nm (554nm/581nm).

V. Discussion

Osteosarcoma is recognized as a very aggressive form of cancer affecting primarily adolescents and the elderly. This is one of the tumour types that is most resistant to therapy (Cannon, 2007; Longhi et al, 2006). The mechanisms that determine the poor treatment response and promote tumour relapse are not fully understood. The concept that a small population of cells that reside within the tumour has the potential to repopulate the tumour after therapy, the so called “tumour initiating cells” (TICs), (Kummermehr J. & Trott K.R., 1996) is a great step forward. These cells are postulated to play a major role for both tumorigenesis, the response to therapy, and tumour recurrence. It was shown that populations of such TICs cells possessing a self renewal potential can be found in different types of tumours (Butof et al; Nguyen et al, 2012; Yang et al, 2011). In studies on human osteosarcoma-derived cell lines and primary osteosarcoma such a subset of cells expressing markers characteristic for TICs and resistance to chemotherapeutic drugs was shown (Tirino et al, 2008; Yang et al, 2011). In spite of this strong indication for the presence of TICs in osteosarcoma, no direct study on the radiosensitivity of these cells has been carried out.

In the present study we have investigated the hypothesis that tumour initiating cells in osteosarcoma possess a unique set of physiological properties, and that they are inherently more radioresistant when compared to the bulk (non-TICs) tumour cells. The goal was to identify and isolate TICs and to evaluate their importance for determining the contribution, if any, of TICs cells for the radiosensitivity of a panel of murine osteosarcoma (MOS) cell lines.

A panel of MOS osteosarcoma cell lines, previously established from α -emitter Th²²⁷ - induced mouse bone tumours, were selected for the study (MOS-R-1929, MOS-R-306, MOS-S-184 and MOS-S-1403) based on their different sensitivities to growth inhibition after exposure to gamma-radiation (Figure 7).

5.1. MOS cell lines showed a large degree of variability in their clonogenic survival, with only a slight correlation with residual DNA double strand breaks

In the first stage of the project we tested differences in radiosensitivity between the four chosen MOS cell lines using a clonogenic cell survival assay. For this purpose we developed a semi-automated fluorescence-based method using 96-wells based on the concept of limiting dilution. We could show that this method allows the quick and high-throughput measurement

of surviving clonogens even in cells that normally do not form colonies *in vitro* (Figure 43). We found that MOS-R-1929 and MOS-R-306 were significantly more resistant to radiation at 4Gy than MOS-S-184 and MOS-S-1403 (Figure 43). This was in line with our predictions based on previous studies (Figure 7). Radiation sensitivity of the different MOS cell lines was compared by determining the radiation doses at which 10% survival (D_{10}) occurs, i.e. the dose of radiation required to inactivate 90% of the cells (Hall, 2012). We observed that MOS-R-306 was less sensitive than MOS-R-1929 by a factor of 1.2, whereas MOS-S-184 was less sensitive by a factor of 1.4 and MOS-S-1403 by a factor of 1.6 (Table 20). The other parameter of survival, SF2, i.e. the survival fraction at 2Gy also varied between the MOS cell lines and varied from 0,66 to 0,38 two-fold (Table 20). Interestingly, the SF2 values are well within the range of published SF2 values for range of cell lines established from human tumours, including medulloblastoma (0.35), breast cancer (0.3), melanoma (0.2-0.7), glioblastoma (0,4-0.74) and colon cancer (0.14-0.75), as well as cell lines established from mouse tumours such as melanoma (0.58) and fibrosarcoma (0.49) (Bristow et al, 1990; Deacon et al, 1984; Taghian et al, 1995). This finding challenges the widespread suggestion that osteosarcoma are inherently radioresistant (Cannon, 2007). At least at the level of the information provided by cell clonogenic survival mouse osteosarcoma must now be considered to be as radiosensitive as most common cancers.

Analysis of the clonogenic survival curves of MOS cells fitted using the linear-quadratic function revealed that the alpha component i.e. estimated unreparable damage induced by radiation for MOS-S-1403 was 0.19 and for MOS-S-184 $\alpha = 0.14$ (Table 20). This was higher than the α values for both relatively resistant cell lines (0.05-0.07) (Table 20). The beta component, i.e. repairable damage induced by radiation, was similar for all four cell lines (0.01-0.02) (Table 20). This may be an indication that sensitive cell lines have to cope with a high amount of unreparable damage after irradiation or that they have an insufficient capacity to repair the radiation damage compared to the more resistant cell lines.

To analyse the relationship between clonogenic radiosensitivity and DNA damage repair we measured γ H2AX and 53BP1 (Markova et al, 2007) foci after 1Gy of irradiation in all four cell lines. Our findings showed that there were more DNA double strand breaks remaining 90 minutes after 1Gy of irradiation in the most resistant MOS-R-1929 cell line (~12 foci per cell) compared to the other resistant MOS-R-306 cell line (~6 foci per cell) (Figure 51). On the other hand, there was the same scale of difference in 90 minutes foci number between the sensitive cell lines MOS-S-1403 (~12 foci per cell) and MOS-S-184 (~6 foci per cell) (Figure 51). Although there is a clear difference in the remaining DNA damage

between the four cell lines no correlation with radiosensitivity was found. This result is in accordance with a previous study showing no correlation between the induction of DNA DSBs and radiosensitivity tested on squamous carcinoma cell lines with moderate and high radiosensitivity (Kasten-Pisula et al, 2009). We found more long-term foci (residual DNA double strand breaks) in the most sensitive MOS-S-1403 cell line compared to the most resistant MOS-R-1929 ($p = 0.02$) (Figure 52). The slight correlation between the radiosensitivity and DNA damage is well in line with suggestions that residual DNA double strand breaks can be used to predict clonogenic cell survival (Menegakis et al, 2009). We also found that repair of radiation-induced DNA double strand breaks in MOS-R-1929 was faster than in the other cell lines, including the other resistant line, MOS-R-306 (Table 24). Surprisingly, we found that MOS-R-1929 used almost only the fast phase of repair. In contrast, the other three MOS cell lines all showed typical biphasic (fast and slow) kinetics of DNA double strand break repair (Figure 50). In previous studies the presence of a p53 point mutation in MOS-R-1929 had been suggested. We could confirm this by using western immunoblot protein analysis, revealing an excess level of p53 in non-irradiated cells (Figure 41 and 42). This is expected only if a mutation in the p53 tumour suppressor gene causes stabilization of the encoded protein. From the literature it is known that p53 plays an important role in cellular radiation sensitivity (Gudkov & Komarova, 2003). Up-regulation of p53 in response to ionising radiation can lead to either induction of growth-arrest or to induction of apoptosis and cell death. The susceptibility of tumours with p53 mutation to therapy is highly dependent on the capabilities of the cells to initiate the p53-dependant apoptosis (Gudkov & Komarova, 2003).

Thus, we suggest that the absence of the slow DNA repair phase (associated with repair by homologous recombination) in MOS-R-1929 may be caused by the mutation of the p53 gene and absence of G1 cycle arrest after irradiation.

5.2. MOS cells possess a distinct subset of cells with the properties of tumour initiating cells

In order to identify and isolate TICs from the selected MOS cell lines we used the side population assay. This method is based on the specific ability of TICs to efflux small molecules, including the DNA binding fluorescent dye Hoechst 33342. The side population cells i.e. cells low in dye retention has been shown in various studies to be composed of cells possessing tumour initiating properties (Fukaya et al, 2010; Hu et al, 2010). In a study of 29

different mesenchymal tumours of human origin Wu showed that side population cells had a significantly higher potential to induce tumours upon serial transplantation in SCID mice *in vivo*, when compared to the remaining SP-depleted main population cells (Wu et al, 2007).

In our study we have established that each of the MOS cell lines has a different proportion of the side population cells (Figure 14). MOS-R-1929 contained the highest fraction of the four MOS cell lines tested, with an average of 15% side population cells compared to MOS-R-306 (0.75%), MOS-S-184 (0.67%) and MOS-1403 (0.14%) (Figure 14). The range of the side population sizes we observed is in agreement with previous studies on human osteosarcoma, where the side population fraction ranged from $\leq 1\%$ in established cell lines such as U2OS, NY and Saos2 to more than 10% in primary human osteosarcomas (Murase et al 2009, Tirino et al 2008, Yang et al 2011). In other non-mesenchymal tumour types the percentage of side population cells measured was also similar to our data, such as the proportion found in human breast carcinoma MCF7 (2%), rat C6 glioma (0.4%), brain glioma (20%), lung cancer cell line A549 (6.3%) (Hirschmann-Jax et al, 2004; Hsu et al, 2011; Kondo et al, 2004).

Interestingly, MOS-R-1929 showed a very pronounced side population fraction and only this cell line was found to have a p53 mutation (Figure 14, Figure 41). It is therefore possible that p53 status is associated with the fraction of TICs. Indeed, it has been demonstrated that the loss of p53 in breast cancer cells led to an increase in the expression of the transcriptional signature of tumour initiating cells (Mizuno et al, 2010).

In order to better characterize the stem-like properties of the side population we collected both the side and the SP-depleted main population cells from MOS-R-1929, MOS-R-306 and MOS-S-184. We found that after sorting and incubating the side population cells for at least seven days they grew mainly as spherical and loosely attached cells, compared to the SP-depleted main population cell (Figure 15). This is consistent with the observation that stem cells exhibit a smaller, more rounded morphology in culture (Murase et al, 2009). We also found that the side population cells cultured from the MOS-R-1929 cell line could repopulate cells of both the side and the main populations (Table 18). During growth of SP-cell in culture the side population cell numbers decreased and at the same time the population of SP-depleted main population cells expanded (Figure 18, Table 18). This suggests the SP cells are capable of asymmetric division and self-renewal *in vitro*. This is in line with previous studies on glioma and bone sarcomas (Kondo et al, 2004; Murase et al, 2009; Yang et al, 2011)

The metabolic properties of tumour initiating cells are not completely understood, TICs are suggested to have in general a lower oxygen consumption and therefore very likely a lower proliferation activity than non TICs (Vlashi et al., 2011). We found that the proliferation activity measured with the MTT assay was indeed lower in the side population cells compared to the SP-depleted main population cell, but this was not consistently seen between all of the tested cell lines (Figure 21). Our data are in line with a report showing that glioblastoma TICs derived from neurospheres were less glycolytic compared to the more differentiated adherent cells (Vlashi et al., 2011). Nevertheless, our data establish that the absolute MTT signal is not a reliable indicator for comparing proliferation activity of the SP and SP-depleted MP cells.

Further, we analysed the side population cells for the expression of known transcription factors involved in self-renewal and cell development during embryogenesis and that are also found to be expressed in TICs (Yang et al., 2011). This study produced conflicting results. On the one hand, the side population sorted from MOS-R-306 showed consistently high expression of three embryonic “core transcription” factors, namely Sox2, Nanog and Oct3/4 compared to the SP-depleted MOS-R-306 main population cells (Figure 26). This suggests that the side population obtained from MOS-R-306 possesses a strong TICs stemness phenotype. This is in accordance with the data showing the expression of stemness genes in TICs derived from osteosarcoma sarcospheres (Tirino et al., 2008; Tirino et al., 2011). On the other hand, the remaining tested cell line, MOS-R-1929, which maintained the highest side population fraction did not confirm this result (Figure 27). This suggests that this particular cell line possesses other pathways for the transcriptional regulation of TICs properties than those tested. Several other candidate genes usually expressed in adult stem cells, such as Bmi1, Klf4 and Nestin, were not up-regulated in the side population cells from any of the tested cell lines (Figure 26, Figure 27). This is in contrast to results showing their role in the maintenance of self-renewal in sarcospheres, hepatocellular carcinomas and induced pluripotent stem cells (Chiba et al., 2008; Takahashi and Yamanaka, 2006; Tirino et al., 2011). Altogether, these findings suggest that the putative stem cell markers are not universally specific for TICs in all investigated tumour cell lines.

One of the characteristic properties of TICs is their capability to produce a tumour upon *in vivo* transplantation experiments (Hewitt, 1958; O'Brien et al, 2007). To evaluate the tumorigenic and clonogenic differences between the MOS cell lines we used the limiting dilution assay as an *in vitro* analogue to the transplantation technique (Traycoff et al, 1995). We found that the cell line with the highest side population fraction, MOS-R-1929, showed a

significantly higher clonogenic potential of the SP cells compared to the SP-depleted MP cells (Figure 22). This is supported by previous studies that showed that far less side population cells from osteosarcoma and glioma are required to produce a tumour *in vivo* compared to SP-depleted main population cells (Kondo et al., 2004; Wu et al., 2007; Yang et al., 2011). The tested MOS-R-306 and MOS-S-184 cell lines did not show a significant difference in clonogenicity between the SP and SP-depleted MP cell populations (Figure 23, Figure 24). This could be due to the fact that in cell lines with a low fraction of SP cells the result of the single cell assays could be influenced by contamination by TICs from the SP-depleted main population cells (Figure 17). For the comparison of clonogenic potential we analysed the number of cells per well that were required to produce 63% of wells with a growing colony. According to the Poisson distribution if every cell plated were a tumour initiating cell expected to produce a colony, 63% of wells would contain colonies (Figure 25). Indeed, MOS-R-1929 side population cells needed only 1-2 cells per well to have 63% of wells with colonies compared to the SP-depleted MP cells where 10x more cells are required to achieve the same result. Thus SP-depleted MP cells do indeed still contain residual SP (TICs) cells. Therefore the ability of MOS-R-1929 SP-depleted MP cells to form colonies is probably due to low level contamination with SP cells. Our data indicates that the analysed side population cells possess tumour initiating properties. MOS-R-306 significantly over-expresses embryonic “core transcription factors”. MOS-R-1929 side population cells have a prominent clonogenic potential compared to the SP-depleted main population. Thus the side population cells express some, but not all, properties of the tumour initiating cells. This warrants further investigation.

5.3. Tumour initiating cells do not show inherent radioresistance

In the clonogenic survival assay we observe that the MOS-R-1929 cell line is almost 50 % more radioresistant (D_{10}) than the most radiosensitive MOS-S-1403 cell line (Table 20). MOS-R-306 shows similar results to MOS-R-1929. This variability corresponds to a study demonstrating that glioblastoma cell lines have an inherently wide range of radiosensitivities (Taghian et al, 1995). Moreover, we could suggest that there is a relationship between the radiosensitivity and the clonogenicity of the side and the SP-depleted main cell populations in MOS-R-1929. Thus, we investigated whether the side population cells are themselves radioresistant.

We performed the limiting dilution clonogenic survival assay with the side population and the SP-depleted main population cells from the MOS-R-1929 cell line (Figure 45). We found that the side population cells are more sensitive to irradiation (D_{10} 5.9Gy) when compared to both unsorted MOS-R-1929 (D_{10} 7.04Gy) and the SP-depleted main population (D_{10} 8.35Gy) (Table 21). These findings indicate that the relative radioresistance of MOS-R-1929 is due to the radioresistance of the SP-depleted MP cells whereas the side population cells that have a high clonogenic potential are radiosensitive.

However, this difference does not exist in the other cell lines, e.g. MOS-R-306, which is relatively radioresistant and where the side population is much smaller (Figure 46, Table 22). Since the SP-depleted main population has a lower plating efficiency more cells have to be used in the experiment. We speculate that an environmental factor plays some role in regulating sensitivity. There is evidence that hypoxic and perivascular tumour initiating cell niches play an important role in the regulation of TICs stemness in glioblastoma and colorectal cancer (Borovski et al, 2011).

The results we obtained are surprising and opposite to our expectation, going against the widely-accepted hypothesis that tumour initiating cells are inherently radioresistant (Woodward & Bristow, 2009). Despite the general assumption, in the literature there is no convincing evidence that tumour initiating cells are indeed radioresistant. In 1967 Van Putten and Kalmann showed in transplantation experiments that there was no difference in *in vivo* survival curves of osteosarcoma cells and cells from other isogenic mouse tumours (Van Putten & Kallman, 1968). In a recent study on glioblastoma Bao reported that after irradiation of the tumour cells the fraction of neurosphere forming CD133⁺ tumour initiating cells increased compared to CD133⁻ cells due to radiation-induced apoptosis of CD133⁻ cells. However, quantitative clonogenic cell survival experiments were not performed (Bao et al., 2006).

5.4. Expression of tumour initiating cells markers in MOS cells does not correlate with their radiosensitivity

In our study we found reproducible differences in the TICs marker mRNA expression between MOS-R-306 side population cells compared to SP-depleted main population cells. These differences were not the same between all four unsorted MOS cell lines. Surprisingly, we found up-regulation of Sox2 (Figure 30) and Nanog (Figure 31) in the MOS-S-1403 cell line compared to the other cell lines, although it has only very a few TICs. In another

relatively radioresistant MOS-S-184 cell line we observed up-regulation of Nestin (Figure 34) and slight up-regulation of Nanog (Figure 31) compared to the more radioresistant cell lines. This could indicate that tumours sustain unlimited proliferation capacity even without a high number of TICs cells, suggesting a high proliferative capacity for the stem-like cells. In the literature it is shown that a pseudogene NanogP8 could modulate the ability of tumour cells to maintain stem-like characteristic (Zhang et al, 2012). One explanation is that transcription of this pseudogene could mediate miRNA levels by attraction of miRNA to corresponding elements (Salmena et al, 2011). Such decoy regulation also may govern the activity of Sox2, Nanog and Nestin.

In the present study we investigated the change in mRNA expression of stem cell markers after irradiation in all four MOS cell lines. Only Sox2 was significantly up-regulated after 4Gy of irradiation in MOS-R-1929, MOS-S-184 and MOS-S-184 without correlation to clonogenic survival (Figure 54). If taking into account the over-expression of Sox2 in untreated MOS-S-1403 compared to other MOS cell lines (Figure 30), where a very small side population fraction is present compared to the other cell lines, these findings suggest that Sox2 up-regulation in MOS cell lines is mainly due to an expression change in the SP-depleted main population cell rather than in the side population. After 4Gy approximately 60-90% of tumour initiating cells are killed (Figure 43) but markers of stemness go up. This finding corresponds to a study where radiation was suggested to reprogram breast cancer cells (Lagadec et al, 2012). In this study the breast cancer cells showed higher level of mammosphere formation after 8Gy of radiation, increased expression of Sox2 and could be tracked by low proteasome activity compared to unirradiated tumour cells. Thus, these cells were induced to obtain TICs properties due to irradiation (Lagadec et al, 2012). However, in our study the mRNA up-regulation of Sox2 after irradiation may be unlikely to be an increase in the stemness of tumour cells as we could not confirm this finding at the protein level (Figure 59).

The other markers (Nanog, Nestin, Klf4, and Bmi1) show very little change after 4Gy. The tendency is rather to go up than down, though not significantly so. This suggests that up-regulation of stemness might occur in the non-tumour initiating cells and warns against the use of such markers as the only criteria for the radiosensitivity, as was shown for induced pluripotent stem cells (Hayashi et al, 2012).

5.5. MOS cell radiosensitivity correlates with the fraction of tumour initiating cells

To further find the relation between TICs and radiosensitivity of the four analysed MOS cell lines we compared the clonogenic cell survival of four cell lines with the fraction of TICs identified by the side population assay. We found that the TICs fraction is in line with D_{10} clonogenic survival data for all four tested MOS cell lines (where D_{10} is a dose required to kill 90% of the cells) (Figure 44).

There is supporting evidence indicating that the fraction of tumour initiating cells influences the curability of a tumour by radiotherapy as was determined by Hill and Milas (Hill & Milas, 1989). In transplantation experiments, where tumour take in recipient mice is determined by the presence of at least 1 or more cells able to initiate a tumour *in vivo*, an inverse correlation between the increase in the TD_{50} (i.e. cell number needed to induce tumour in 50% of recipient animals) and the increase of the TCD_{50} (i.e. radiation dose needed to achieve a local tumour control in 50% of treated animals) for 12 different tumours was reported (Hill & Milas, 1989). In tumours of mesenchymal origin, it was described that there is a correlation between the clinical aggressiveness of a tumour and the side population fraction (Wu et al, 2007). Trott and Kummermehr estimated that a difference of one order of magnitude in the stem cell (or TICs) fraction would cause a 15% difference in the mean curative dose or a 15-30% difference in the probability of cure (Kummermehr J. & Trott K.R., 1996). This suggests that, besides the tumour size, the stem cell fraction is an important factor determining therapy outcome.

5.6. Outlook

As was already discussed, the quantitative analysis of the growth potential of tumour cells is one of the most important and reliable tools to analyse TICs. Whilst *in vitro* colony formation is a robust technique it does not reproduce the *in vivo* situation. Therefore, to allow future studies on osteosarcoma TICs tumour formation we developed a new model. We have produced an experimental osteosarcoma mouse model that will allow *in vitro* as well as *in vivo* examination of the sensitivity of osteosarcoma cell lines to radiation (Figure 62).

We were able to stably transfect a MOS cell line with red fluorescent proteins tdTomato (pCAG-Tomato vector system). We also successfully induced tumours *in vivo* in experimental syngenic mice and used a non-invasive quantitative molecular epi-fluorescent imaging as a tool for *in vivo* small animal imaging and tumour follow up. TdTomato fits all of the criteria for optimal deep tissue imaging application (Winnard et al, 2006) with light absorption occurring in a range where mammalian tissues are practically optically transparent and have minimal autofluorescence. Our study shows that the transfection of the tdTomato protein does not alter the radiosensitivity of the respective cells and that molecular fluorescent imaging appears to be a very useful non-invasive and precise *in vivo* tool to follow tumour formation (Winnard et al, 2006), offers future possibilities for the analysis of tumour re-growth in response to radiotherapy.

5.7. Conclusion

In the present study we showed the tested MOS cell lines vary significantly in their clonogenic radiosensitivity. We observed a slight correlation between the DNA double strand breaks repair and cell radiation response.

Our study confirms the presence of tumour initiating cells (TICs) in MOS cells lines. Surprisingly, we found that isolated TICs are not inherently radioresistant compared to non TICs. On the other hand, we found that the fraction of TICs correlates well with the radiosensitivity of MOS cell lines. This suggests an influential role of the tumour initiating cells interaction with their tumour surrounding environmental (niche) in the tumour radiation response rather than individual tumour initiating cells inherent radioresistance.

Our *in vivo* mouse osteosarcoma fluorescent model showed potential for the further investigation of TICs *in vivo*.

VI. References

- Alvi AJ, Clayton H, Joshi C, Enver T, Ashworth A, Vivanco M, Dale TC, Smalley MJ (2003) Functional and molecular characterisation of mammary side population cells. *Breast Cancer Res* **5**: R1-8
- Banath JP, Klokov D, MacPhail SH, Banuelos CA, Olive PL (2010) Residual gammaH2AX foci as an indication of lethal DNA lesions. *BMC Cancer* **10**: 4
- Bao S, Wu Q, McLendon RE, Hao Y, Shi Q, Hjelmeland AB, Dewhirst MW, Bigner DD, Rich JN (2006) Glioma stem cells promote radioresistance by preferential activation of the DNA damage response. *Nature* **444**: 756-760
- Basu-Roy U, Basilico C, Mansukhani A (2012a) Perspectives on Cancer Stem Cells in Osteosarcoma. *Cancer Lett*
- Basu-Roy U, Seo E, Ramanathapuram L, Rapp TB, Perry JA, Orkin SH, Mansukhani A, Basilico C (2012b) Sox2 maintains self renewal of tumor-initiating cells in osteosarcomas. *Oncogene* **31**: 2270-2282
- Bauer HC, Tempfer H, Bernroider G, Bauer H (2006) Neuronal stem cells in adults. *Exp Gerontol* **41**: 111-116
- Baumann M, Krause M, Thames H, Trott K, Zips D (2009) Cancer stem cells and radiotherapy. *Int J Radiat Biol* **85**: 391-402
- Berry RJ, Andrews JR (1961) Quantitative relationships between radiation dose and the reproductive capacity of tumor cells in a mammalian system in vivo. *Radiology* **77**: 824-830
- Borovski T, De Sousa EMF, Vermeulen L, Medema JP (2011) Cancer stem cell niche: the place to be. *Cancer Res* **71**: 634-639
- Boyer LA, Lee TI, Cole MF, Johnstone SE, Levine SS, Zucker JP, Guenther MG, Kumar RM, Murray HL, Jenner RG, Gifford DK, Melton DA, Jaenisch R, Young RA (2005) Core transcriptional regulatory circuitry in human embryonic stem cells. *Cell* **122**: 947-956
- Brandsma I, Gent DC (2012) Pathway choice in DNA double strand break repair: observations of a balancing act. *Genome Integr* **3**: 9
- Bristow RG, Hardy PA, Hill RP (1990) Comparison between in vitro radiosensitivity and in vivo radioresponse of murine tumor cell lines. I: Parameters of in vitro radiosensitivity and endogenous cellular glutathione levels. *Int J Radiat Oncol Biol Phys* **18**: 133-145
- Brunner TB, Kunz-Schughart LA, Grosse-Gehling P, Baumann M (2012) Cancer stem cells as a predictive factor in radiotherapy. *Semin Radiat Oncol* **22**: 151-174
- Butof R, Dubrovskaya A, Baumann M Clinical perspectives of cancer stem cell research in radiation oncology. *Radiother Oncol*

- Bütöf R, Dubrovská A, Baumann M Clinical perspectives of cancer stem cell research in radiation oncology. *Radiotherapy and Oncology*
- Cade S (1955) Osteogenic sarcoma; a study based on 133 patients. *J R Coll Surg Edinb* **1**: 79-111
- Cannon RSaSR (2007) Osteosarcoma. In *Oxford Textbook of Oncology*, 13.4. Oxford University Press, USA
- Chang F, Syrjänen S, Kurvinen K, Syrjänen K (1993) The p53 tumor suppressor gene as a common cellular target in human carcinogenesis. *Am J Gastroenterol* **88**: 174-186
- Chiba T, Miyagi S, Saraya A, Aoki R, Seki A, Morita Y, Yonemitsu Y, Yokosuka O, Taniguchi H, Nakauchi H, Iwama A (2008) The polycomb gene product BMI1 contributes to the maintenance of tumor-initiating side population cells in hepatocellular carcinoma. *Cancer Res* **68**: 7742-7749
- Chmelevsky D, Kellerer AM, Land CE, Mays CW, Spiess H (1988) Time and dose dependency of bone-sarcomas in patients injected with radium-224. *Radiat Environ Biophys* **27**: 103-114
- Chuthapisith S. (2011) Cancer Stem Cells and Chemoresistance, Cancer Stem Cells Theories and Practice. In Shostak PS (ed.).
- Combs SE, Ellerbrock M, Haberer T, Habermehl D, Hoess A, Jakel O, Jensen A, Klemm S, Munter M, Naumann J, Nikoghosyan A, Oertel S, Parodi K, Rieken S, Debus J (2010) Heidelberg Ion Therapy Center (HIT): Initial clinical experience in the first 80 patients. *Acta Oncol* **49**: 1132-1140
- Deacon J, Peckham MJ, Steel GG (1984) The radioresponsiveness of human tumours and the initial slope of the cell survival curve. *Radiother Oncol* **2**: 317-323
- DeLaney TF, Park L, Goldberg SI, Hug EB, Liebsch NJ, Munzenrider JE, Suit HD (2005) Radiotherapy for local control of osteosarcoma. *Int J Radiat Oncol Biol Phys* **61**: 492-498
- Dikomey E, Dahm-Daphi J, Brammer I, Martensen R, Kaina B (1998) Correlation between cellular radiosensitivity and non-repaired double-strand breaks studied in nine mammalian cell lines. *Int J Radiat Biol* **73**: 269-278
- Dincbas FO, Koca S, Mandel NM, Hiz M, Dervisoglu S, Secmezacar H, Oksuz DC, Ceylaner B, Uzel B (2005) The role of preoperative radiotherapy in nonmetastatic high-grade osteosarcoma of the extremities for limb-sparing surgery. *Int J Radiat Oncol Biol Phys* **62**: 820-828
- Dittfeld C, Dietrich A, Peickert S, Hering S, Baumann M, Grade M, Ried T, Kunz-Schughart LA (2010) CD133 expression is not selective for tumor-initiating or radioresistant cell populations in the CRC cell line HCT-116. *Radiother Oncol* **94**: 375-383
- Franken NA, Rodermond HM, Stap J, Haveman J, van Bree C (2006) Clonogenic assay of cells in vitro. *Nat Protoc* **1**: 2315-2319

- Fry SA (1998) Studies of U.S. radium dial workers: an epidemiological classic. *Radiat Res* **150**: S21-29
- Fukaya R, Ohta S, Yamaguchi M, Fujii H, Kawakami Y, Kawase T, Toda M (2010) Isolation of cancer stem-like cells from a side population of a human glioblastoma cell line, SK-MG-1. *Cancer Lett* **291**: 150-157
- Gao Q, Geng L, Kvalheim G, Gaudernack G, Suo Z (2009) Identification of cancer stem-like side population cells in ovarian cancer cell line OVCAR-3. *Ultrastruct Pathol* **33**: 175-181
- Geller DS, Gorlick R (2010) Osteosarcoma: a review of diagnosis, management, and treatment strategies. *Clin Adv Hematol Oncol* **8**: 705-718
- Gong C, Yao H, Liu Q, Chen J, Shi J, Su F, Song E (2010) Markers of tumor-initiating cells predict chemoresistance in breast cancer. *PLoS One* **5**: e15630
- Goodell MA, Brose K, Paradis G, Conner AS, Mulligan RC (1996) Isolation and functional properties of murine hematopoietic stem cells that are replicating in vivo. *J Exp Med* **183**: 1797-1806
- Gössner W, Hug O, Luz A, Muller WA (1976) Experimental induction of bone tumors by short-lived bone-seeking radionuclides. *Recent Results Cancer Res*: 36-49
- Grenman R, Burk D, Virolainen E, Buick RN, Church J, Schwartz DR, Carey TE (1989) Clonogenic cell assay for anchorage-dependent squamous carcinoma cell lines using limiting dilution. *Int J Cancer* **44**: 131-136
- Gudkov AV, Komarova EA (2003) The role of p53 in determining sensitivity to radiotherapy. *Nat Rev Cancer* **3**: 117-129
- Hall EJ (ed) (2012) *Radiobiology for the Radiologist*: Lippincott Williams & Wilkins
- Halperin E.C., Perez C.A., Brady L.W. (eds) (2008) *Perez and Brady's principles and practice of radiation oncology, 5th edition*. Philadelphia, USA: Lippincott Williams & Wilkins
- Harris MB, Gieser P, Goorin AM, Ayala A, Shochat SJ, Ferguson WS, Holbrook T, Link MP (1998) Treatment of metastatic osteosarcoma at diagnosis: a Pediatric Oncology Group Study. *J Clin Oncol* **16**: 3641-3648
- Hayashi N, Monzen S, Ito K, Fujioka T, Nakamura Y, Kashiwakura I (2012) Effects of ionizing radiation on proliferation and differentiation of mouse induced pluripotent stem cells. *J Radiat Res* **53**: 195-201
- Hewitt HB (1953) Studies of the quantitative transplantation of mouse sarcoma. *Br J Cancer* **7**: 367-383
- Hewitt HB (1958) Studies of the dissemination and quantitative transplantation of a lymphocytic leukaemia of CBA mice. *Br J Cancer* **12**: 378-401

- Hewitt HB, Blake ER, Walder AS (1976) A critique of the evidence for active host defence against cancer, based on personal studies of 27 murine tumours of spontaneous origin. *Br J Cancer* **33**: 241-259
- Hill RP, Milas L (1989) The proportion of stem cells in murine tumors. *Int J Radiat Oncol Biol Phys* **16**: 513-518
- Hirschmann-Jax C, Foster AE, Wulf GG, Nuchtern JG, Jax TW, Gobel U, Goodell MA, Brenner MK (2004) A distinct "side population" of cells with high drug efflux capacity in human tumor cells. *Proc Natl Acad Sci U S A* **101**: 14228-14233
- Hsu HS, Lin JH, Huang WC, Hsu TW, Su K, Chiou SH, Tsai YT, Hung SC (2011) Chemoresistance of lung cancer stemlike cells depends on activation of Hsp27. *Cancer* **117**: 1516-1528
- Hu L, McArthur C, Jaffe RB (2010) Ovarian cancer stem-like side-population cells are tumorigenic and chemoresistant. *Br J Cancer* **102**: 1276-1283
- Iliakis G, Wang H, Perrault AR, Boecker W, Rosidi B, Windhofer F, Wu W, Guan J, Terzoudi G, Pantelias G (2004) Mechanisms of DNA double strand break repair and chromosome aberration formation. *Cytogenet Genome Res* **104**: 14-20
- Jiang Y, Jahagirdar BN, Reinhardt RL, Schwartz RE, Keene CD, Ortiz-Gonzalez XR, Reyes M, Lenvik T, Lund T, Blackstad M, Du J, Aldrich S, Lisberg A, Low WC, Largaespada DA, Verfaillie CM (2002) Pluripotency of mesenchymal stem cells derived from adult marrow. *Nature* **418**: 41-49
- Kallman RF, Silini G, Van Putten LM (1967) Factors influencing the quantitative estimation of the in vivo survival of cells from solid tumors. *J Natl Cancer Inst* **39**: 539-549
- Kasten-Pisula U, Menegakis A, Brammer I, Borgmann K, Mansour WY, Degenhardt S, Krause M, Schreiber A, Dahm-Daphi J, Petersen C, Dikomey E, Baumann M (2009) The extreme radiosensitivity of the squamous cell carcinoma SKX is due to a defect in double-strand break repair. *Radiother Oncol* **90**: 257-264
- Kondo T, Setoguchi T, Taga T (2004) Persistence of a small subpopulation of cancer stem-like cells in the C6 glioma cell line. *Proc Natl Acad Sci U S A* **101**: 781-786
- Koshurnikova NA, Gilbert ES, Sokolnikov M, Khokhryakov VF, Miller S, Preston DL, Romanov SA, Shilnikova NS, Suslova KG, Vostrotin VV (2000) Bone cancers in Mayak workers. *Radiat Res* **154**: 237-245
- Kummermehr J., Trott K.R. (1996) Tumour stem cells. In *Stem Cells*, Potten CS (ed), pp 363-399. Academic Press Inc
- Lagadec C, Vlashi E, Della Donna L, Dekmezian C, Pajonk F (2012) Radiation-induced reprogramming of breast cancer cells. *Stem Cells* **30**: 833-844
- Lapidot T, Sirard C, Vormoor J, Murdoch B, Hoang T, Caceres-Cortes J, Minden M, Paterson B, Caligiuri MA, Dick JE (1994) A cell initiating human acute myeloid leukaemia after transplantation into SCID mice. *Nature* **367**: 645-648

- Livak KJ, Schmittgen TD (2001) Analysis of relative gene expression data using real-time quantitative PCR and the $2(-\Delta\Delta C(T))$ Method. *Methods* **25**: 402-408
- Longhi A, Errani C, De Paolis M, Mercuri M, Bacci G (2006) Primary bone osteosarcoma in the pediatric age: state of the art. *Cancer Treat Rev* **32**: 423-436
- Luz A, Muller WA, Linzner U, Strauss PG, Schmidt J, Muller K, Atkinson MJ, Murray AB, Gossner W, Erfle V, et al. (1991) Bone tumor induction after incorporation of short-lived radionuclides. *Radiat Environ Biophys* **30**: 225-227
- Machak GN, Tkachev SI, Solovyev YN, Sinyukov PA, Ivanov SM, Kochergina NV, Ryjkov AD, Tepliakov VV, Bokhian BY, Glebovskaya VV (2003) Neoadjuvant chemotherapy and local radiotherapy for high-grade osteosarcoma of the extremities. *Mayo Clin Proc* **78**: 147-155
- Malkin D, Li FP, Strong LC, Fraumeni JF, Jr., Nelson CE, Kim DH, Kassel J, Gryka MA, Bischoff FZ, Tainsky MA, et al. (1990) Germ line p53 mutations in a familial syndrome of breast cancer, sarcomas, and other neoplasms. *Science* **250**: 1233-1238
- Markova E, Schultz N, Belyaev IY (2007) Kinetics and dose-response of residual 53BP1/gamma-H2AX foci: co-localization, relationship with DSB repair and clonogenic survival. *Int J Radiat Biol* **83**: 319-329
- Matsunobu A, Imai R, Kamada T, Imaizumi T, Tsuji H, Tsujii H, Shioyama Y, Honda H, Tatezaki SI (2012) Impact of carbon ion radiotherapy for unresectable osteosarcoma of the trunk. *Cancer* **118**: 4555-4563
- Menegakis A, Yaromina A, Eicheler W, Dorfler A, Beuthien-Baumann B, Thames HD, Baumann M, Krause M (2009) Prediction of clonogenic cell survival curves based on the number of residual DNA double strand breaks measured by gammaH2AX staining. *Int J Radiat Biol* **85**: 1032-1041
- Mizuno H, Spike BT, Wahl GM, Levine AJ (2010) Inactivation of p53 in breast cancers correlates with stem cell transcriptional signatures. *Proc Natl Acad Sci U S A* **107**: 22745-22750
- Mo SL, Li J, Loh YS, Brown RD, Smith AL, Chen Y, Joshua D, Roufogalis BD, Li GQ, Fan K, Ng MC, Sze DM (2011) Factors influencing the abundance of the side population in a human myeloma cell line. *Bone Marrow Res* **2011**: 524845
- Murase M, Kano M, Tsukahara T, Takahashi A, Torigoe T, Kawaguchi S, Kimura S, Wada T, Uchihashi Y, Kondo T, Yamashita T, Sato N (2009) side population cells have the characteristics of cancer stem-like cells/cancer-initiating cells in bone sarcomas. *Br J Cancer* **101**: 1425-1432
- Nguyen LV, Vanner R, Dirks P, Eaves CJ (2012) Cancer stem cells: an evolving concept. *Nat Rev Cancer* **12**: 133-143
- O'Brien CA, Pollett A, Gallinger S, Dick JE (2007) A human colon cancer cell capable of initiating tumour growth in immunodeficient mice. *Nature* **445**: 106-110

- Olweus J, Lund-Johansen F, Terstappen LW (1994) Expression of cell surface markers during differentiation of CD34+, CD38-/lo fetal and adult bone marrow cells. *Immunomethods* **5**: 179-188
- Ottaviani G, Jaffe N (2009) The epidemiology of osteosarcoma. *Cancer Treat Res* **152**: 3-13
- Pautke C, Schieker M, Tischer T, Kolk A, Neth P, Mutschler W, Milz S (2004) Characterization of osteosarcoma cell lines MG-63, Saos-2 and U-2 OS in comparison to human osteoblasts. *Anticancer Res* **24**: 3743-3748
- Peitzsch C, Kurth I, Kunz-Schughart L, Baumann M, Dubrovskaja A (2013) Discovery of the cancer stem cell related determinants of radioresistance. *Radiother Oncol*
- Petritz J (2007) Flow cytometry of the side population (SP). *Curr Protoc Cytom* **Chapter 9**: Unit9 23
- Pevsner-Fischer M, Levin S, Zipori D (2011) The origins of mesenchymal stromal cell heterogeneity. *Stem Cell Rev* **7**: 560-568
- Phillips TM, McBride WH, Pajonk F (2006) The response of CD24(-/low)/CD44+ breast cancer-initiating cells to radiation. *J Natl Cancer Inst* **98**: 1777-1785
- Puck TT, Marcus PI (1956) Action of x-rays on mammalian cells. *J Exp Med* **103**: 653-666
- Raymond AK, Ayala AG, Knuutila S (2002) Conventional osteosarcoma. In *WHO Classification of Tumours. Pathology and Genetics: Tumours of Soft Tissue and Bones*, Christopher D.M. Fletcher KKV, F. Mertens (ed), 11, pp 264-270. Lyon: IARC Press
- Reya T, Morrison SJ, Clarke MF, Weissman IL (2001) Stem cells, cancer, and cancer stem cells. *Nature* **414**: 105-111
- Ricci-Vitiani L, Lombardi DG, Pilozzi E, Biffoni M, Todaro M, Peschle C, De Maria R (2007) Identification and expansion of human colon-cancer-initiating cells. *Nature* **445**: 111-115
- Rodda DJ, Chew JL, Lim LH, Loh YH, Wang B, Ng HH, Robson P (2005) Transcriptional regulation of nanog by OCT4 and SOX2. *J Biol Chem* **280**: 24731-24737
- Rodriguez-Galindo C, Daw NC, Kaste SC, Meyer WH, Dome JS, Pappo AS, Rao BN, Pratt CB (2002) Treatment of refractory osteosarcoma with fractionated cyclophosphamide and etoposide. *J Pediatr Hematol Oncol* **24**: 250-255
- Rogakou EP, Pilch DR, Orr AH, Ivanova VS, Bonner WM (1998) DNA double-stranded breaks induce histone H2AX phosphorylation on serine 139. *J Biol Chem* **273**: 5858-5868
- Rosemann M, Lintrop M, Favor J, Atkinson MJ (2002) Bone tumorigenesis induced by alpha-particle radiation: mapping of genetic loci influencing predisposition in mice. *Radiat Res* **157**: 426-434

- Rowland RE, Stehney AF, Lucas HF, Jr. (1978) Dose-response relationships for female radium dial workers. *Radiat Res* **76**: 368-383
- Sakurai N, Iwamoto S, Miura Y, Nakamura T, Matsumine A, Nishioka J, Nakatani K, Komada Y (2013) Novel p53 splicing site mutation in Li-Fraumeni-like syndrome with osteosarcoma. *Pediatr Int* **55**: 107-111
- Salmena L, Poliseno L, Tay Y, Kats L, Pandolfi PP (2011) A ceRNA hypothesis: the Rosetta Stone of a hidden RNA language? *Cell* **146**: 353-358
- Saulnier N, Puglisi MA, Lattanzi W, Castellini L, Pani G, Leone G, Alfieri S, Michetti F, Piscaglia AC, Gasbarrini A (2011) Gene profiling of bone marrow- and adipose tissue-derived stromal cells: a key role of Kruppel-like factor 4 in cell fate regulation. *Cytotherapy* **13**: 329-340
- Seo E, Basu-Roy U, Zavadil J, Basilico C, Mansukhani A (2011) Distinct functions of Sox2 control self-renewal and differentiation in the osteoblast lineage. *Mol Cell Biol* **31**: 4593-4608
- Smit JK, Faber H, Niemantsverdriet M, Baanstra M, Bussink J, Hollema H, van Os RP, Plukker JT, Coppes RP (2013) Prediction of response to radiotherapy in the treatment of esophageal cancer using stem cell markers. *Radiother Oncol*
- Spiess H (1995) The RA-224 Study: Past, Presence and Future. In *Proceedings of the International Seminar on Health Effects of Internally Deposited Radionuclides: Emphasis on Radium and Thorium*, van Kaick G, Karaoglou A, Kellerer AM (eds), pp 157-163. World Scientific Publishing Co. Pte. Ltd
- Spike BT, Wahl GM (2011) p53, Stem Cells, and Reprogramming: Tumor Suppression beyond Guarding the Genome. *Genes Cancer* **2**: 404-419
- Taghian A, DuBois W, Budach W, Baumann M, Freeman J, Suit H (1995) In vivo radiation sensitivity of glioblastoma multiforme. *Int J Radiat Oncol Biol Phys* **32**: 99-104
- Takahashi K, Yamanaka S (2006) Induction of pluripotent stem cells from mouse embryonic and adult fibroblast cultures by defined factors. *Cell* **126**: 663-676
- Tirino V, Desiderio V, d'Aquino R, De Francesco F, Pirozzi G, Graziano A, Galderisi U, Cavaliere C, De Rosa A, Papaccio G, Giordano A (2008) Detection and characterization of CD133+ cancer stem cells in human solid tumours. *PLoS One* **3**: e3469
- Toguchida J, Ishizaki K, Nakamura Y, Sasaki MS, Ikenaga M, Kato M, Sugimoto M, Kotoura Y, Yamamuro T (1989) Assignment of common allele loss in osteosarcoma to the subregion 17p13. *Cancer Res* **49**: 6247-6251
- Traycoff CM, Kosak ST, Grigsby S, Srouf EF (1995) Evaluation of ex vivo expansion potential of cord blood and bone marrow hematopoietic progenitor cells using cell tracking and limiting dilution analysis. *Blood* **85**: 2059-2068
- Van Putten LM, Kallman RF (1968) Oxygenation status of a transplantable tumor during fractionated radiation therapy. *J Natl Cancer Inst* **40**: 441-451

- Veselska R, Hermanova M, Loja T, Chlapek P, Zambo I, Vesely K, Zitterbart K, Sterba J (2008) Nestin expression in osteosarcomas and derivation of nestin/CD133 positive osteosarcoma cell lines. *BMC Cancer* **8**: 300
- Visvader JE, Lindeman GJ (2008) Cancer stem cells in solid tumours: accumulating evidence and unresolved questions. *Nat Rev Cancer* **8**: 755-768
- Ward IM, Minn K, Jorda KG, Chen J (2003) Accumulation of checkpoint protein 53BP1 at DNA breaks involves its binding to phosphorylated histone H2AX. *J Biol Chem* **278**: 19579-19582
- Ward P, Packman S, Loughman W, Sparkes M, Sparkes R, McMahon A, Gregory T, Ablin A (1984) Location of the retinoblastoma susceptibility gene(s) and the human esterase D locus. *J Med Genet* **21**: 92-95
- Winnard PT, Jr., Kluth JB, Raman V (2006) Noninvasive optical tracking of red fluorescent protein-expressing cancer cells in a model of metastatic breast cancer. *Neoplasia* **8**: 796-806
- Wong FL, Boice JD, Jr., Abramson DH, Tarone RE, Kleinerman RA, Stovall M, Goldman MB, Seddon JM, Tarbell N, Fraumeni JF, Jr., Li FP (1997) Cancer incidence after retinoblastoma. Radiation dose and sarcoma risk. *JAMA* **278**: 1262-1267
- Woodward WA, Bristow RG (2009) Radiosensitivity of cancer-initiating cells and normal stem cells (or what the Heisenberg uncertainty principle has to do with biology). *Semin Radiat Oncol* **19**: 87-95
- Wu C, Wei Q, Utomo V, Nadesan P, Whetstone H, Kandel R, Wunder JS, Alman BA (2007) Side population cells isolated from mesenchymal neoplasms have tumor initiating potential. *Cancer Res* **67**: 8216-8222
- Yang M, Yan M, Zhang R, Li J, Luo Z (2011) Side population cells isolated from human osteosarcoma are enriched with tumor-initiating cells. *Cancer Sci* **102**: 1774-1781
- Yoshikawa T, Kashino G, Ono K, Watanabe M (2009) Phosphorylated H2AX foci in tumor cells have no correlation with their radiation sensitivities. *J Radiat Res* **50**: 151-160
- Zhang J, Espinoza LA, Kinders RJ, Lawrence SM, Pfister TD, Zhou M, Veenstra TD, Thorgeirsson SS, Jessup JM (2012) NANOG modulates stemness in human colorectal cancer. *Oncogene*

Curriculum Vitae

Name: Klymenko Olena (Viktorivna)

Born in Kyiv, Ukraine, 07.05.1982

E-mail address: olenaklymenko@yahoo.com

Languages spoken

Ukrainian (mother tongue), Russian (mother tongue), English (fluent), German (basic)

Educational history

Doctor of Philosophy in Medical Life Science and Technology – Medical faculty, Technical University Munich, Munich, Germany (April 2010 – March 2014)

Master of Science in Radiation Biology– University College London, London, UK (September 2008–October 2009)

Postgraduate training – Medical Academy of Postgraduate Education, Kyiv, Ukraine – Certified Radiation Therapist (2007)

Internship – Medical Academy of Postgraduate Education, Kyiv, Ukraine – Radiology, Radiation therapy, Nuclear Medicine (September 2005- July 2007)

M.D. – National Medical University, Kyiv, Ukraine. Specialty – General Medical Practice (September 1999– July 2005)

Kyiv Gymnasium 178 (high school), Kyiv, Ukraine – (September 1990 - July 1999)

Professional experience

15. 03. 2010 – present time – PhD student, Institute of Radiation Biology, Helmholtz Center Munich, German Research Center for Environmental Health, Neuherberg, Germany

23.11.2009 – 28.02.2010 – Research assistant, Institute of Radiation Biology Helmholtz Center Munich, German Research Center for Environmental Health, Neuherberg, Germany

01.05.2009 – 15.10 2009 - Master student, Institute of Radiation Biology, Helmholtz Center Munich - German Research Center for Environmental Health, Neuherberg, Germany.

01.08.2007 – 22.09.2008 – Radiation therapist, Department of Radiation Therapy, Kyiv City Oncology Hospital, Kyiv, Ukraine.

Publications

Gonzalez-Vasconcellos I, Anastasov N, Sanli-Bonazzi B, Klymenko O, Atkinson M J, Rosemann M. “Rb1 haploinsufficiency promotes telomere attrition and radiation-induced genomic instability.” *Cancer Research*, 2013

Bannik K, Rössler U, Faus-Kessler T, Gomolka M, Hornhardt S, Dalke C, Klymenko O, Rosemann M, Trott KR, Atkinson M, Kulka U, Graw J. “Are mouse lens epithelial cells more sensitive to γ -irradiation than lymphocytes?” *Radiat Environ Biophys*. 2013 Jan 16

O.Klymenko, K.-J. Heiliger, I. Gonzalez Vasconcellos, C. Dalke, M. J. Atkinson, M. Rosemann. "Molecular changes in radiation induced thyroid carcinomas in mice" Radiobiology and Environmental Security, NATO Science for Peace and Security Series C: Environmental Security, Springer, 2011

Co-author of scientific publication in Ukraine: Лазар, Д. А, Чеботарьова Т.І., Говоруха Т.М., Клименко О.В. Супровідна терапія при лікуванні хворих на високоступіньові гліоми головного мозку. Український радіологічний журнал, 311-313, (ukrainian). „Support therapy during treatment of high grade gliomas, Ukrainian Journal of Radiology”

Awards

Fridericus Foundation “PhD research stipend award” for the period January 2013-June 2013

Award for best presentation by an early career geneticist awarded by the Genetics Society of America. At the 3rd International Conference on Modern Problems in Genetics, Radiobiology, Radioecology and Evolution, 14 October 2010 Alushta, Ukraine

Fridericus Foundation “Master research stipend award” for the period October 2009-October 2010